# DIGITAL HOLOGRAPHY FOR NONDESTRUCTIVE TESTING

SUWAN PLAIPICHIT

A THESIS SUBMITTED IN FULFILLMENT
OF THE REQUIREMENT FOR THE DEGREE OF
DOCTOR OF PHILOSOPHY IN APPLIED PHYSICS
FACULTY OF SCIENCE
KING MONGKUT'S INSTITUTE OF TECHNOLOGY LADKRABANG
2014

KMITL-2014-SC-D-030-051

# DIGITAL HOLOGRAPHY FOR NONDESTRUCTIVE TESTING

**SUWAN PLAIPICHIT**

**A THESIS SUBMITTED IN FULFILLMENT**

**OF THE REQUIREMENT FOR THE DEGREE OF**

**DOCTOR OF PHILOSOPHY IN APPLIED PHYSICS**

**FACULTY OF SCIENCE**

**KING MONGKUT'S INSTITUTE OF TECHNOLOGY LADKRABANG**

**2014**

**KMITL-2014-SC-D-030-051**

**คณะวิทยาศาสตร์**
**สถาบันเทคโนโลยีพระจอมเกล้าเจ้าคุณทหารลาดกระบัง**
**ใบรับรองวิทยานิพนธ์**

---

**หัวข้อวิทยานิพนธ์** ดิจิตอลโฮโลกราฟีสำหรับการตรวจสอบแบบไม่ทำลาย
DIGITAL HOLOGRAPHY FOR NONDESTRUCTIVE TESTING

**นักศึกษา** นายสุวรรณ พลายพิชิต
**รหัสประจำตัว** 53650101
**ปริญญา** ปรัชญาดุษฎีบัณฑิต
**สาขาวิชา** ฟิสิกส์ประยุกต์
**อาจารย์ที่ปรึกษาวิทยานิพนธ์** ดร.ประธาน บุรณศิริ

| คณะกรรมการสอบวิทยานิพนธ์ | | ลายมือชื่อ |
|---|---|---|
| รศ.ดร.วราวุฒิ | เถาลัดดา | |
| รศ.วิชาญ | เตชิตธีระ | |
| ดร.เชรษฐา | รัตนพันธ์ | |
| ผศ.ดร.รัชภาคย์ | จิตต์อารี | |
| ดร.ประธาน | บุรณศิริ | |

**วัน / เดือน/ ปี ที่สอบ** 28 พฤศจิกายน พ.ศ. 2557 เวลา 13.00 – 16.00 น.
**สถานที่สอบ** ณ ห้อง 307 ชั้น 3 อาคารจุฬาภรณวลัยลักษณ์ 1



**คณะวิทยาศาสตร์รับรองแล้ว**

**(รองศาสตราจารย์ ดร.ดุษณี ธนะบริพัฒน์)**
**คณบดีคณะวิทยาศาสตร์**
**วันที่**.....15.....**เดือน**.....ธ.ค.....**พ.ศ**.....57.....

**หัวข้อวิทยานิพนธ์** ดิจิตอลโฮโลกราฟีสำหรับการตรวจสอบแบบไม่ทำลาย

**นักศึกษา** นายสุวรรณ พลายพิชิต

**รหัสประจำตัว** 53650101

**ปริญญา** ปรัชญาดุษฎีบัณฑิต

**สาขาวิชา** ฟิสิกส์ประยุกต์

**พ.ศ.** 2557

**อาจารย์ที่ปรึกษา** ดร.ประธาน บุรณศิริ

## บทคัดย่อ

วิทยานิพนธ์ฉบับนี้ได้เสนอวิธีการตรวจสอบแบบไม่ทำลายด้วยเทคนิคดิจิตอลโฮลกราฟี โดยมีตัวอย่างที่นำมาทำการตรวจสอบทั้งหมดสามชนิด ได้แก่ ลายนิ้วมือ ขวดแก้ว และโฟโตรีแฟรคทีฟเกรตติงของผลึกแบเรียมไททาเนตชนิดเจือด้วยซีเรียม โดยทุกการติดตั้งอุปกรณ์เพื่อตรวจสอบนั้นจะใช้เลเซอร์ไดโอดที่มีความยาวคลื่น 635 นาโนเมตรเป็นแหล่งกำเนิดแสง และใช้กล้องถ่ายรูปที่มีเซ็นเซอร์ชนิดซีมอส (CMOS) เป็นตัวรับภาพอันดับแรกในการตรวจสอบความชื้นของนิ้วมือนั้น วิทยานิพนธ์นี้ได้ทำการรวมเทคนิกการถ่ายลายนิ้วมือด้วยหลักการสะท้อนกลับหมดและดิจิตอลโฮโลกราฟีแบบสะท้อนเข้าด้วยกัน ผลของการถ่ายแผ่นทดสอบที่มีเส้นทึบหนา 200 ไมโครเมตร ด้วยเทคนิกดิจิตอลโฮโลกราฟีแบบส่งผ่านกับแบบสะท้อนแสดงให้เห็นว่าทั้งสองวิธีให้ผลของการสร้างภาพโฮโลแกรมที่เหมือนกันดังนั้นเทคนิกที่คิดค้นขึ้นนี้จึงถูกนำมาใช้กับการถ่ายลายนิ้วมือที่มีความชื้นต่างกันดังนี้ 39% 54% 69% และนิ้วมือที่เปียกต่อมาทำการตรวจสอบขวดแก้วด้วยดิจิตอลโฮโลกราฟี ซึ่งสิ่งที่ตรวจสอบได้แก่รัศมีความโค้งและจุดบกพร่องในเนื้อแก้ว ในการตรวจสอบหารัศมีความโค้งนั้นจะใช้แสงขนานส่องผ่านแผ่นทดสอบที่มีเส้นดำทึบไปยังผิวโค้งของแก้ว จากนั้นแสงสะท้อนที่ประกอบด้วยภาพของแผ่นทดสอบเส้นทึบจากผิวแก้วจะถูกบันทึกลงบนกล้อง รัศมีความโค้งของขวดแก้วสามารถคำนวณได้จากสมการกระจกโค้ง โดยใช้ระยะภาพที่ได้จากการสร้างภาพด้วยดิจิตอลโฮโลกราฟี ในส่วนของการตรวจหารอยบกพร่องจะใช้แสงขนานส่องผ่านรอยบกพร่องในขวดแก้วและทำการบันทึกภาพ เมื่อทำการสร้างภาพดิจิตอลโฮโลแกรมจะพบรอยบกพร่อง ในการตรวจสอบสิ่งสุดท้ายคือโฟโตรีแฟรคทีฟเกรตติงภายในผลึกแบเรียมไททาเนต ในการสร้างเกรตติงในผลึกจะทำการแบ่งแสงจากฮีเลียมนีออนเลเซอร์ที่มีกำลัง 10 มิลลิวัตต์

เป็นสองลำให้ตกกระทบบนผลึกเป็นมุมต่างๆ จากนั้นทำการหามุมที่ทำให้แสงเลี้ยวเบนมีความเข้มสูงสุด ซึ่งเป็นมุมที่ทำให้เกรตติงมีความแข็งแรงที่สุดด้วย จากผลการสังเกตพบว่า ที่มุมตกกระทบ 20 องศาจะให้แสงเลี้ยวเบนมีความเข้มสูงสุด ในการสังเกตเกรตติงภายในผลึกจะใช้แสงจากเลเซอร์ไดโอดส่องผ่านไปยังผลึก และใช้เลนส์ช่วยขยายขนาดของเกรตติงก่อนทำการบันทึกภาพ จากนั้นจึงทำการสร้างภาพดิจิตอลโฮโลกราฟีของเกรตติงภายในผลึกเพื่อวัดความกว้างของเกรตติง

**คำสำคัญ:** ดิจิตอลโฮโลกราฟี, การตรวจสอบแบบไม่ทำลาย, ลายนิ้วมือ, วัสดุผิวโค้ง, โฟโตรีแฟรค-ทีพ, การเลี้ยวเบนด้วยตัวเอง

| | |
|---|---|
| **Thesis Title** | Digital holography for nondestructive testing |
| **Student** | Suwan Plaipichit |
| **Student ID** | 53650101 |
| **Degree** | Doctor of Philosophy |
| **Program** | Applied Physics |
| **Year** | 2014 |
| **Thesis Advisor** | Dr. Prathan Buranasiri |

## ABSTRACT

In this thesis, digital in-line holography (DIH) has been used as a tool for nondestructive testing technique. Three different samples *i.e.* fingerprint, glass bottle, and photorefractive grating inside Ce:$BaTiO_3$ crystal have been investigated by using this technique. All our DIH nondestructive systems have been composed of a laser diode with 635 nm and a CMOS camera. First, the moisture effect in fingerprint scanner based on total internal reflection which is the important concept in optical finger print scanner has been explored. The reflected and transmitted DIH have been set up and compared the results by using positive resolution test target with line width of 200 μm. From the experimental results, the reconstructed image of reflected DIH is as perfect as the image of transmitted DIH. Due to the advantage for opaque object imaging of reflected DIH, reflected DIH based on TIR has been selected to investigate moisture effect of the fingerprint. The fingerprints with different moistures of 39%, 54%, 69%, and soaked up finger have been observed. Second, the technique for investigating the quality of glass bottle by using DIH has been proposed. The collimated beam laser diode incident on a glass bottle then the image bearing reflected beam consisting of quality profile of the glass bottle has been recorded on a CMOS camera. By using the experimental results and numerically reconstructed images, the defects inside the glass bottle can be detected and the curvature radius of the bottle can be directly calculated by putting the reconstructed distance into mathematical model of a mirror equation. Finally, the grating period of photorefractive anisotropic self-diffraction inside Ce:$BaTiO_3$ has been investigated by using DIH technique. To write grating inside the crystal, a beam with

wavelength of 632.8 nm and power of 10 mW from a He-Ne laser has been separated into two beams and then incident on the crystal with different angles. The highest efficiency of diffraction beams have been founded when the angle between both beams is 20 degrees. To observe the gratings inside the crystal, the transmitted probe beam with opposite polarization of the writing beams has been expanded and incident on the crystal. The transmitted beam has been recorded on a digital camera. To explore the grating periods, both phase and amplitude of the images were reconstructed by numerical process using a computer. Then, the grating periods in photorefractive anisotropic self-diffraction have been measured.

**Keywords:** digital in-line holography, nondestructive testing, fingerprint, curvature surface, photorefractive, self-diffraction.

# ACKNOWLEDGEMENT

This thesis could not be successfully completed without support and help from many people. First, I would like to express my sincere thanks to my thesis advisor, Dr. Prathan Buranasiri for his invaluable suggestions and correction since the start until the completion of this thesis. Moreover, he is the person, who introduced me to the research fields of photorefractive effect and digital holography. I also would like to thank my thesis committees, Assoc. Prof. Dr. Warawoot Thowladda, Assoc. Prof. Wicharn Techitdheera, Dr. Chesta Rattanapun, and Asst. Prof. Dr. Ratchapak Chitaree, for their valuable discussions to improve this thesis.

I would like to give a special thank Dr. Surawut Wicharn, my colleague at Photon Dynamics Laboratory at Physics Department (PDL), KMITL, for his suggestion in computer programming. I also would like to thank graduated and undergraduate students at PDL for their supporting. I would like to thank Mr. Matthew Beals for supporting the reconstructed tool "HoloViewer" [41], that I used to study and develop the code to reconstruct digital hologram. Moreover, I would like to special thank the Science Achievement Scholarship of Thailand (SAST) for financially supporting during my study in Ph.D. program.

Last but not least, I would like to especially thank my father and mother, who are the most important people in my life. They not only give financial support but also encouragement when I felt down. This thesis would not be completed without them.

Suwan Plaipichit

November 28, 2014

# TABLE OF CONTENTS

ABSTRACT (THAI) ..... I

ABSTRACT (ENGLISH) ..... III

ACKNOWLEDGEMENT ..... V

TABLE OF CONTENTS ..... VI

LIST OF FIGURES ..... IX

LIST OF TABLES ..... XII

**CHAPTER 1 INTRODUCTION ..... 1**

1.1 Background and motivation. ..... 1

1.1.1 Nondestructive testing. ..... 1

1.1.2 Digital holography and its configuration. ..... 2

1.1.3 Optical fingerprint scanner. ..... 3

1.1.4 Glass bottle inspection. ..... 4

1.1.5 Photorefractive grating. ..... 4

1.2 Objective of thesis. ..... 5

1.3 Scope of work. ..... 5

1.4 Thesis outline. ..... 6

**CHAPTER 2 THEORY ..... 7**

2.1 Diffraction and Fourier optics ..... 7

2.1.1 Light wave. ..... 7

2.1.2 Diffraction of light ..... 8

2.1.3 Fourier transformation. ..... 10

2.1.4 Convolution theorem. ..... 11

2.2 Holography and digital holography. ..... 11

2.2.1 Holography. ..... 11

2.2.2 Holographic term. ..... 13

2.2.3 Digital holography. ..... 14

2.2.4 Method of reconstruction. ..... 16

2.2.4.1 Huygens convolution method. ..... 16

2.2.4.2 Angular spectrum method. ..... 17

2.2.5 Comparison of method. ..... 20

2.2.5.1 Simulation of diffraction. ..... 20

2.2.5.2 Reconstruction. ..... 21

2.3 Digital holography configurations. ..... 24

2.3.1 Digital off-axis holography (DOH) configuration. ..... 24

2.3.2 Digital in-line holography (DIH) configuration. ..... 24

2.4 Photorefractive nonlinear optics. ..... 28

2.4.1 Photorefractive effect. ..... 28

2.4.2 Anisotropic self-diffraction (ASD) ..... 30

**CHAPTER 3 FINGERPRINT MOISTURE INVESTIGATION ..... 32**

3.1 Optical fingerprint scanner. ..... 32

3.2 TDIH and RDIH configuration. ..... 33

3.2.1 Experimental results of test target hologram. ..... 35

3.3 Experimental setup for investigating moisture effect in optical fingerprint scanner using TIRDIH. ..... 37

3.3.1 Experimental results of fingerprint hologram. ..... 38

**CHAPTER 4 GLASS BOTTLE INSPECTION ..... 41**

4.1 Mathematical method. ..... 41

4.2 Experimental setup for measuring radius of curvature. ..... 42

4.3 Experimental setup for defect detection in glass bottle. ..... 43

4.4 Experimental results. ..... 44

**CHAPTER 5 MEASUREMENT OF PHOTOREFRACTIVE GRATING ..... 46**

5.1 Experimental setup for determining the optimum angle of higher order ASD. ..... 46

5.2 Experimental setup for measuring the width of PR grating. ..... 48

5.3 Experimental results. ..... 49

**CHAPTER 6 CONCLUSIONS** ..... **52**

6.1 Summary of fingerprint moisture investigation using TIRDIH. ..... 52

6.2 Summary of glass bottle inspection using DIH ..... 52

6.3 Summary of direct measurement of PR grating in $BaTiO_3$ crystal. ..... 53

6.4 Future work. ..... 53

**REFERENCES** ..... **54**

**APPENDICES** ..... **58**

APPENDIX A ..... **58**

APPENDIX B ..... **60**

APPENDIX C ..... **64**

**AUTHOR BIOGRAPHY** ..... **80**

# LIST OF FIGURES

**Figure 2.1** Fresnel diffraction.....9

**Figure 2.2** Fraunhofer diffraction.....9

**Figure 2.3** Huygen's principle.....9

**Figure 2.4** Geometry of diffraction from 2D aperture. .....10

**Figure 2.5** Conventional hologram recording. .....12

**Figure 2.6** conventional hologram reconstructions. .....12

**Figure 2.7**The holographic term; (a) hologram recording, (b) hologram reconstruction with reference wave $E_R$, and (c) hologram reconstruction with conjugate of reference wave $E_R^*$. .....14

**Figure 2.8** Concept of digital holography .....15

**Figure 2.9** Coordinating system for numerical reconstruction.....17

**Figure 2.10** The wave vector $\vec{k}$ .....19

**Figure 2.11** Diagram of the diffracted simulation.....20

**Figure 2.12** Diffracted simulation image at each distance of; (a) HCM and (b) ASM.....21

**Figure 2.13** Diagram of experimental setup for computing the reconstruct method. .....22

**Figure 2.14** The set of digital hologram; (a) recorded images, (b) reconstructed images with HCM, and (c) reconstructed image with ASM. .....22

**Figure 2.15** The flow chart of reconstruction algorithm .....23

**Figure 2.16** Off axis configuration.....24

**Figure 2.17** In-line configuration. .....25

**Figure 2.18** Gabor configuration.....25

**Figure 2.19** Multi plane DIH configuration. .....25

**Figure 2.20** Recorded digital hologram. .....26

**Figure 2.21** Reconstructed digital hologram;

(a)at plane z = 150 mm and (b) at plane z = 250 mm.(c) at plane z = 350 mm.....26

(c) at plane z = 350 mm,(d) at plane z = 450 mm, and (e) at plane z = 550 mm. .....27

**Figure 2.22** Band transport model.....29

**Figure 2.23** The distribution of charge under illuminating region. .....30

**Figure 2.24** The interference fringe from two incident beam with angle $2\theta_i$ . .....30

**Figure 2.25** Wave vector diagram of anisotropic self-diffraction. .....31

**Figure 3.1** Concept of optical fingerprint scanner. .....33

**Figure 3.2** Experimental setup for recording resolution test target by TDIH configuration. .....34

**Figure 3.3** Experimental setup for recording resolution test target by RDIH configuration .....34

**Figure 3.4** Hologram and its profile from TDIH: (a) recorded hologram, (b) reconstructed hologram, and (c) transverse intensity profile of (b). .....35

**Figure 3.5** Hologram and its profile from RDIH: (a) recorded hologram, (b) reconstructed hologram, and (c) transverse intensity profile of (b). .....36

**Figure 3.6** The schematic of digital holographic fingerprint scanner using TIRDIH. .....37

**Figure 3.7** Recorded hologram: (a) with moisture of 54.0%. Reconstructed holograms: (b) with moisture of 39.0%, (c) with moisture of 54.0%, (d) with moisture of 69.0%, and (e) soak fingerprint. .....39

**Figure 3.8** Transverse intensity profiles of fingerprint with moisture of 54.0%. .....40

**Figure 3.9** The small ridge and valley at the edge of fingerprint. .....40

**Figure 4.1** The concept of radius of curvature measurement configuration .....42

**Figure 4.2** The experimental setup for the measurement of radius of curvature using DIH. .....43

**Figure 4.3** The experimental setup for defect detection using DIH. .....43

**Figure 4.4** Digital hologram of; (a) recorded image by using flat mirror; (b) numerical Reconstruction image of (a) at distance 194.7 mm, (c) recorded image by using glass bottle, and (d) numerical reconstruction image of (c) at distance 4370 mm. .....44

**Figure 4.5** Defect inside glass bottle; (a) bubble, (b) recorded image of bubble using DIH configuration, (c) numerical reconstructed image of (b), (d) line scratch, (e) recorded image of line scratch using DIH configuration, and (f) numerical reconstructed image of (e). .....45

**Figure 5.1** Experimental setup for observing grating; P, polarizer; M's, mirror; BS, beam splitter; L's, lenses. ..... 46

**Figure 5.2** The characteristic of incident angle and diffraction power. ..... 47

**Figure 5.3** The pattern of zero and first order of anisotropic self-diffraction. ..... 47

**Figure 5.4** Snell's laws. ..... 48

**Figure 5.5** Recorded hologram of standard grating.. ..... 49

**Figure 5.6** Reconstructed hologram of standard grating. ..... 49

**Figure 5.7** Transverse intensity profile of Fig. 5.6. ..... 50

**Figure 5.8** Reconstructed hologram of phase grating inside the crystal. ..... 51

**Figure 5.9** Transverse intensity profile of Fig. 5.7 ..... 51

**Figure A.1** The sample of image; (a) square aperture, (b) FFT, (c) triangle aperture, (d) FFT of triangle aperture, (e) circle aperture, and FFT of circle aperture ..... 59

# LIST OF TABLES

**Table A.1** MATLAB code example for transforming image with FFT function.....58

**Table B.1** MATLAB code example for reconstructing digital hologram using HCM. .....60

**Table B.2** MATLAB code example for reconstructing digital hologram using ASM.....62

# CHAPTER 1

# INTRODUCTION

## 1.1 Background and motivation

In this thesis, the digital in-line holography, which is the one of optical characterization, has been applied to nondestructive testing technique. Therefore, there are mainly five articles have been described in this topic: nondestructive testing, digital holography, fingerprint scanner, glass bottle inspection, and photorefractive grating.

### 1.1.1 Nondestructive testing

The measurement is the important process in various fields, i.e. industrial factory, medical profession, forensic science, general laboratory, and so on. There are two analysis techniques to investigate the properties of material, component or system; the method that invasively evaluate the systems called destructive testing (DT) and the method that non-invasively evaluate the systems called nondestructive testing (NDT). NDT techniques have been widely applied to various fields such as industrial factory, aerospace field, medical imaging, and so on [1]. NDT can be mainly classified into five major methods; radiological testing, acoustical/vibration testing, electromagnetic testing, thermal/infrared testing and visual/optical testing. Each method has some limitations to use. For example, radiographic testing method is the technique that uses ionizing radiation (X-ray and $\gamma$-ray) investigates material or system. Due to the high energy of ionizing radiation, users must have radiograph license and wear an individual direct reading pocket dosimeter and either a film badge or thermo luminescent dosimeter while doing their work [2]. Acoustical testing technique use mechanical wave to investigate mechanical properties inside material or system. This technique makes vibration that may annoy some system that not needs the vibration such as optical system.

Visual/optical testing methods are the fastest-growing NDT technique. They can evaluate both micro and macro scales. Because they are non-contact testing, they can investigate irregular

object and non-planar surfaces. This method can be developed to observe object in three dimensions (3D) via holography or digital holography technique [3-15]. However, a lot of systems are not still evaluated by using digital holography technique. In this research, the NDT using digital in-line holography (DIH) has been proposed. There are three samples have been investigated; fingerprint, properties of glass bottle, photorefractive grating inside $BaTiO_3$.

### 1.1.2 Digital holography and its configurations

Holography, the imaging technique recorded and reconstructed image in three dimensions was invented by Gabor [3-5]. The recording process is required the interference of object beam and reference beam on photographic film. Then, it uses the reading beam shine on the photographic film to see image in three dimensions. This process is called reconstruction. Due to the conventional holography waste photographic film, digital holography was developed. The image, which consists of phase and amplitude, is recorded on electronics devices such as charge couple devices (CCDs) or complementary metal oxide semiconductors (CMOS). The three dimensional image is numerically reconstructed by using computer [6]. Digital holography would be typically classified into two type i.e. an off-axis and an in-line configuration. The digital in-line holography (DIH) is the simplest configuration to record hologram. There are various configurations of DIH such as transmission, reflection, and total internal reflection (TIR). Transmission DIH (TDIH) could record and reconstruct interferogram, which place difference plane [7]. An example of TDIH, the particle was characterized by shining the collimated light through it and then the transmitted beam was recorded and reconstructed [8-12]. However, TDIH configuration has some limitation. It may not use in investigation the surface of opaque object, so the reflected DIH (RDIH) has been developed. As normal holography, RDIH need the interference of object beam and reference beam to complete the recording process. By using the reference-delayed technique, however, the system could record hologram with only one input beam. In this configuration, two reflected beam from object, which consist of phase difference, were interfered and recorded on CCD camera [13]. As describe above, DIH is the simplest configuration, therefore the system can be setup in small area and it may be easy assemble as the compact measured device. Hence, all of

the experimental setup based on DIH. Moreover, in this thesis, the RDIH configuration has been developed to record with only one beam. This system is simpler than the past and it can useful. The fingerprint is the sample tested with this new RDIH technique. The detail of this technique will be described in chapter 3.

### 1.1.3 Optical fingerprint scanner

By using the technique of TIR holographic microscopy, recently, some properties of biology cells have been explored [14, 15]. They shined the collimated light to the leg of right angle prism. The object beam undergoes TIR at hypotenuse of right angle prism then interferes and record on camera. The cells that have non-homogeneous of index of refraction provide phase difference in digital hologram. In addition, the basic concept of TIR was widely applied in fingerprint scanner application [16, 17]. The early system, however, provided unsharp patterns. A number method has been invented for resolving this problem. For example, the holographic plate which placed on prism was used to correct the distortion of pattern [18, 19]. Another example, asymmetrical aspheric lens was invented to get the better contrast of fingerprint pattern [20]. Recently, the fingerprint patterns were explored using digital holography technique based on angular spectrum method [21], based on Michelson interferometer. In our previous work, the digital hologram patterns of fingerprint pattern were obtained by using reflection from glass slide [22]. There were interference pattern from top and bottom occurred and distributed in recorded images.

However, from the point of view, the imaging technique of fingerprint has been still valued for continuing to explore. In this thesis, digital holographic fingerprint scanner based on combination of RDIH and TIR have been presented. In this configuration, instead of using two input beam as previous systems, only one input beam is used so the system may be cheaper and more compact. The reflected field, which is diffracted at the edge, of the fingerprint pattern is interfered with nondiffracted field. In chapter 3, there also show that the reconstructed of RDIH provide the same results as TDIH. By using this technique, the results of some various moistures on fingerprint have been explored and shown.

### 1.1.4 Glass bottle inspection

Generally, there are mainly two configuration to measure shape; multi illumination point method and multi wavelength method [23, 24]. Phase shifting digital holography technique is the one of multi illumination point methods that used mirror mounted on piezoelectric transducer (PZT) to shift stepwise the phase of reference wave [25]. Due to the sensitive to external disturbances of conventional phase shifting digital holography technique, Doppler phase shifting technique was developed [26]. The time variation of intensity at a pixel of digital hologram from the mirror movement with perturbed table was extracted by Fourier transform into frequency domain. By picking the actual frequency peak to reconstruct process, the clearly shape under perturbation was obtain. The phase shifting technique can be measure shape and also the radius of curvature. However, the phase shifting technique generally needs at least three interferograms with mutual phase shifting to reconstruct image. In this thesis we propose the method to investigate radius of curvature and defect inside glass bottle using digital in-line hologram (DIH) configuration by using only one interferogram. By using geometrical optics; lens and mirror equations, the radius of curvature are easy to obtain with reconstructed distance. Moreover, the defects inside glass bottle, bubble and line scratch are clearly to detect.

### 1.1.5 Photorefractive grating

Photorefractive effect was the dynamic grating which found by Askin *et. al.* The refractive index of $LiNbO_3$ and $LiTaO_3$ were changed by optically induced and called “optical damage” [27]. Several years later, this phenomenon has been studied on $BaTiO_3$ by using holographic storage technique [28]. Because the properties and applications of $BaTiO_3$ have value to study, there were several researches try to observe these properties such as intensity dependence, phase conjugate, and so on [29-32]. Kukhtarev et al. first found that polarization of incident beam and diffracted beam of $BaTiO_3$ crystal were perpendicular each other and called “anisotropic self diffraction (ASD)” [33]. Then Temple and Warde found that higher order anisotropic diffraction can be occurred on other photorefractive crystals such as BaTiO3, SBN and BSKNN [34]. After that, there were some applications of ASD with $BaTiO_3$ have been studied by several authors [35,

36]. They show that the index of refraction of $BaTiO_3$ can be change by the change of temperature. So, the change of index of refraction directly affect to the diffraction angle of higher order. This concept was applied to temperature measurement. Moreover, the wavelength absorption coefficient of $BaTiO_3$ crystal depends on impurity doped in crystal. Changxi Yang et. al. shown that the Cerium doped level cause the properties of $BaTiO_3$ change, i.e. responsible wavelength shifted to red wavelength [37]. On the other words, Cerium doped Barium Titanate ($Ce:BaTiO_3$) can be operated with red light (undoped $BaTiO_3$ is good response in blue light). The wavelength dependence of Cerium doped Barium Titanate ($Ce:BaTiO_3$) has been essential investigated [38].

However, it was hardly to observe photorefractive effect inside material with non-destruction and there were still few study dynamic grating on $LiNbO_3$ photorefractive crystals [39, 40]. In this thesis, digital holography has been applied for nondestructive testing technique to investigate photorefractive grating of higher order ASD in $Ce:BaTiO_3$.

## 1.2 Objectives of thesis

1.2.1 To study the principle and configuration of DIH.

1.2.2 To applied DIH for nondestructive testing technique to investigate fingerprint, glass bottle and photorefractive grating inside a Ce: BaTiO3 crystal.

1.2.3 To study the condition of ASD grating inside Ce: $BaTiO_3$ crystal.

## 1.3 Scope of work

The scope of this research is focused on the application of DIH for nondestructive testing. Firstly, the different moistures of fingerprint by using fingerprint scanner based on DIH technique have been investigated. Then, the DIH technique has been applied to measure the radius of curvature of glass bottle and detect defect inside glass bottle. Finally, ASD in Ce: $BaTiO_3$ crystal has been explored and then the grating inside the crystal has been observed by using DIH.

## 1.4 Thesis outline

Chapter 1 provides background (literature review) and motivation, object, scope, and outline of the thesis. The background and motivation have been divided into five topics: nondestructive testing, digital in-line holography, moisture effect in optical fingerprint scanner, glass bottle inspection, and photorefractive grating.

Chapter 2 will present the theory of diffraction and Fourier optics, holography and digital holography, the configuration of digital holography, photorefractive nonlinear optics. The diffraction and Fourier optics are the basic principle to describe that how digital holography works. In this chapter will describe the difference of conventional holography, digital holography and their configuration. The two kinds of reconstruction methods; Huygens convolution and angular spectrum, will be compare here. The phenomenon of photorefractive effect will be described by band transport model. Finally, the principle of anisotropic self diffraction in a photorefractive Ce: $BaTiO_3$ crystal, the one of photorefractive effect, will be described.

Chapter 3 will show that RDIH developed in this thesis will be applied to digital holographic fingerprint recording. The moisture effect of optical fingerprint scanner will be investigated by digital holography in this chapter.

Chapter 4 will show the technique to measure radius of curvature using DIH based on geometrical optics (lens and mirror equation). Then we will show that DIH is also applied to detect defect inside glass bottle.

Chapter 5 will present the measurement of PR grating inside Ce:$BaTiO_3$ crystal. First, the optimum angle that provides the strongest grating will be investigated. Then this grating will be measured using DH technique.

Chapter 6 will present the summaries and the future work of this thesis.

# CHAPTER 2

# THEORY

This chapter presents the theory which is important to this thesis. We begin by describe the propagation of light wave which follow Maxwell equation and plane wave equation. The diffracted wave from the object is described by two methods. One is Huygens convolution method (HCM) and the other is angular spectrum method (ASM). Moreover, these two methods also are applied to reconstruct the digital hologram. Then, the diffracted simulation and reconstructed images by using these two methods are compared. The flow chart of reconstruction algorithm that we used in this thesis also shows in this chapter. Then the configuration of digital holography will be described. In the end, the band transport model, which is the basic of the photorefractive effect, has been discussed. Here, the photorefractive effect is the basic phenomena that generate the ASD grating observed by DIH.

## 2.1 Diffraction and Fourier optics

Diffraction and Fourier optics are the essential theory in description of digital holographic process. The propagation of optical fields of light from object plane to hologram plane and the reconstructed hologram fields at image plane can be mathematically described by these theories.

### 2.1.1 Light wave

By following Maxwell equation, the propagating of light can be described by the wave equation in vacuum

$$\nabla^2 \vec{E} - \frac{1}{c^2}\frac{\partial^2 \vec{E}}{\partial t^2} = 0 \tag{2-1}$$

where $\vec{E}$ is the electric fields, c is speed of light in vacuum and $\nabla^2$ is the Laplace operator which defined as

$$\nabla^2 = \frac{\partial^2}{\partial x^2} + \frac{\partial^2}{\partial y^2} + \frac{\partial^2}{\partial z^2} \tag{2-2}$$

The vibration of electric fields $\vec{E}$ can vibrate in any direction which perpendicular to propagated direction. However, the wave vibrates in single plane in many light application and called linear polarized light. Often in optics, it is sufficient to consider light using scalar wave equation. Let $E$ be the scalar of electric fields. Therefore, Eq. (2-1) is rewritten in scalar wave equation

$$\nabla^2 E - \frac{1}{c^2}\frac{\partial^2 E}{\partial t^2} = 0 \tag{2-3}$$

Then, the simplest solution of Eq. (2-3), plane wave solution, is given by

$$\begin{aligned} E(x,y,z,t) &= \exp[\, j(\omega t - \vec{k}\cdot\vec{R})] \\ &= \exp[\, j(\omega t - \alpha\hat{x} - \beta\hat{y} - \gamma\hat{z})] \end{aligned} \tag{2-4}$$

where $\omega = 2\pi f$, $\vec{R} = x\hat{x} + y\hat{y} + z\hat{z}$, and $\vec{k} = \alpha\hat{x} + \beta\hat{y} + \gamma\hat{z}$ are angular frequency, position vector, and wave vector, respectively ( $\hat{x}$, $\hat{y}$, and $\hat{z}$ denote the unit vector in $x$, $y$, and $z$ direction). The ratio of k named wave number is calculated by

$$\left|\vec{k}\right| \equiv k = \frac{2\pi}{\lambda} \tag{2-5}$$

### 2.1.2 Diffraction of light

Diffraction of light is the phenomenon that the light wave hits an obstacle, ahole, or a slit. This characteristic behavior will occur with the condition that the wavelength of incident plane wave must be in the range of obstacle or slit. The diffraction can be classified into two type by consider with the length of diffraction.In near field of diffraction, the diffracted wavefront is considered as spherical wave called Fresnel diffraction as shown in Fig 2.1. On the other hand, as illustrate in Fig 2.2 the diffracted wave front is considered as plane wave at far field of diffraction called Fraunhofer diffraction.

Diffraction, the bending of wave around the edge of slit or obstacle, can be explained with Huygens' principle (as illustrate in Fig. 2.3):

*Every point of a wavefront can be considered as a source point for secondary spherical waves. The wavefront at any other place is the coherent superposition of these secondary waves.*

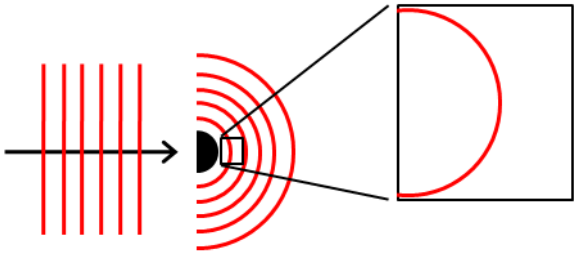

**Figure 2.1** Fresnel diffraction**.**

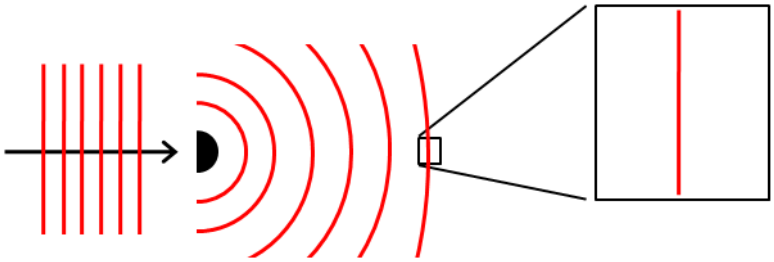

**Figure 2.2** Fraunhofer diffraction.

**Figure 2.3** Huygens' principle

By consider that the light propagates along z-direction as show in Fig. 2.4, when the light propagates through aperture or hit on edge of obstacle, it will be diffractedby the edge of aperture or obstacle. This called diffraction from 2D aperture.

When the light propagated through Fourier plane $(\xi,\eta)$ such as lens, grating or obstacle, the approximation solution of wave equation can be given by

$$E_{diff}(x,y,z,t)=\frac{1}{j\lambda}\iint E_{tran}(\xi,\eta)\frac{\exp(jk\rho)}{\rho}dxdy \tag{2-6}$$

where $E_{trans}(\xi,\eta)$ is the fraction of field that transmit through the aperture and it will be equal to zero if any points $\xi$ and $\eta$ are block by aperture. $\rho$ is the distance between aperture plane $(\xi,\eta)$ to observing plane $(x,y)$ i.e. hologram plane or recorded plane.

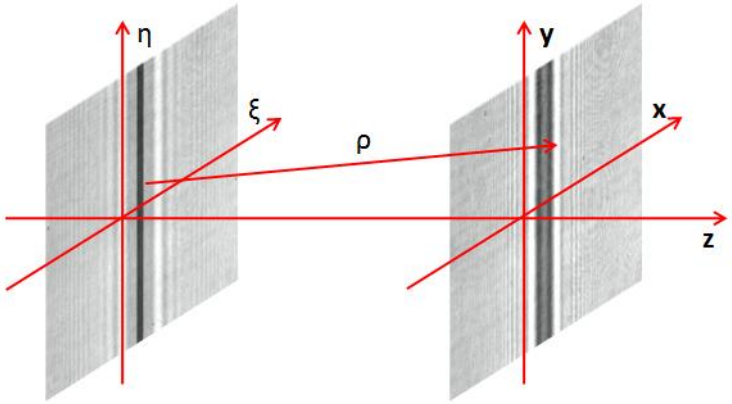


**Figure 2.4** Geometry of diffraction from 2D aperture.

### 2.1.3 Fourier transformation

In electrical system which concerned signal as function of time, one dimensional (1D) Fourier transform is applied to solve the problem in the system. On the other hand, in optic, i.e. image or optical field, there are two spatial variables x and y must be consider. Hence, the two dimensional (2D) spatial signal can be considered using Fourier transform and defined as

$$\mathcal{F}\{f\}=\int_{-\infty}^{\infty}\int_{-\infty}^{\infty}f(x,y)\exp[-j2\pi(f_x x+f_y y)]dxdy \tag{2-7}$$

The corresponding inverse 2D Fourier transformation is defined as

$$\mathcal{F}^{-1}\{F\}=\int_{-\infty}^{\infty}\int_{-\infty}^{\infty}F(f_x,f_y)\exp[j2\pi(f_x x+f_y y)]df_x df_y \tag{2-8}$$

The function $f(x,y)$ and $F(f_x,f_y)$ are called Fourier transform pair

### 2.1.4 Convolution theorem

Due to the some part of numerical reconstructed process in this thesis used convolution method, this topic will describe the definition of convolution.The 2D convolution of two functions $f(x,y)$ and $g(x,y)$ can be defined as

$$f(x,y)\otimes g(x,y)=\int_{-\infty}^{\infty}\int_{-\infty}^{\infty} f(\xi,\eta)g(x-\xi,y-\eta)d\xi d\eta \tag{2-9}$$

where the $\otimes$ is the convolution operation. The convolution theorem can apply with Fourier transformation. If $\mathcal{F}\{f(x,y)\}=F(f_x,f_y)$ and $\mathcal{F}\{g(x,y)\}=G(f_x,f_y)$, then

$$\mathcal{F}\{f(x,y)\otimes g(x,y)\}=F(f_x,f_y)G(f_x,f_y) \tag{2-10}$$

## 2.2 Holography and digital holography

### 2.2.1 Holography

The basic principle of holography, which record and reconstruct image in 3D, consists of two processes; record and reconstruction. The recording process based oninterference ofthe reflected or transmit wave from obstacle called object wave and the wave which is not reflect from anything called reference wave is shown in Fig. 2.5. To reconstructed hologram, the other reference wave is shined on the recording medium or hologram to see the image which consists of phase and amplitude as shown in Fig. 2.6.

By consider the kind of recording medium, there are two type hologram; static and dynamic hologram. The static hologram use thin medium such as photographic film or image sensor (it will describe in the future topic and called digital holography) to record the interference of object and reference wave or hologram. When image was recorded in static hologram medium, it cannot be changed anyway. Therefore, this called static hologram. By recording hologram in thick medium i.e. photorefractive crystals ($BaTiO_3$, $LiNbO_3$, etc), the hologram in this medium can be changed. Hence, this called dynamic hologram (sometimes called volume hologram). The

dynamic hologram can occur because of the properties of photorefractive material (it will be described in future topic).

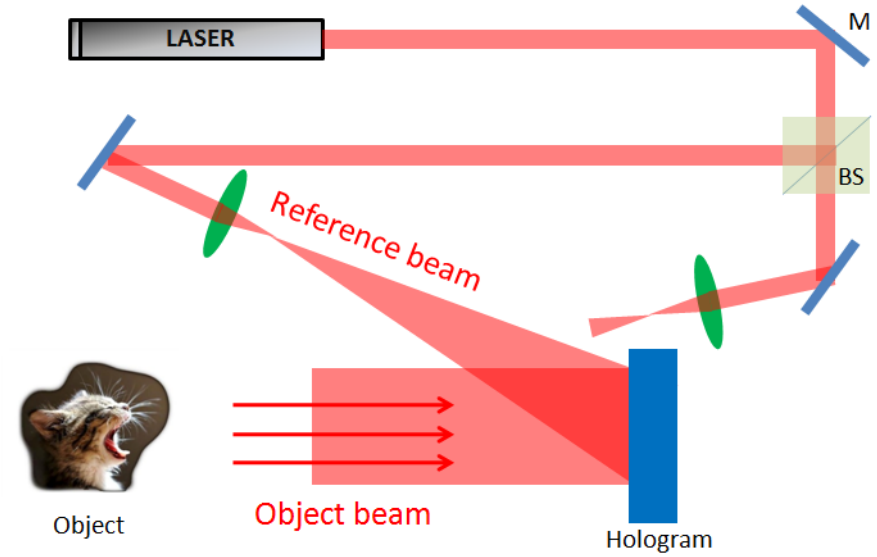


**Figure 2.5** Conventional hologram recording.

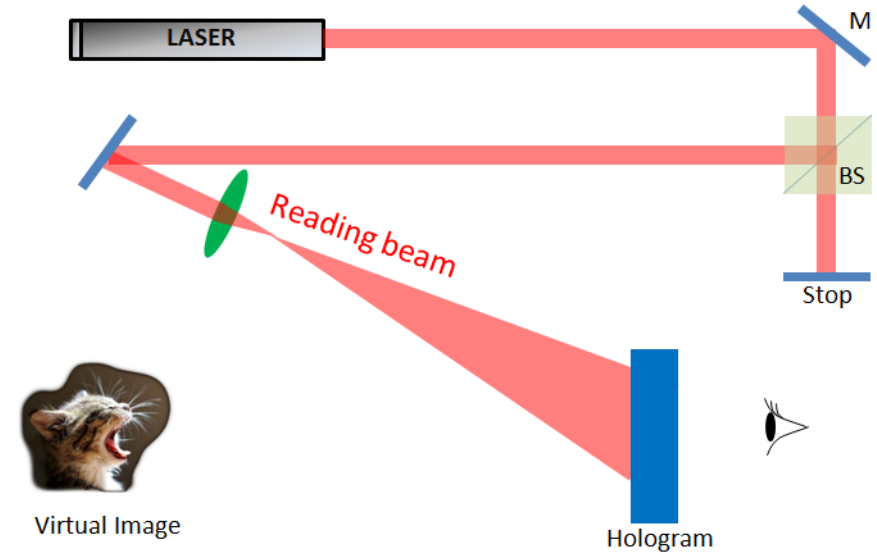


**Figure 2.6** Conventional hologram reconstruction.

### 2.2.2 Holographic term

By following Fig. 2.7(a), suppose that $E_O$ and $E_R$ are illumination of object field and reference field respectively, the intensity of interference field of $E_O$ and $E_R$ recorded on hologram mediumis calculated by

$$\begin{aligned} I &= \left|E_R + E_O\right|^2 \\ &= \left|E_R\right|^2 + \left|E_O\right|^2 + E_R^* E_O + E_R E_O^* \end{aligned} \tag{2-11}$$

where $E_O^*$ and $E_R^*$ are the conjugate pair of object field and reference field respectively. For reconstruction, the reference field $E_R$ (reading beam) illuminated again on the hologram then the transmitted field is

$$\begin{aligned} E &= E_R I \\ &= E_R \left|E_R + E_O\right|^2 \\ &= E_R \left|E_R\right|^2 + E_R \left|E_O\right|^2 + \left|E_R\right|^2 E_O + E_R^2 E_O^* \end{aligned} \tag{2-12}$$

The firsttwo terms represent the nondiffracted wave pass through the hologram calledzero diffraction order. The third term is the reconstructed object wave which forms the virtual image on the same side as the object. The fourth term is the distorted real image generated by spatial varying complex factor $E_R^2$. These last two terms are the complex object field and its conjugate called first order twin image.The hologram term is illustrates in Fig. 2.7(b).

To eliminate the distorted real image, the undistorted real can be generated by using conjugated reference beam $E_R^*$ as describe

$$\begin{aligned} E &= E_R^* I \\ &= E_R^* \left|E_R + E_O\right|^2 \\ &= E_R^* \left|E_R\right|^2 + E_R^* \left|E_O\right|^2 + E_R^{*2} E_O + \left|E_R\right|^2 E_O^* \end{aligned} \tag{2-13}$$

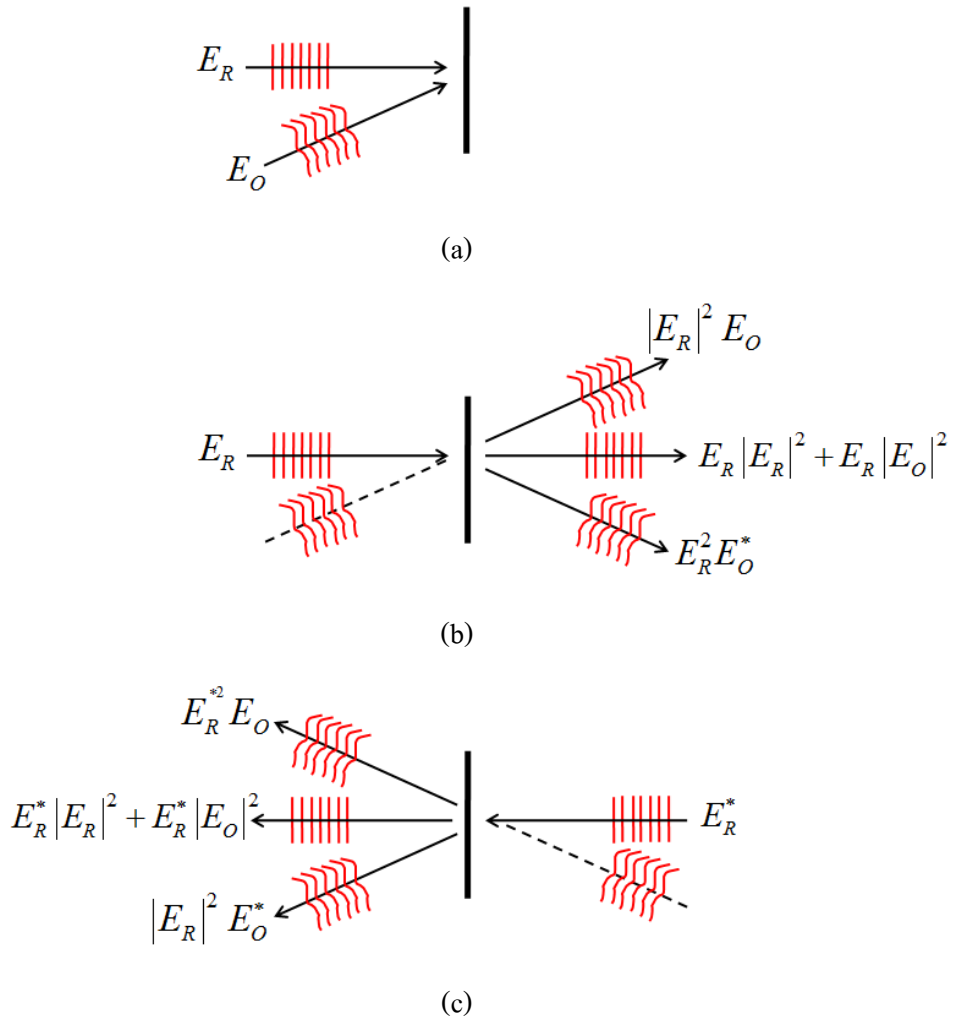


**Figure 2.7** The holographic term; (a) hologram recording, (b) hologram reconstruction with reference wave $E_R$, and (c) hologram reconstruction with conjugate of reference wave $E_R^*$.

### 2.2.3 Digital holography

The concept of digital holography is the recording on anelectronic image sensor, i.e. CCD or CMOS, instead of the conventional one which record on photographic film. By record with electronic devices, the digital hologram profiles are kept in digital files, i.e. JPEG, PNG, TIF etc, which can be opened by digital electronics devices or computers. There are many advantages of the electronic recoding. First, digital recorded holograms have long life time because they are kept in digital storage such as hard disk drive, flash drive, and memory stick, and moreover, the digital image can be duplicated and save in any location or directory. The second advantage, the digital recording use only one recorded sensor, therefore it is not waste the recording medium like

the convention holography which use a film as recording medium. Third, the digital hologram is easier to read than the conventional one. There is not the process called “photographic film development” which acts in dark room. Moreover, digital image can be digitally process (such as scale measurement, brightness and contrast adjustment) by computer.

As shown in Fig. 2.8(a), the light propagated through the object and then recorded on recorded plane. The image recorded on this plane has blur pattern like out of focus image due to the diffraction along propagated distance. After insert the numerical lens instead of recorded media on recorded plane, the image will be focus as shown in Fig. 2.8(b). So this is the regime of digital holography.

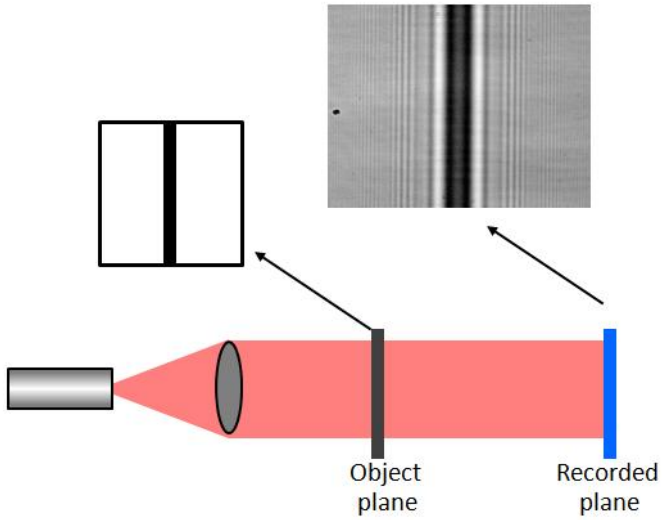


(a)

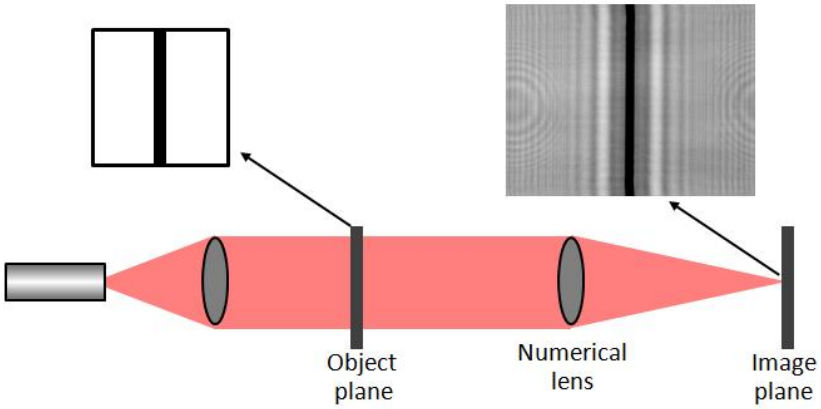


(b)

**Figure 2.8** Concept of digital holography.

### 2.2.4 Methods of reconstruction

#### 2.2.4.1 Huygens convolution method

HCM is the reconstructed method that based on Fresnel diffraction principle and convolution theorem. Suppose that $h(x, y)$ represents the two dimensional diffracted optical field, which propagated along z direction to the recorded plane (hologram plane) as shown in Fig. 2.9. By using Huygens – Fresnel principle [42] which explains the diffraction of light via aperture in rectangular coordinates, the diffracted optical field can be expressed as

$$h(x, y) = \frac{z}{j\lambda} \iint O(\xi, \eta) \frac{\exp(jk\rho)}{\rho^2} d\xi d\eta \tag{2-14}$$

where $O(\xi, \eta)$ is optical field at object plane, $\rho = [z^2 + (x-\xi)^2 + (y-\eta)^2]^{1/2}$ is the distance from any point on object plane $(\xi, \eta)$ to hologram plane $(x, y)$ , z is the propagation distance, and $k = 2\pi / \lambda$ is the wavenumber with the wavelength $\lambda$ . By using the convolution method, the hologram function can be rewritten as

$$h(x, y) = \mathcal{F}^{-1}\{\mathcal{F}[O(\xi, \eta)] \cdot \mathcal{F}[g(\xi, \eta, x, y)]\} \tag{2-15}$$

where the kernel $g(\xi, \eta, x, y)$ is given by

$$g(\xi, \eta, x, y) = \frac{z}{j\lambda} \frac{\exp(jk\rho)}{\rho^2} \tag{2-16}$$

Due to the pixels size of recorded media (CMOS or CCD) is very small when compare with propagated distance, the parameter $\rho^2$ can be reduced to $z^2$ . Thus the kernel is rewritten as

$$g(\xi, \eta, x, y) = \frac{\exp(jk\rho)}{j\lambda z} \tag{2-17}$$

The optical field at the image plane $R(\xi', \eta')$ can be reconstructed by using inverse Fourier transform of filtered Huygens – Fresnel as:

$$R(\xi', \eta') = \mathcal{F}^{-1}\{\mathcal{F}[h(x, y)] \cdot \mathcal{F}[g(\xi, \eta, x, y)]\} \tag{2-18}$$

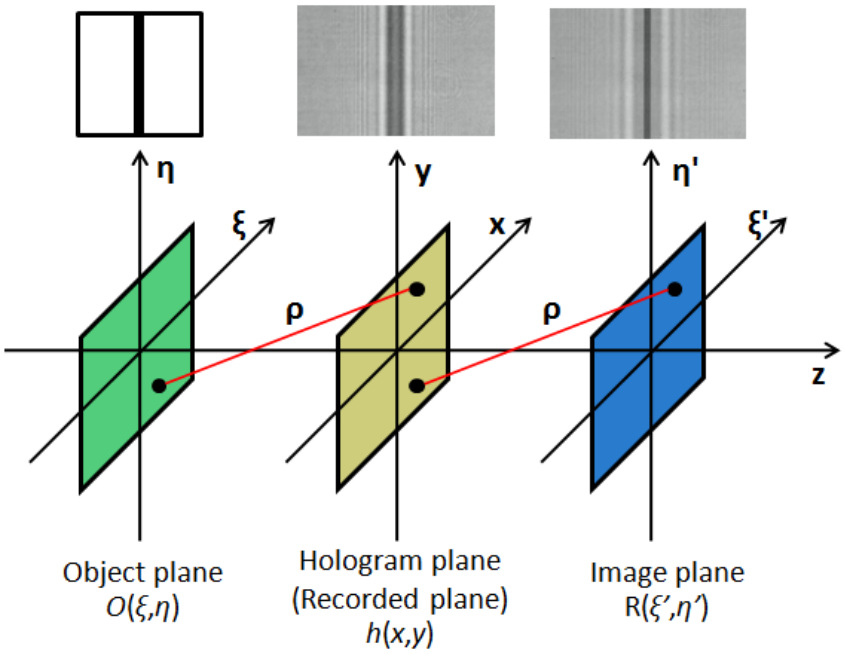


**Figure 2.9** Coordinating systems for numerical reconstruction.

#### 2.2.4.2 Angular spectrum method

ASM, the mathematical technique, is used to describe the optical field of the plane of propagated light and also is used to reconstruct the digital hologram. This method uses Fourier transformation and inverse Fourier transformation to reconstruct digital hologram as the HCM, but it has the advantage in reconstructed distance. ASM can rightly reconstruct the digital hologram in nearer distance when compare with HCM, and will be shown in the next topics.

Suppose that at plane $z=0$ is the object plane $(\xi,\eta)$, as shown Fig. 2.9, the field of object plane $O(\xi,\eta)$ has a two-dimensional Fourier transform that given by

$$\begin{aligned} O'\left(f_\xi, f_\eta; 0\right) &= \mathcal{F}\left\{O\left(\xi,\eta,0\right)\right\} \\ &= \int_{-\infty}^{\infty}\int_{-\infty}^{\infty} O(\xi,\eta,0)\exp[-j2\pi(f_\xi\xi + f_\eta\eta)]d\xi d\eta \end{aligned} \tag{2-19}$$

and the inverse Fourier transform of its angular spectrum can be given by

$$\begin{aligned} O(\xi,\eta,0) &= \mathcal{F}^{-1}\left\{O'\left(f_\xi, f_\eta;0\right)\right\} \\ &= \int_{-\infty}^{\infty}\int_{-\infty}^{\infty} O'(f_\xi, f_\eta;0)\exp[-j2\pi(f_\xi\xi + f_\eta\eta)]df_\xi df_\eta \end{aligned} \tag{2-20}$$

where $f_\xi$ and $f_\eta$ are the components of spatial frequency. By consider as plane wave propagating with direction cosines as illustrated in Fig. 2.10, the component of spatial frequency can be given by

$$\alpha = \lambda f_\xi \;\; \beta = \lambda f_\eta \;\; \gamma = \sqrt{1-\left(\lambda f_\xi\right)^2 - \left(\lambda f_\eta\right)^2} \tag{2-21}$$

Hence, the Eq. 2-19 becomes

$$O'\left(\frac{\alpha}{\lambda},\frac{\beta}{\lambda};0\right) = \int_{-\infty}^{\infty}\int_{-\infty}^{\infty} O(\xi,\eta,0)\exp[-j2\pi(\frac{\alpha}{\lambda}\xi+\frac{\beta}{\lambda}\eta)]d\xi d\eta \tag{2-22}$$

After propagation over distance $z$, the component in exponential will acquire a factor $\exp\left(-j\frac{2\pi}{\lambda}\gamma z\right)$. The angular spectrum of object field can be expressed by

$$\begin{aligned} O'\left(\frac{\alpha}{\lambda},\frac{\beta}{\lambda};z\right) &= \int_{-\infty}^{\infty}\int_{-\infty}^{\infty} O(\xi,\eta,0)\exp[-j2\pi(\frac{\alpha}{\lambda}\xi+\frac{\beta}{\lambda}\eta)]\exp(-j\frac{2\pi}{\lambda}\gamma z)d\xi d\eta \\ &= \mathcal{F}\left\{O(\xi,\eta,0)\exp(-j\frac{2\pi}{\lambda}\gamma z)\right\} \end{aligned} \tag{2-23}$$

And its inverse Fourier transform is

$$\begin{aligned} O(\xi,\eta,z) &= \int_{-\infty}^{\infty}\int_{-\infty}^{\infty} O'(\frac{\alpha}{\lambda},\frac{\beta}{\lambda};0)\exp[-j2\pi(\frac{\alpha}{\lambda}\xi+\frac{\beta}{\lambda}\eta)]\exp(-j\frac{2\pi}{\lambda}\gamma z)d\frac{\alpha}{\lambda}d\frac{\beta}{\lambda} \\ &= \mathcal{F}^{-1}\left\{O'(\frac{\alpha}{\lambda},\frac{\beta}{\lambda};0)\exp(-j\frac{2\pi}{\lambda}\gamma z)\right\} \end{aligned} \tag{2-24}$$

Due to the wave propagate from object plane $(\xi,\eta)$ to hologram plane $(x,y)$ over a distance z , the optical field on hologram plane can be expressed

$$\begin{aligned} h(x,y,z) &= O(\xi,\eta,z) \\ &= \int_{-\infty}^{\infty}\int_{-\infty}^{\infty} O'(\frac{\alpha}{\lambda},\frac{\beta}{\lambda};0)\exp[-j2\pi(\frac{\alpha}{\lambda}\xi+\frac{\beta}{\lambda}\eta)]\exp(-j\frac{2\pi}{\lambda}\gamma z)d\frac{\alpha}{\lambda}d\frac{\beta}{\lambda} \\ &= \mathcal{F}^{-1}\left\{O'(\frac{\alpha}{\lambda},\frac{\beta}{\lambda};0)\exp(-j\frac{2\pi}{\lambda}\gamma z)\right\} \\ &= \mathcal{F}^{-1}\left\{\mathcal{F}\{O(x,y,0)\}\exp(-j\frac{2\pi}{\lambda}\gamma z)\right\} \end{aligned} \tag{2-25}$$

Similarly, the optical field on reconstruction plane $R(\xi',\eta')$ can be written in inverse Fourier transform form of hologram field

$$R(\xi',\eta',z) = \mathcal{F}^{-1}\left\{\mathcal{F}\{h(x,y,0)\}\exp(-j\frac{2\pi}{\lambda}\gamma z)\right\} \tag{2-26}$$

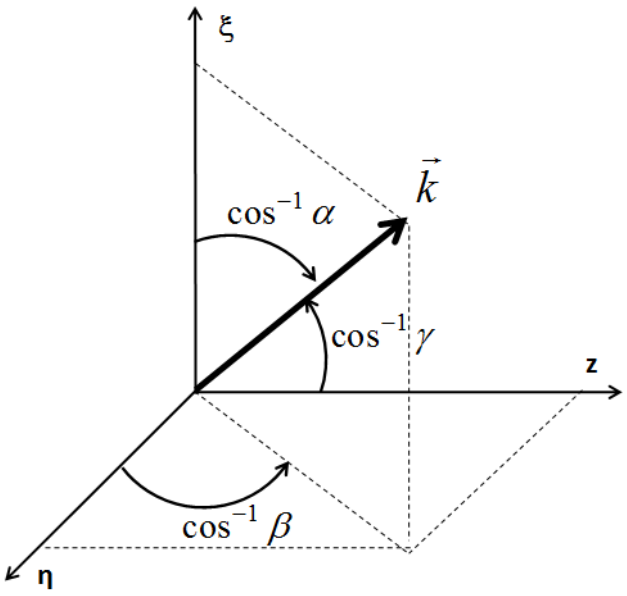


**Figure 2.10** The wave vector $\vec{k}$ .

### 2.2.5 Comparison of methods

Previously, the concepts of reconstruction method were described. In this topic, the reconstructed images of two methods are compared. We will show that the ASM has more advantage than HCM.

#### 2.2.5.1 Simulation of diffraction

We simulate the diffraction pattern of two method which shown in Fig. 2.11. The wave length of light source in this simulation is 635 nm. The distance of diffracted simulation has been varied from 0 mm to 500 mm. The simulated results at each plane are shown in Fig. 2.12. HCM has good simulated diffracted imaged at distance over 150 mm as shown in Fig. 2.12(a). On the other hand, it cannot simulate the diffraction at short distance (less than 150 mm). Moreover, the diffracted simulation of HCM at 0 mm give the over bright image because of $1/z$ factor. By input the distance $z=0$, the intensity of image will increase to infinite value. In contrast to the HCM, ASM can simulate the diffraction with all distance (also include zero) as illustrated in Fig. 2.12(b). The difference between HCM and ASM in Eq. 2-18 and Eq. 2-26 is the replacement of $\mathcal{F}[g(\xi,\eta,x,y)]$ with $\exp(-j\frac{2\pi}{\lambda}\gamma z)$. The ASM has no $1/z$ factor that make the invalid image like HCM, this is the reason that why ASM can simulate the diffraction at all distance.

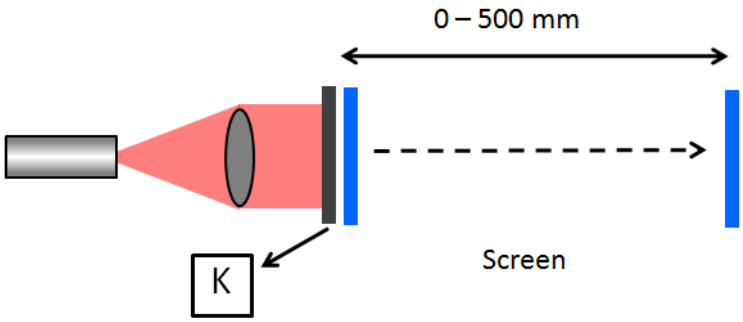


**Figure 2.11** Diagram of the diffracted simulation.

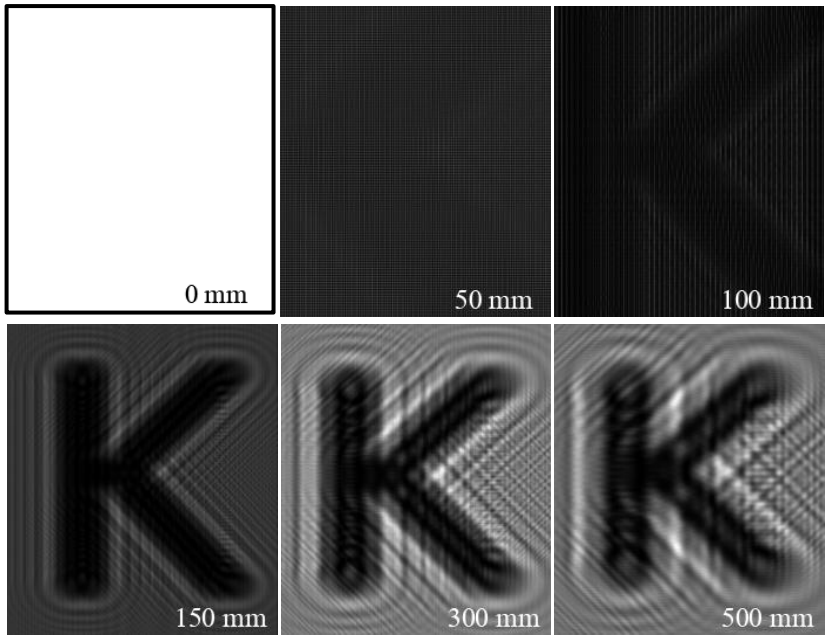


(a)

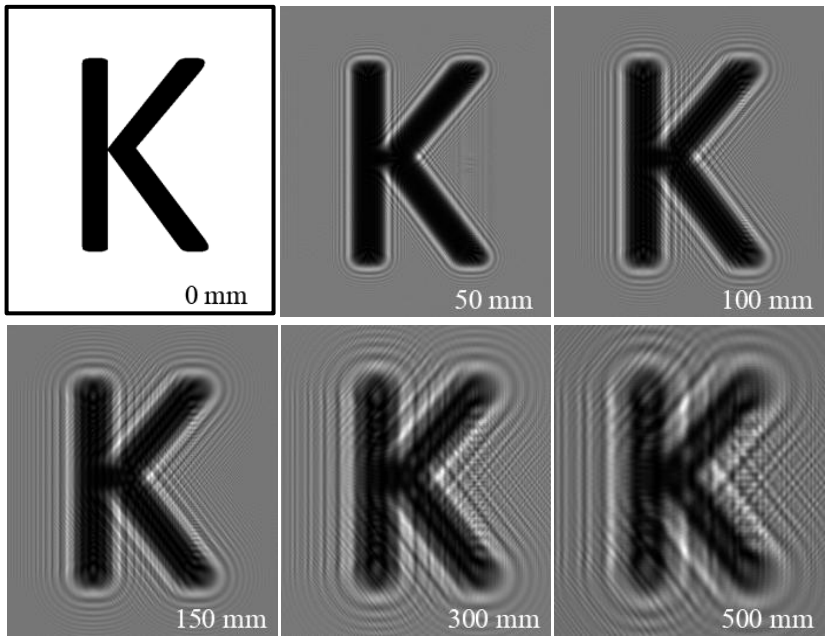


(b)

**Figure 2.12** Diffracted simulation image at each distance of; (a) HCMand (b) ASM.

#### 2.2.5.2 Reconstruction

The diagram of experimental setup for comparing the reconstruction method has been shown in Fig. 2.13. The collimated beam with wavelength of 635 nm has been shined through the letter "K" and then recorded on CMOS. The recording distance has been varied from 50 mm to 500 mm (50 mm, 100 mm, 150 mm, 300 mm, and 500 mm). The recorded digital holograms are shown in

Fig. 2.14(a). Figure 2.14(b) shows the reconstructed image at each distance of HCM. The recorded images at distance below 150 mm cannot be completely reconstructed. This mean the HCM has limitation to reconstruct image at near distance. On the other hand, the ASM can reconstruct at all distance without any limitation as shown in Fig. 2.14(c).

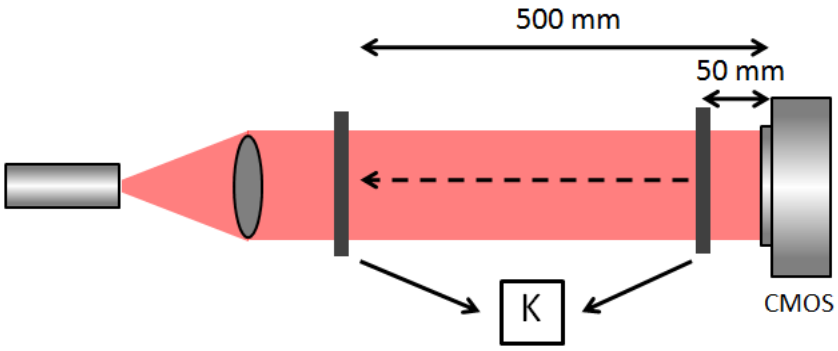


**Figure 2.13** Diagram of experimental setup for comparing the reconstruction method.

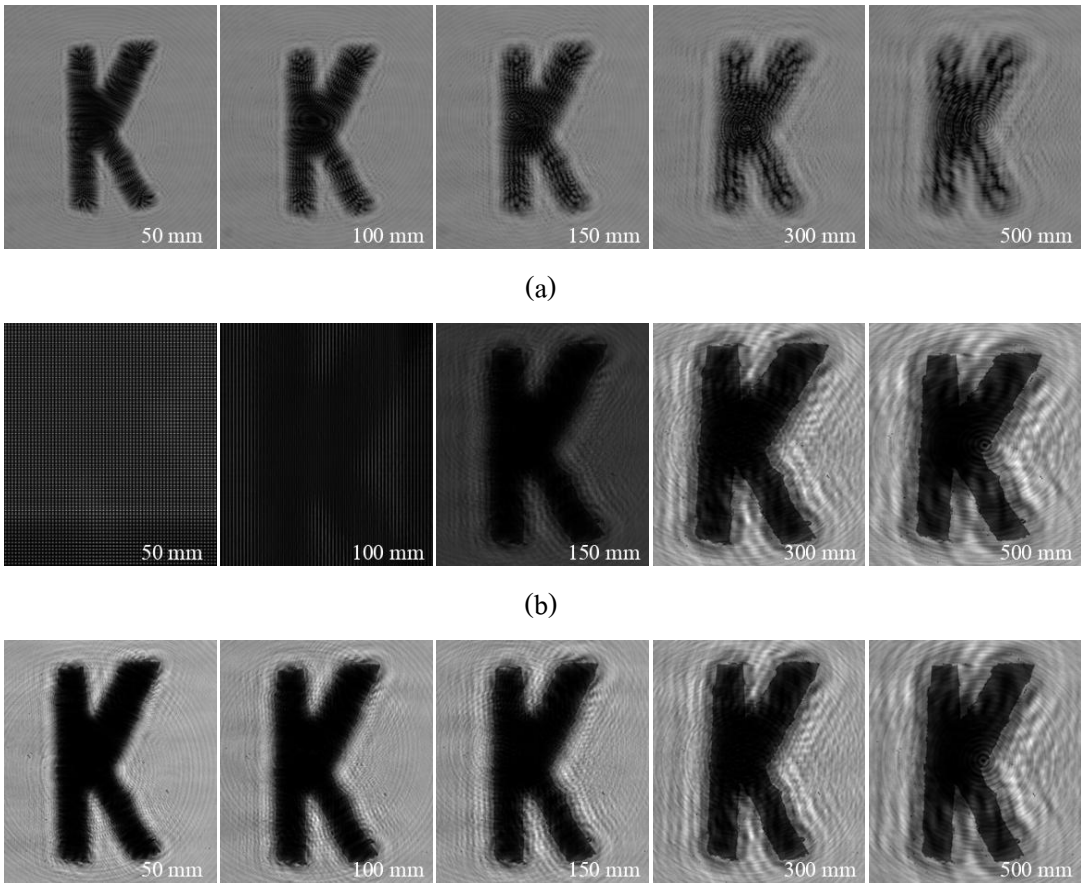


**Figure 2.14** The set of digital hologram; (a) recorded images, (b) reconstructed images with HCM, and (c) reconstructed images with ASM.

From the results of reconstruction, the ASM has more advantage than HCM; therefore ASM has been used to reconstruct digital hologram in this thesis. A schematic flow chart diagram of the digital hologram reconstructed process is shown in Fig. 2.15. There are three mainly step processes in this digital hologram reconstructed algorithm. First, compute the Fast Fourier Transformation (FFT) of hologram (FFT is the one function in MATLAB® program), then multiply the results from FFT by kernel $g(z) = \exp\left(-j\frac{2\pi}{\lambda}\gamma z\right)$. Last, the reconstructed digital hologram is obtained by computing with Inverse Fast Fourier Transformation (IFFT) of the multiplied result.

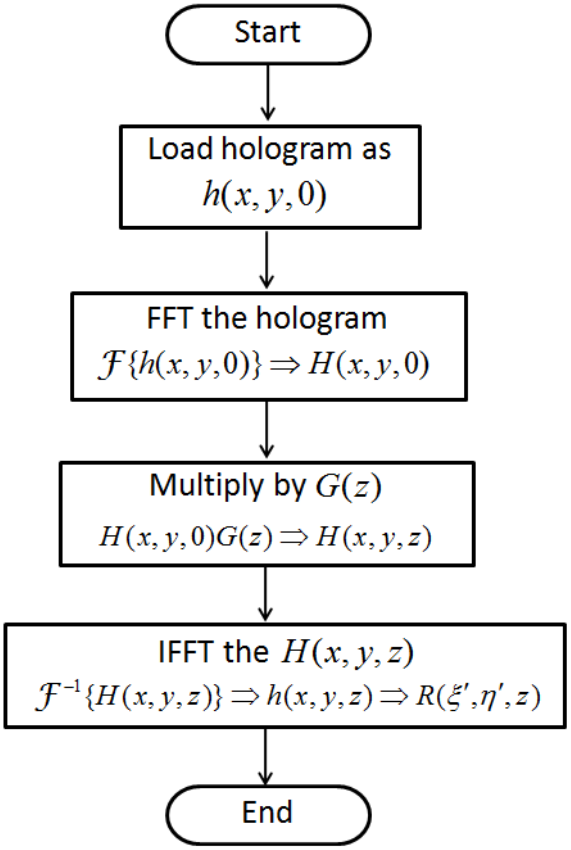


**Figure 2.15** The flow chart of reconstruction algorithm.

## 2.3 Digital holography configurations

As describe in chapter 1, there are two mainly configurations of digital holography, off axis and in-line configuration.

### 2.3.1 Digital off-axis holography (DOH) configuration

As shown in Fig. 2.16, the off axis configuration,the reference and object wave are interfere with angle $\theta$. The maximum angle $\theta_{max}$ can be calculated by (W. Jueptner, chapter 3, 2005)[43]

$$\theta_{max} = 2\arcsin\left(\frac{\lambda}{4\Delta x}\right) \approx \frac{\lambda}{2\Delta x} \tag{2-27}$$

where $\lambda$ and $\Delta x$ are wavelength of recording light and resolution of recording medium. The angle $\theta$ in this configuration can be up to 180 degree by using photographic film as the recording medium with the resolution $\Delta x$ up to 0.2 µm. However, the maximum resolution of imaging sensor (CCD or CMOS) is in order of 5 µm. Therefore, the maximum angle in this case (the wavelength of light source in this thesis is 635 nm) is about 3.6 degree.

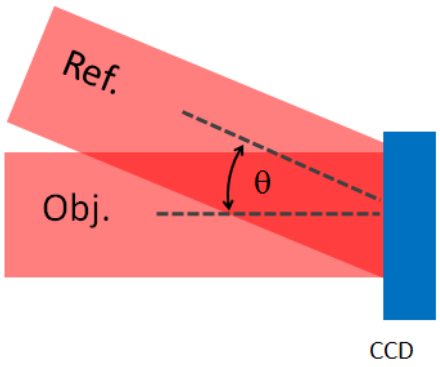


**Figure 2.16** Off axis configuration.

### 2.3.2 Digital in-line holography (DIH) configuration

The recording angle of digital holography is factually close to 0 degree and called in-line configuration as shows in Fig. 2.17. Moreover, there are the other one configuration called Gabor configuration, which is invented by D. Gabor, who the first invent holography technique. As shown in Fig 2.18 the light illuminate to obstacle and there are two consider wave this configuration. First, the light diffract at the edge of obstacle called object wave. Second, the other

part of light that not scatter on obstacle called reference wave. These two waves interfere on sensorlike the other configurations. However, in this thesis called Gabor configuration as in-line configuration because most of research call this configuration as in-line [7-12].

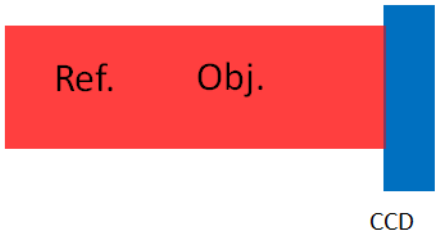


**Figure 2.17** In-line configuration.

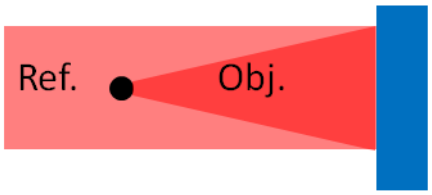


**Figure 2.18** Gabor configuration

Figure 2.19 shows the multi plane in-line configuration. The collimate light illuminate through five letters (K, M, I, T, and L) which place difference plane by 100 mm. Figure 2.20 shows record image which very poor pattern (a lot of diffraction pattern, out of focus image). The numerical reconstruction at distance 150 mmgive first letter which place nearest the sensor, K, is focus as shown in Fig. 2.21 (a). Then reconstructed image at distance 250 mm, 350 mm, 450 mm, 550mmthe MITL will be focus simultaneously as shown in Fig 2.21 (b), (c), (d), and (e).

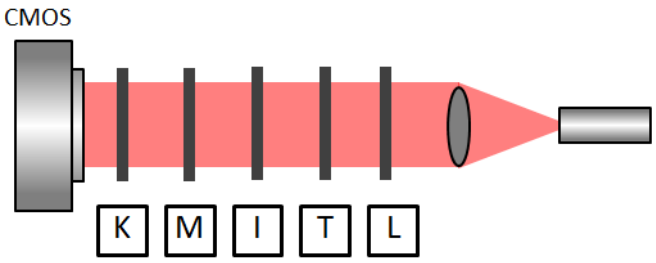


**Figure 2.19** Multi plane DIH configuration.

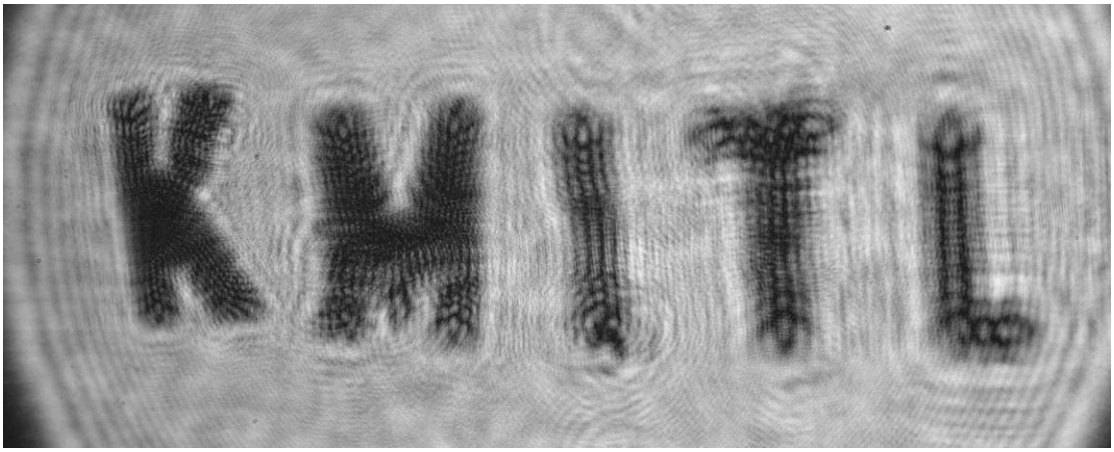


**Figure 2.20** Recorded digital hologram

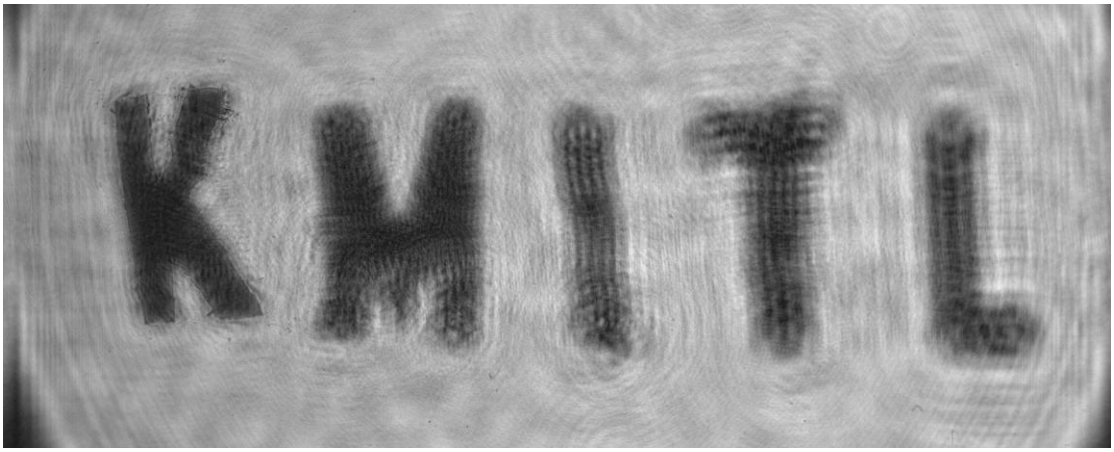


(a)

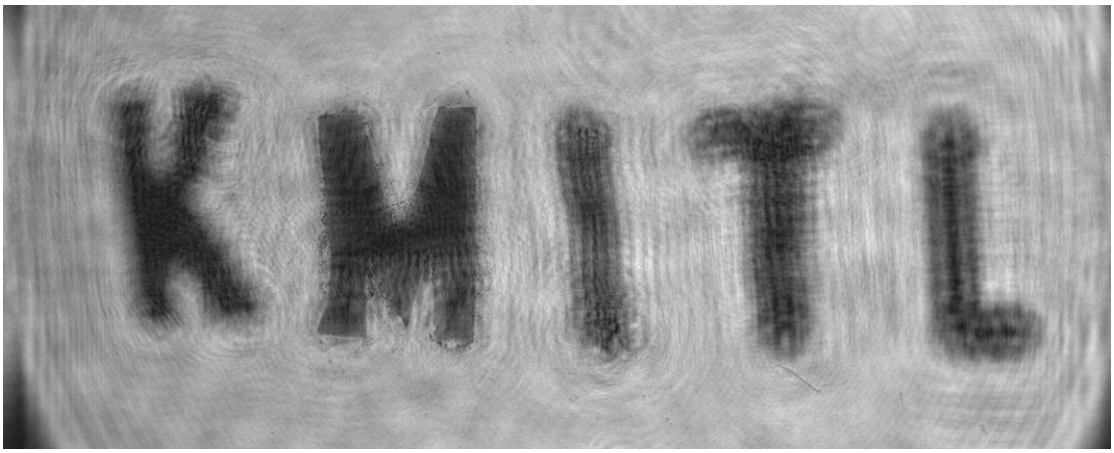


(b)

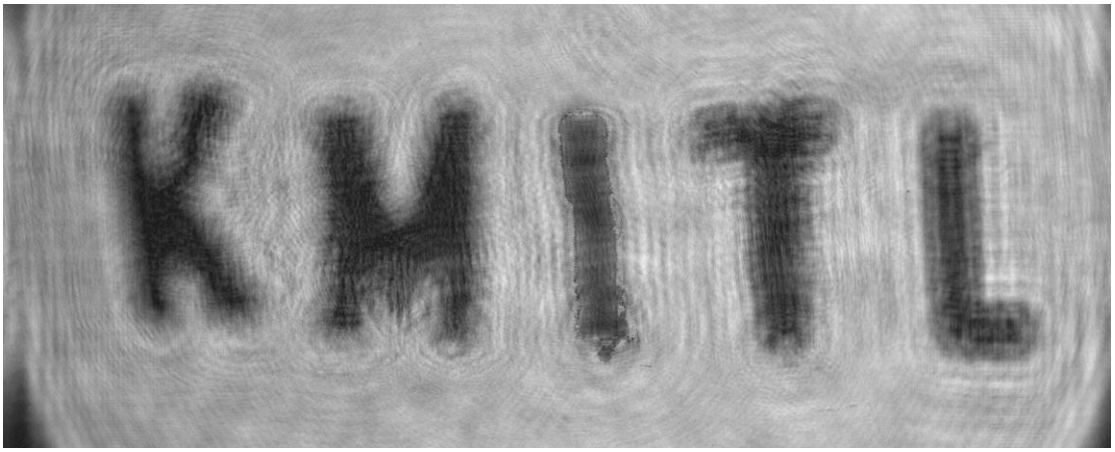


(c)

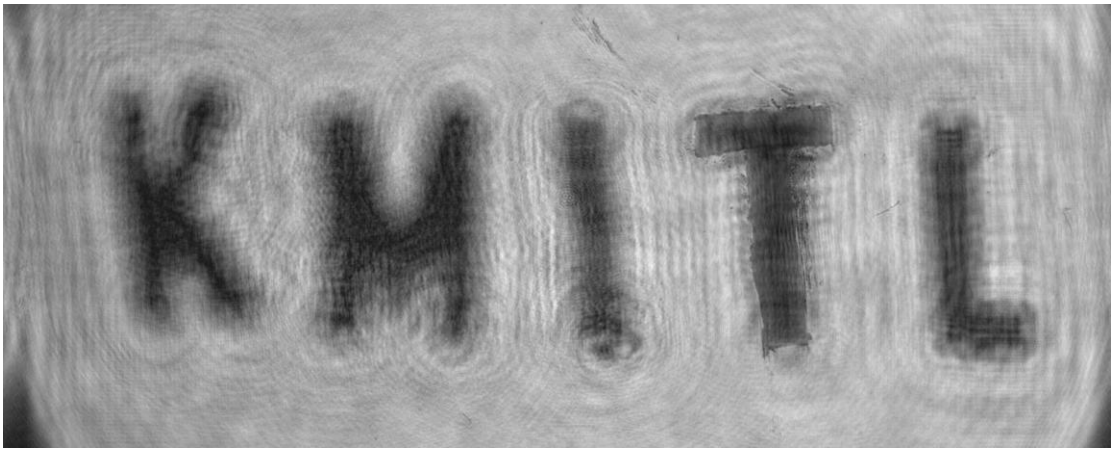


(d)

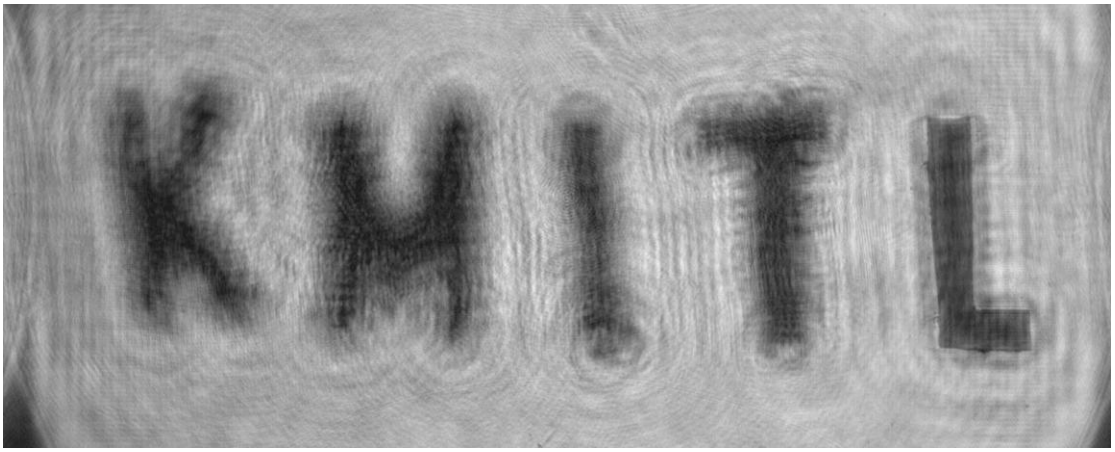


(e)

**Figure 2.21** Reconstructed digital hologram; (a) at plane z = 150 mm, (b) at plane z = 250 mm, (c) at plane z = 350 mm, (d) at plane z = 450 mm, and (e) at plane z = 550 mm.

## 2.4 Photorefractive nonlinear optics

Generally, the refractive index of medium depends on the arrangement and distribution of atoms and electrons. In linear optics, the index of refraction of medium is depending on the wavelength of the incident light but it independent with the intensity of light beam.This occurs because the electric field of the light beam is smaller compare with the intra-atomic electric field. Perversely, the index of refraction is dependent with the intensity of light, if the electric field is comparable with the intra-atomic electric field. This is the concept of nonlinear optics.

### 2.4.1 Photorefractive effect

Photorefractive effect is the one phenomenon of nonlinear optics that the index of refraction can be changed by the spatial variable of intensity of light. This phenomenon can be explained by band transport model as illustrated in Fig. 2.22. Thephotorefractive crystals, i.e. $LiNbO_3$, $BaTiO_3$, SBN, and BSO, normally have donor band and acceptor band between valence band and conduction band due to the impurities in the crystal. When the electrons in donor band is excited by incoming light, they will ionized to conduction band and leaving the empty state behind. Therefore they can be trapped again by donor band. The rate equation for the density of donor ionization can be express as

$$\frac{\partial N_D^i}{\partial t} = sI(N_D - N_D^i) - \gamma_R N N_D^i \tag{2-28}$$

where $s$ is cross section for photo-excitation, $I$ is light intensity, $N_D$ and $N_D^i$ are density of donor impurity and ionization, $\gamma_R$ is electron-ionized trap recombination rate, and $N$ is electron density. The first term describe the rate of electron generation which is depended the intensity of light, whereas the second term is the rate of trap capture.Because he electron density may be affected by electron transport insidephotorefractive crystal, the rate equation for electron density $N_D$ and $N_D^i$ has been concerned and defined as

$$\frac{\partial N}{\partial t} - \frac{\partial N_D^i}{\partial t} = \frac{1}{q}\nabla \cdot \vec{J} \tag{2-29}$$

where $q$ is the electron and $\vec{J}$ is current density which defined by the consists of contributions from the drift of charge carrier due to the electric field and the diffusion due to the gradient of carrier density as Eq. (2-30)

$$\vec{J} = qN\mu\vec{E} + k_B T\mu\nabla N \tag{2-30}$$

where $\mu$, $\vec{E}$, and $k_b T$ are the mobility tensor, electric field, and the product of the Boltzmann constant and temperature respectively. By following Poisson equation, the electric field can be written as

$$\begin{aligned} \nabla \cdot \varepsilon\vec{E} &= \rho(\vec{r}) \\ &= -q(N + N_A - N_D^i) \end{aligned} \tag{2-31}$$

where $\varepsilon$, $\rho(\vec{r})$, and $N_A$ are dielectric tensor charge density, acceptor impurity density respectively. The Eq. (2-28) – (2-31) have been called Kukhtarev's equation.

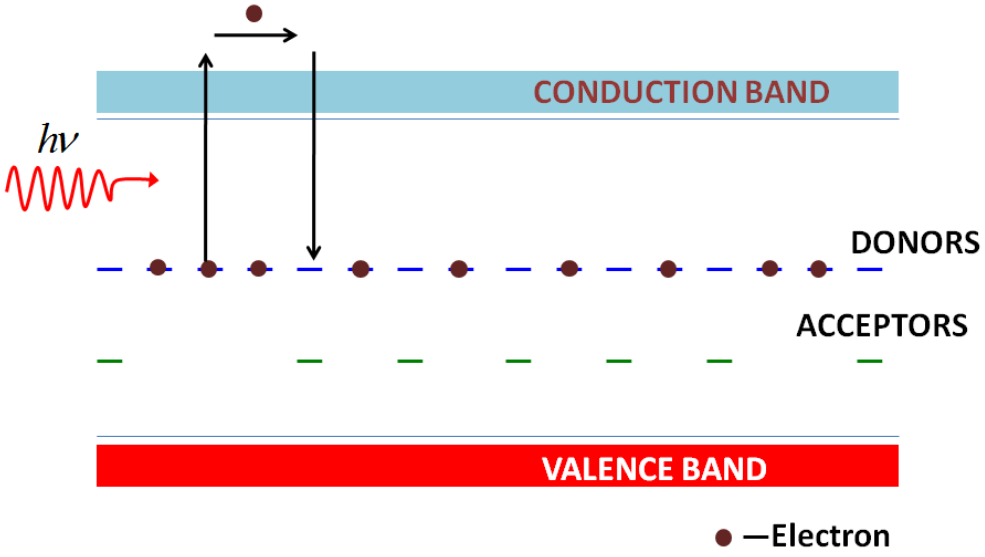


**Figure 2.22** Band transport model.

Under the non-homogeneous illumination, the electrons density in this area is not uniform too. As shown in Fig. 2.23, the electrons, which migrate from the bright area to dark area, affect the electron density in bright area is lower than the electron in dark area. Therefore, the refractive index under bright illumination is lower than dark illumination.

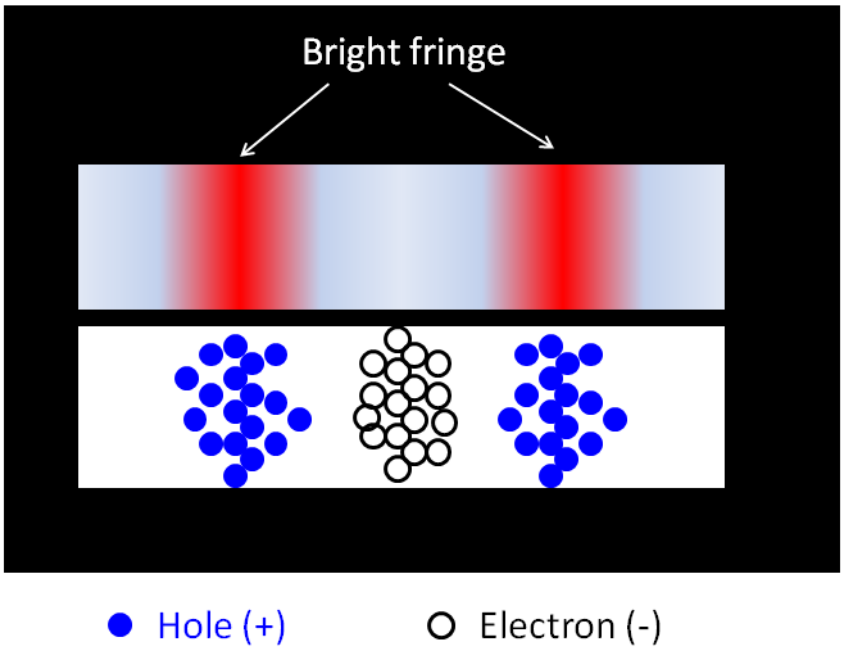


**Figure 2.23** The distribution of charge under illuminating region.

### 2.4.2 Anisotropic self-diffraction (ASD)

Anisotropic self-diffraction is the phenomena in photorefractive effect that the transmitted wave diffracted by itself and changed polarization perpendicular to incident wave. The period of photorefractive grating which generated by the interference of incident wave can be explained by Fig. 2.24 and calculated by

$$\Lambda = \frac{\lambda}{2\sin\theta_i} \tag{2-32}$$

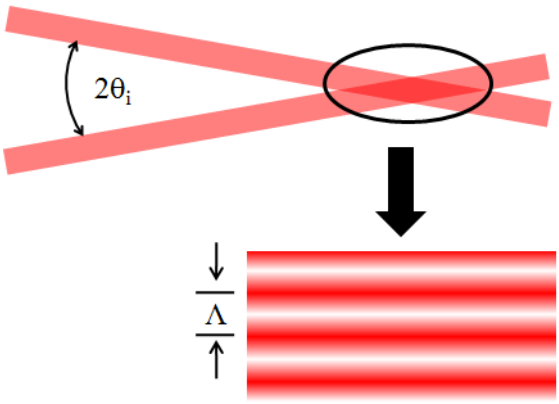


**Figure 2.24** The interference fringe from two incident beam with angle $2\theta_i$ .

In an anisotropic bulk crystal, the phase matching conditions need to be satisfied to create the anisotropic self diffraction. As shown in Fig. 2.25, the optical axis is in the direction parallel to the plane of incident. $K_{e1}$ and $K_{e2}$ are the wave vectors of two writing beams with extraordinary polarization. $K_{o1}$ and $K_{o2}$ are the wave vectors of diffracted beams with direction of polarization perpendicular to c-axis(ordinary polarization). Thus, the grating wave vector, $K_g$, can be defined by

$$K_g = K_{e2} - K_{e1} \tag{2-33}$$

Now, the wave vectors of the diffracted higher order beams can be written as

$$K_{o1} = K_{e1} - K_g \tag{2-34}$$

$$K_{o2} = K_{e2} - K_g \tag{2-35}$$

The incident angle outside crystal can be expressed as [35]

$$\theta_{io} = \sin^{-1}\left[\left(\frac{n_o^2 - n_e^2}{8}\right)^{1/2}\right] \tag{2-36}$$

where $n_o$ is the ordinary refractive index and the $n_e$ is extraordinary refractive index of the crystal. Furthermore, under Bragg condition as shown in Figure 2.25, the incident light $K_{e1}$ and $K_{e2}$ (the zero order beams) not only construct the grating $K_g$ but also couple to first order beams, $K_{o1}$ and $K_{o2}$, respectively. This is the regime of anisotropic self- diffraction.

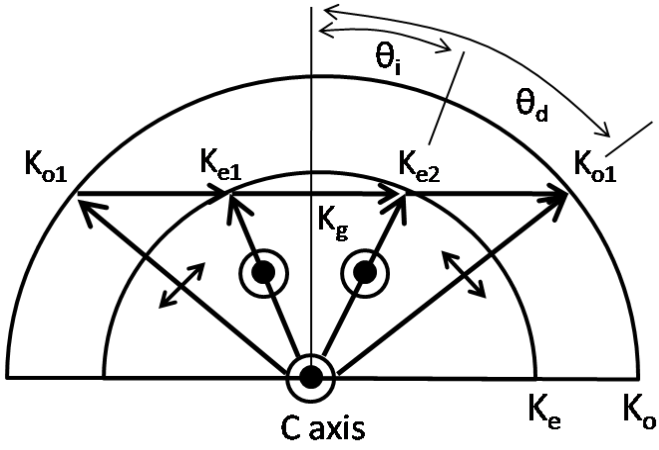


**Figure 2.25** Wave vector diagram of anisotropic self-diffraction.

# CHAPTER 3

# FINGERPRINT MOISTURE INVESTIGATION

As describe in chapter 1, generally, total internal reflection (TIR) was the concept of optical fingerprint scanner. Due to the scatter and diffraction of light at the edge of the ridge of fingerprint, there were some researches try to improve the quality of fingerprint. For example, to eliminate the distorting pattern, they resolve the problem by use focusing lens, the holographic plate, and digital holography. In fact, the diffraction of light at the edge of pattern is easily resolved by using digital holography technique. This technique can reduce the dimension of the system when compare with the technique that use focusing lens. In this thesis, the TIR and DIH technique have been combined to record fingerprint and called TIRDIH. The total internal reflected light with diffract at the edge of the ridge of fingerprint interfere with nondiffracted from the valley of fingerprint. This is the concept of TIRDIH that use to record fingerprint in this thesis. The detail of this technique will be described in the next topic. However, the moisture can directly affect to the fingerprint patterns which are obtained by optical technique. Therefore the TIRDIH has been applied to investigate the moisture on fingerprint.

## 3.1 Optical fingerprint scanner

The concept of conventional optical fingerprint scanner has been shown in Fig 3.1. The light propagates into prism and incident at the side that finger place on. There are two areas obtained pattern in fingerprint imaging based on TIR. First, the light undergo with total internal reflection from the valley of fingerprint provide bright pattern Second, the other light scatter at the ridge of fingerprint provide the dark pattern.

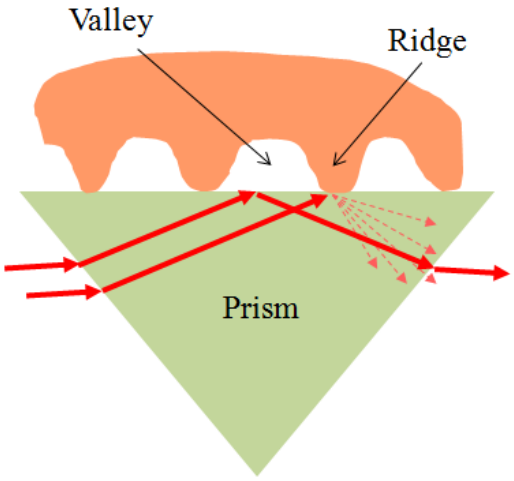


**Figure 3.1** Concept of optical fingerprint scanner.

## 3.2 TDIH and RDIH configuration

Following the DIH configuration as described in chapter 2, the system record the transmitted light which consists of the interference of object and reference wave, so it is called transmitted digital in-line holography (TDIH). However, this configuration has limitation to apply with opaque medium such as fingerprint. Hence, the reflected digital in-line holography has been developed to record the opaque object.

In experimental setup in this thesis (chapter 2 - 5), the laser diode (LDM115G/633/1, 1 mW, 635 nm) has been used as the light source for recording digital hologram, because it is lower cost and smaller size when compare with the other type of laser. Moreover, due to the compact size of laser diode, it may be easy to assemble as a prototype of compacted nondestructive testing instrument using digital holography in the future. A plano convex lens with focal length of 175 mm and diameter of 25.4 mm has been used as the expanded and collimated lens laser. Furthermore, all of the digital holograms were recorded with CMOS camera (Canon EOS 350D, Japan, 3456 x 2304 pixels, and 6.41 μm pixel pitch).

In this topic, the RDIH configuration has been verified that it can use instead of TDIH configuration with the same results. Figure 3.2 shows the experimental setup of TDIH configuration. An expanded beam propagates through the positive pattern test target. Then, it is

separated into two beams, i.e. object and reference beams, by thin opaque line of the target. The object beam is diffracted by the object pattern; the other one is a reference beam, since it just transmitted through the target without any distortion. The holographic interference pattern is obtained by the superposition of these two beams and then recorded on CMOS camera.

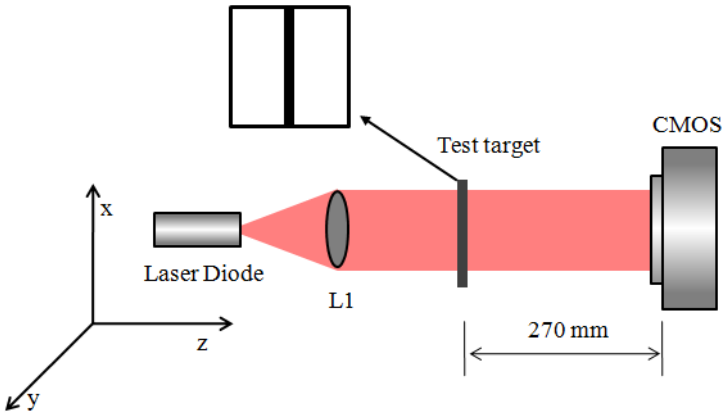


**Figure 3.2** Experimental setup for recording resolution test target by TDIH configuration.

The concept of RDIH is illustrated in Fig. 3.3. The expanded beam is incident on the target, which has thin opaque line and then reflects back due to the polished surface. There are two different beams reflected at this surface. The first one reflects with diffraction at the edge of the opaque pattern; the other one reflects on the clear surface of the target without any diffraction. The interference of these two beams was recorded on CMOS camera and then was numerical reconstructed as the same way in basic DIH.

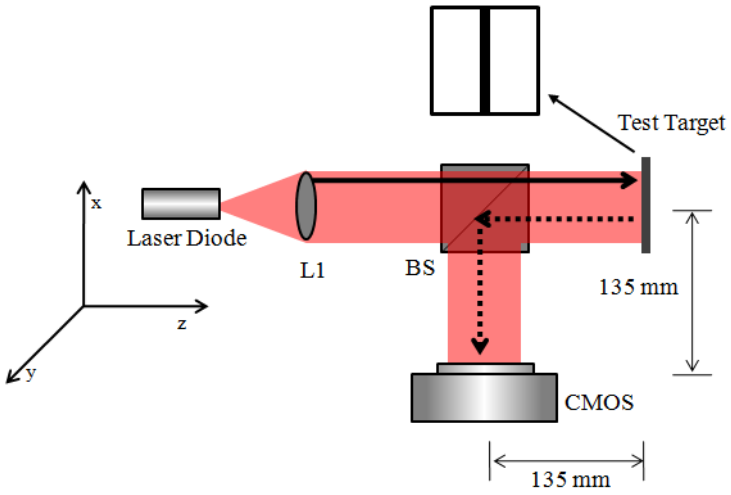


**Figure 3.3** Experimental setup for recording resolution test target by RDIH configuration.

### 3.2.1 Experimental results of test target hologram

The experimental results of TDIH and RDIH have been shown in Fig. 3.4 and 3.5. Figure 3.4(a) shows the transmitted hologram, which was recorded in the experimental setup from Fig. 3.2. The image recorded on CMOS plane appears as defocused pattern. The numerical reconstruction of Fig. 3.4(a) at the plane of z = 270 mm from CMOS is shown in Fig. 3.4(b). At this plane, the pattern of test target is focused. The transverse intensity profile of Fig. 3.4(b) is illustrated in Fig. 3.4(c). The cross section plot have been found corresponding to the standard value of the width of resolution test target (200 μm).

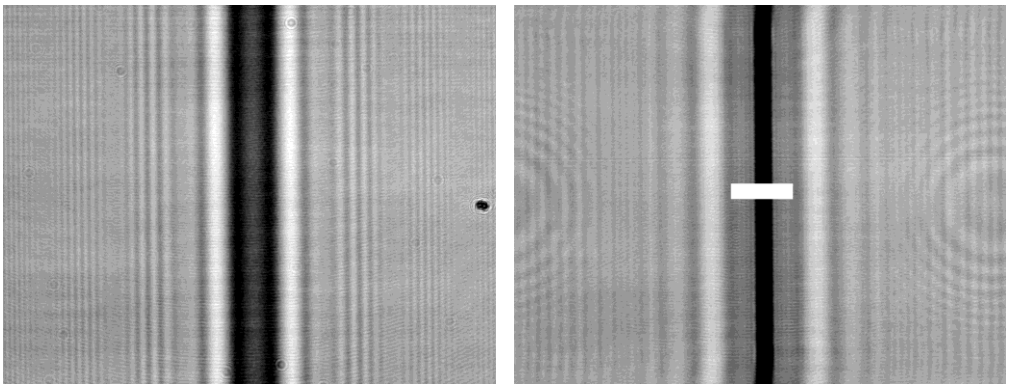

(a) (b)

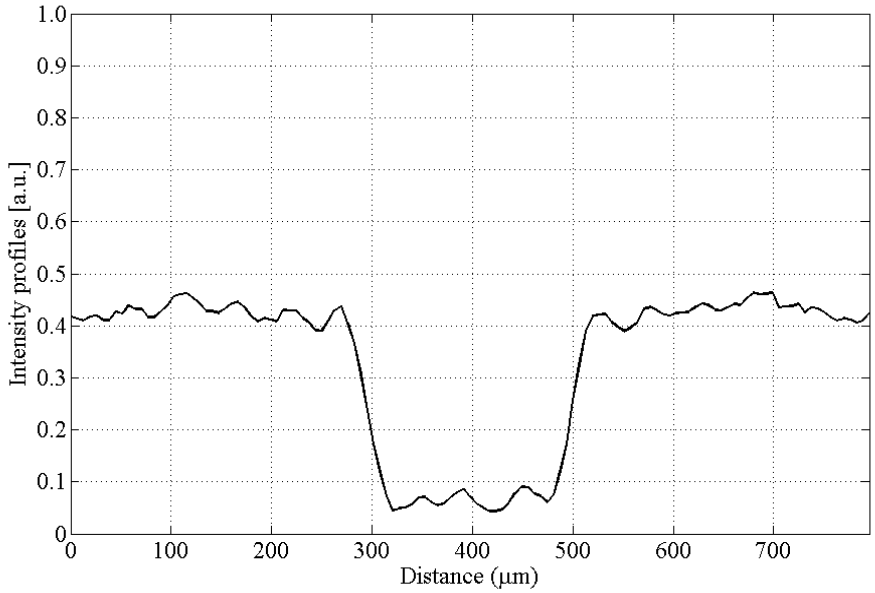


(c)

**Figure 3.4** Hologram and its profile from TDIH: (a) recorded hologram, (b) reconstructed hologram, and (c) transverse intensity profile of (b).

Figure 3.5(a) – (c) represent the recorded hologram pattern, reconstructed hologram pattern, and its transverse intensity profile of RDIH configuration. From our RDIH results, the image can be reconstructed as in the case of TDIH. The pattern of test target is focused at the plane of z = 270 mm as in TDIH case. Moreover, the pattern width is the same as TDIH case.

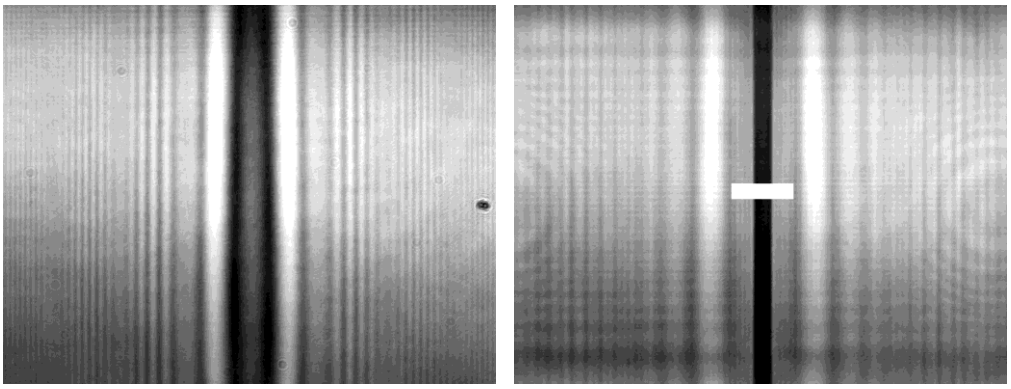

(a) (b)

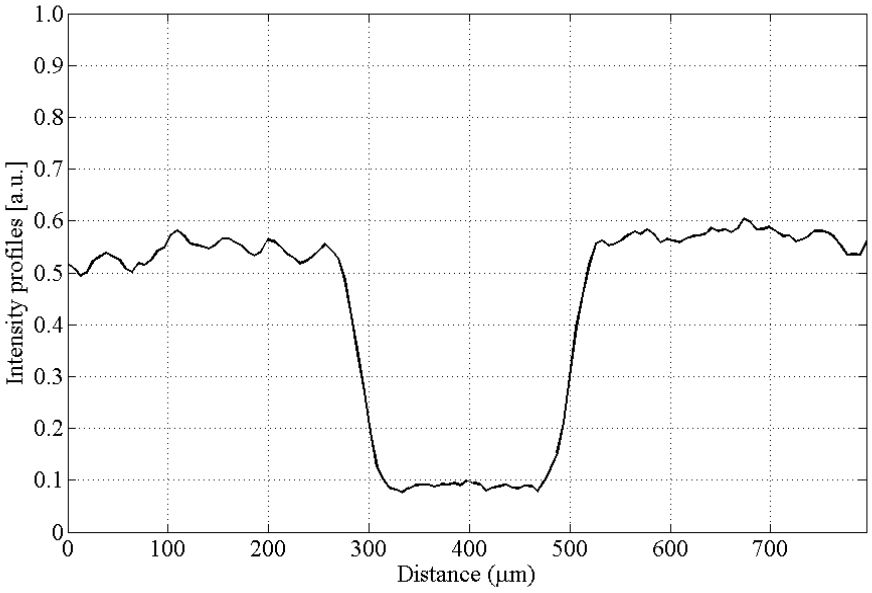


(c)

**Figure 3.5** Hologram and its profile from RDIH: (a) recorded hologram, (b) reconstructed hologram, and (c) transverse intensity profile of (b).

## 3.3 Experimental setup for investigating moisture effect in optical fingerprint scanner using TIRDIH

From the previous topic, the reflected light from fingerprint actually consists of diffraction from the edge of the ridge and valley of it, and RDIH configuration verified that it can record and reconstruct the hologram of opaque object. By combining the TIR and RDIH, the experimental setup of TIRDIH configuration is shown in Fig 3.6. The expanded beam from laser diode incident on equilateral glass prism (N-BK7 with refractive index: n=1.52) with angle $\theta_{io}$. The refracted beam transmits through the prism and then reflects at the boundary between the prism and air with angle $\theta_{ii}$. In the experiment, the TIR between the boundary of the prism and air was obtained when $\theta_{io}$ is equal to 29.0 degree, (i.e. $\theta_{ii}$ = 41.14 degree). Then, the interference patterns of various moistures of fingerprints were recorded with CMOS camera.

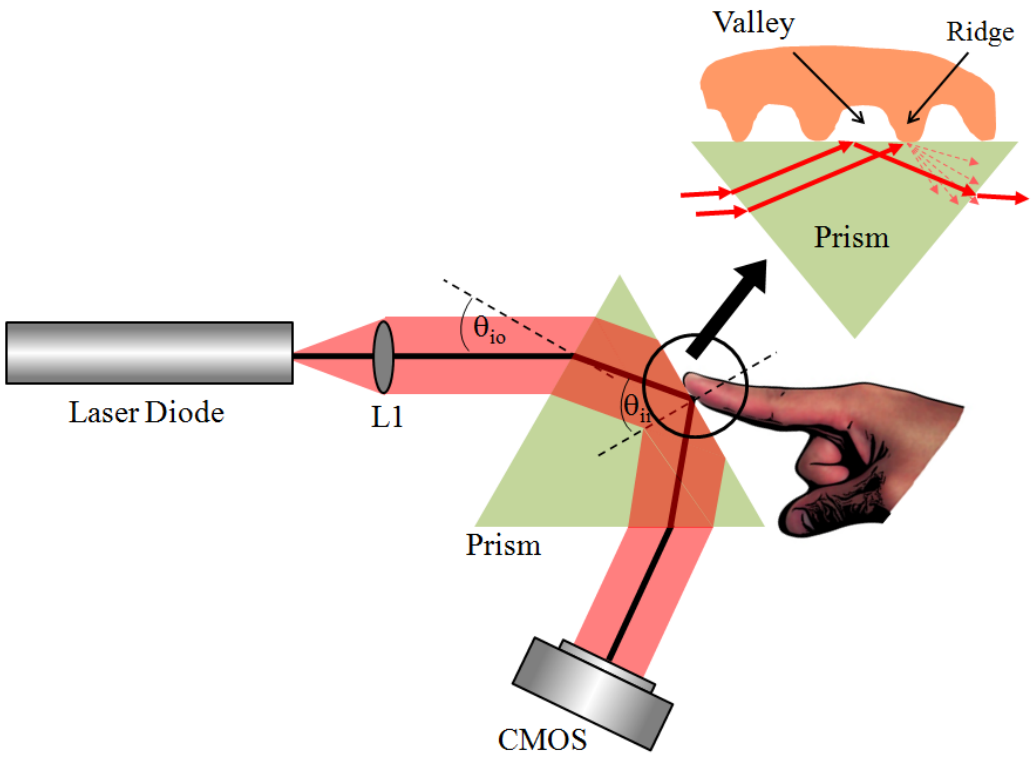


**Figure 3.6** The schematic of digital holographic fingerprint scanner using TIRDIH.

Four samples of different moistures of fingerprint, i.e. 39%, 54%, 69% and soak fingerprint were used in the experiment. Since the maximum measurable range of the skin moisture checker (Scalar model MY808s, Japan) is only about 70%, so 69% of moisture was used as the highest one to avoid the saturated value of the instrument.

### 3.3.1 Experimental results of fingerprint hologram

The hologram pattern of fingerprint with moisture of 54.0% and its best numerical reconstructed image are shown in Fig. 3.7 (a) and 3.7 (c), respectively. The reconstructed image is in better profile than the recorded image. Figure 3.7(b) – 3.7(e) represent the best reconstructed fingerprint hologram of different moistures. From our observation, the image of fingerprint with moisture of 39.0% [Fig. 3.7(b)] is incomplete because the ridge of the fingerprint is not completely close to glass prism. In fact, there are small ridges and valleys in the ridge of fingerprint as illustrated in Fig. 3.9. The small ridges of fingerprint with low moisture can well reflect the light, so the image of ridge has bright pattern due to the air gap between the ridges and the prism (From the optical fingerprint scanner concept, they should actually provide the dark pattern). When the fingerprint had enough moisture for coupling the fingerprint with prism, the fingerprint pattern image would be perfected as illustrated in Fig. 3.7(c). We observed that the ridge of fingerprint as the dark patterns is obtained from the scattering of light and the valley of fingerprint as the bright patterns is obtained from the TIR of light inside prism as described in topic 3.1. However, the fingerprint with too much moisture may give the worse image pattern as shown in Fig. 3.7(d). Since, the gaps between fingerprint valleys and prism are full of moisture, the TIR cannot be occurred. Therefore, the ridge patterns still occurred while the valley patterns were darker than the image of fingerprint with moisture of 54.0%. The wet fingerprint gives the worst pattern because there is a lot of water between fingerprint and prism. In this case, the ridge and valley of fingerprint cannot be distinguished as presented in Fig. 3.7(e). Moreover, the intensity of image will be decreased when the moisture of fingerprint increase. The transverse intensity profile of fingerprint pattern from Fig. 3.7(c) is shown in Fig. 3.8. The width of fingerprint had been measured and it is about 150 μm.

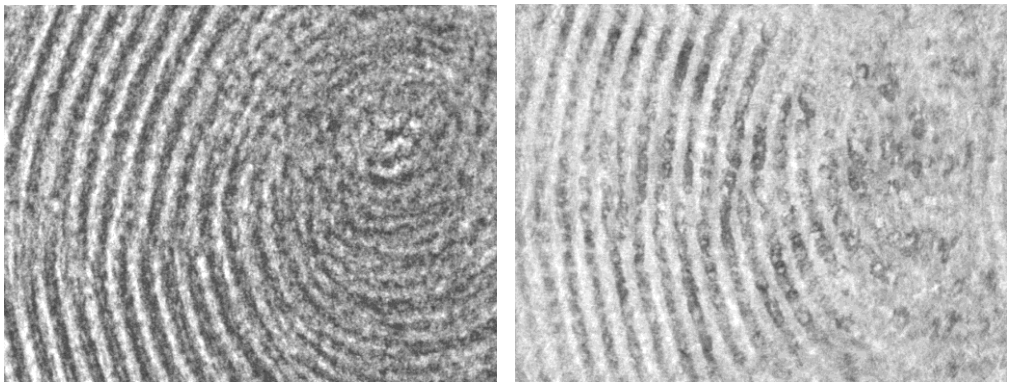

(a) (b)

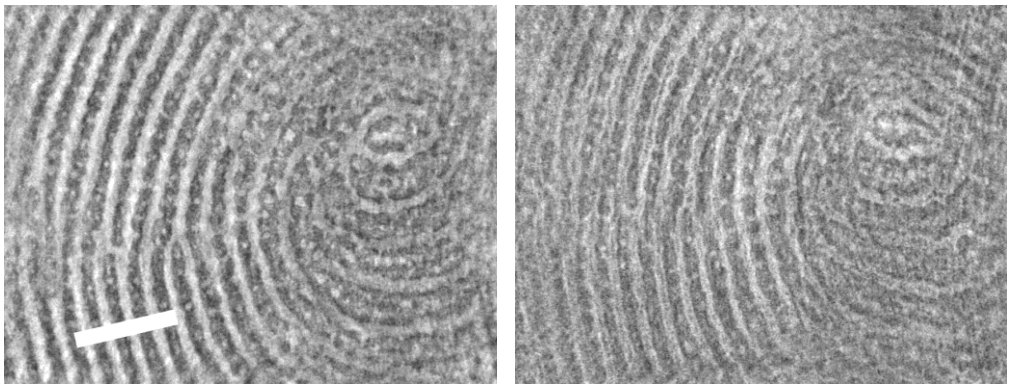

(c) (d)

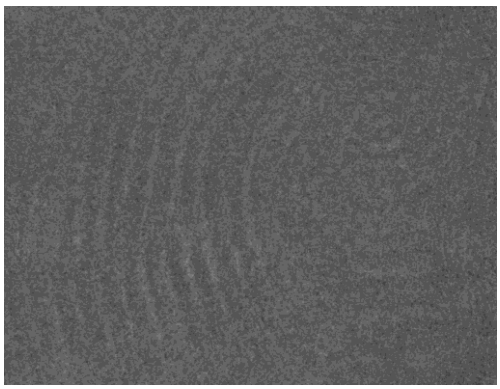

(e)

**Figure 3.7** Recorded hologram: (a) with moisture of 54.0%. Reconstructed holograms: (b) with moisture of 39.0%, (c) with moisture of 54.0%, (d) with moisture of 69.0%, and (e) soak fingerprint.

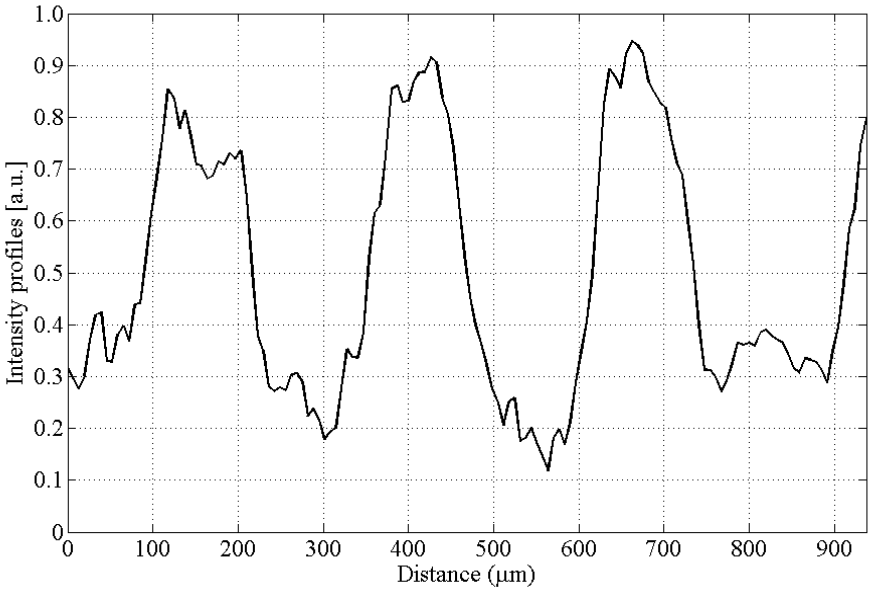


**Figure 3.8** Transverse intensity profiles of fingerprint with moisture of 54.0%.

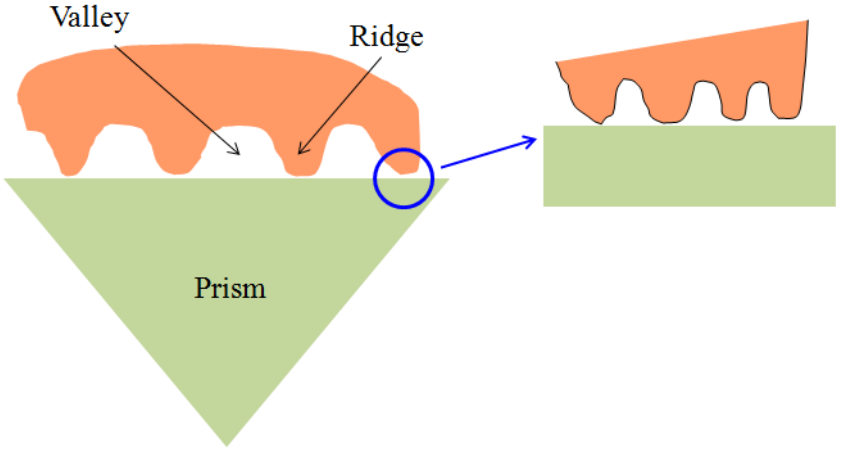


**Figure 3.9** The small ridge and valley at the ridge of fingerprint.

# CHAPTER 4

# GLASS BOTTLE INSPECTION

As described in chapter 1, phase shifting was the technique that measuring the surface shape with uses at least three recorded holograms to reconstruct image. In this chapter we propose the different method that uses only one interferogram to investigate radius of curvature of glass bottle. By using geometrical optics (lens and mirror equation), the radius of curvature is easy to obtain with reconstructed distance which obtained by DH technique. Moreover, DH technique not only investigates the surface shape but also clearly to detect the defect inside glass bottle such as bubble and line scratch.

## 4.1 Mathematical method

The concept of radius of curvature measurement is shown in Fig. 4.1. The collimated beam propagates through the object and then reflects on curvature surface. Then, the expanded image bearing beam will be focused by numerical lens $L_n$ at distance $d_i$. By using lens equation the virtual object distance $d_{ov}$ can be written as

$$d_{ov} = \frac{f_{nl} d_i}{d_i - f_{nl}} \tag{4-1}$$

where $d_i$ is image distance which obtained by reconstruction via digital holography technique and $f_{nl}$ is the focal length of numerical lens which equal to $d_o / 2$ (do is the propagated distance from object to numerical lens). By using mirror equation, the radius of curvature can be expressed as

$$R = 2\frac{-vu}{v-u} \tag{4-2}$$

where $u$ is a distance between object and curvature surface and $v$ is a distance between virtual object to curvature surface and can be directly calculated by

$$v = d_{ov} - a \tag{4-3}$$

where $a$ is a distance between curvature surface to numerical lens. By insert (4-1) and (4-3) into (4-2), the radius of curvature can be now rewritten as

$$R = 2\frac{-\left(\frac{f_{nl}d_i}{d_i - f_{nl}} - a\right)u}{-\left(\frac{f_{nl}d_i}{d_i - f_{nl}} - a\right) - u} \tag{4-4}$$

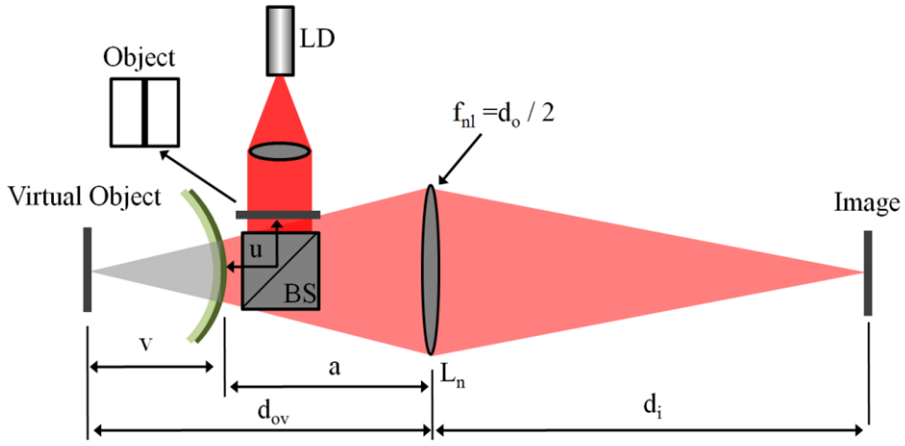


**Figure 4.1** The concept of radius of curvature measurement configuration.

## 4.2 Experimental setup for measuring radius of curvature

The configuration of the experimental setup for the measurement of radius of curvature using DIH is illustrated in Fig. 4.2. The collimated beam from laser diode propagates through object and then reflects on glass bottle. To evaluate the focal length of numerical lens which described in previous section, flat mirror was firstly placed instead of glass bottle. In this experiment, the distance between glass bottle and CMOS plane, $a$, is 82.65 mm, and the propagated distance from

object to glass bottle, $u$, is 81 mm. The image bearing beam which, expands by the curve of glass bottle, was recorded on CMOS camera.

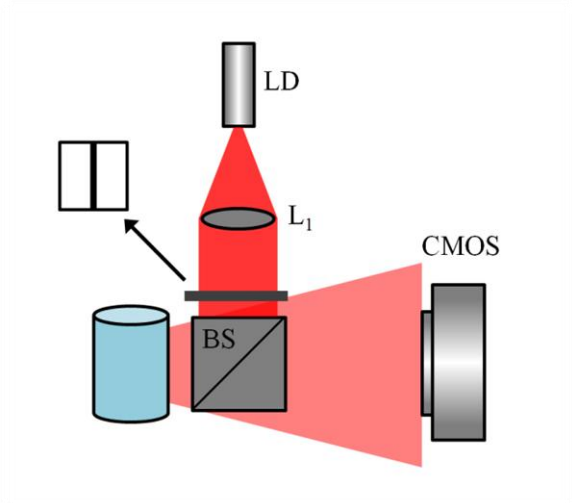


**Figure 4.2** The experimental setup for the measurement of radius of curvature using DIH.

## 4.3 Experimental setup for defect detection in glass bottle

To investigate defect inside glass bottle, the configuration which shows in Fig. 4.3 has been selected. The collimated beam propagates through glass bottle that has the defect and then records on CMOS camera. Two sample of defects; bubble and scratch, were investigated by DIH technique in this thesis.

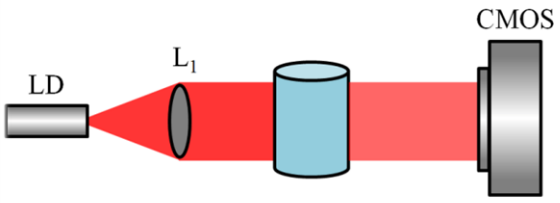


**Figure 4.3** The experimental setup for defect detection using DIH.

## 4.4 Experimental results

Figure 4.4 shows digital hologram of a line pattern object. After numerical reconstructed process at distance of 194.7 mm, the image reflected from flat mirror is focus as shown in Fig. 4.4(b). Therefore focal length of numerical lens, $f_{nl}$, is equal to 97.35 mm. The recorded image reflected from glass bottle [Fig. 4.4(c)] has larger pattern and more scratch than those of the image from flat mirror [Fig. 4.4(a)] due to their surface. In our experiment, the reconstructed image from glass bottle, $d_i$, is found to be focused at the distance of 4370 mm as illustrated in Fig. 4.4(d). After input these numerical parameters into Eq. (4-4), the radius of curvature has been obtained. From our calculation, the radius of curvature of glass bottle is found equal to 42.78 mm (the real value is 40 mm).

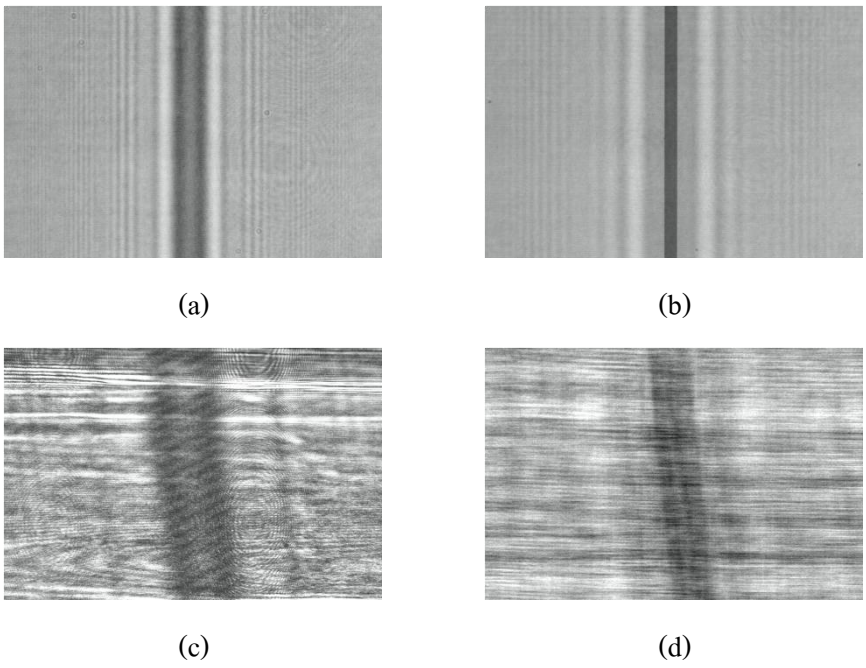

(a) (b)

(c) (d)

**Figure 4.4** Digital hologram of; (a) recorded image by using flat mirror, (b) numerical reconstructed image of (a) at distance 194.7 mm, (c) recorded image by using glass bottle, and (d) numerical reconstructed image of (c) at distance 4370 mm.

Figure 4.5 shows two kinds of defects inside glass bottle; bubble and line scratch. The recorded image of bubble in Fig. 4.5(a) is shown in Fig.4.5 (b). The out of focus image shows diffraction pattern from the edge of bubble. By using numerical reconstruction, the image is

focused and get sharper. With the same explanation for Fig. 4.5(a) - (c), the defect of line scratch are shown in Fig. 4.5(d) - (f).

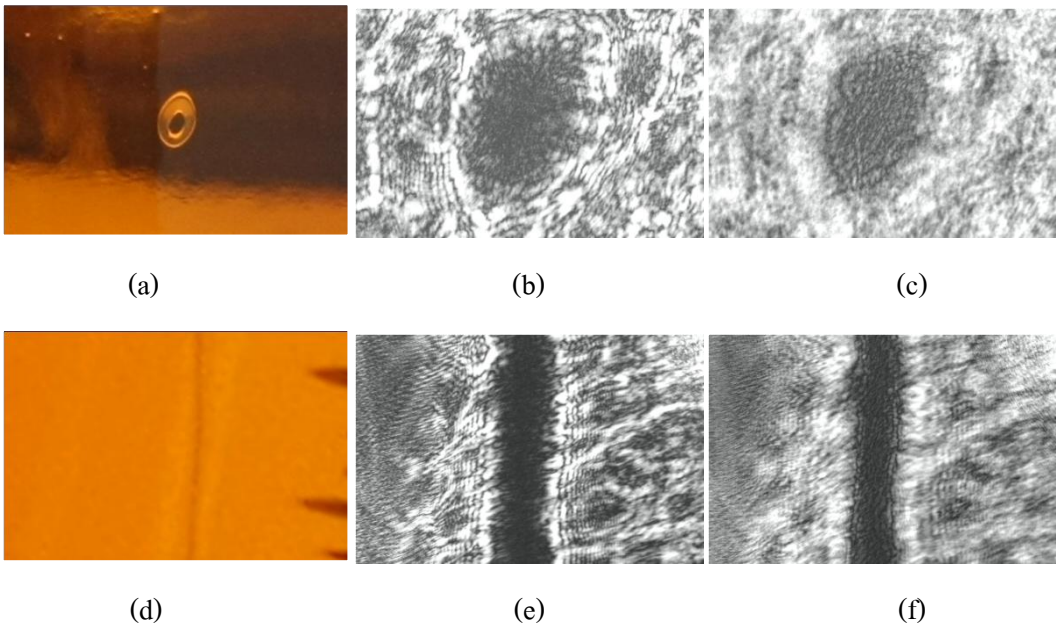

(a) (b) (c)

(d) (e) (f)

**Figure 4.5** Defect inside glass bottle; (a) bubble, (b) recorded image of bubble using DIH configuration, (c) numerical reconstructed image of (b), (d) line scratch, (e) recorded image of line scratch using DIH configuration, and (f) numerical reconstructed image of (e).

# CHAPTER 5

# MEASUREMENT OF PHOTOREFRACTIVE GRATING

This chapter presents the technique that measures directly the photorefractive grating inside Ce: $BaTiO_3$ crystal using DH technique. The experiment is divided into two steps. First, determine the optimum angle that provides the strongest grating. Second, measure the width of PR grating of higher order anisotropic self-diffraction using DH technique.

## 5.1 Experimental setup for determining the optimum angle of higher order ASD

As illustrated in Fig. 5.1, the unpolarized He – Ne laser with wavelength of 632.8 nm has been used to produced the PR grating. The polarized beam from polarizer, $P$, is separated by beam splitter, and then incident on PR Ce:$BaTiO_3$ crystal. The incident angle of two beams on the crystal was calculated by using trigonometry function $2\theta_{io} = \tan^{-1}(y/x)$, where $y$ is distance between beam splitter, $BS$, to mirror, $M_2$, and $x$ is distance between beam splitter to crystal. The dimensions of the crystal are 5.6 mm ×5.6 mm × 6.4 mm (a × b × c). The intensity of self-diffracted beam was measured by using power meter.

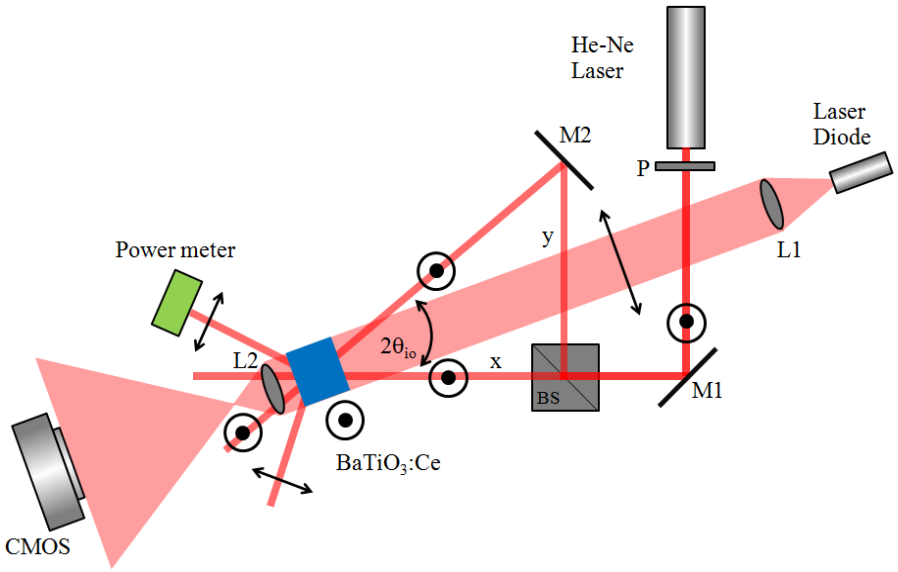


**Figure 5.1** Experimental setup for observing grating: $P$ 's, polarizer; $M$ 's, mirror; $BS$, beam splitter; $L$ 's, lenses.

The optical characteristic between incident angle and the intensity of higher order is shown in Fig. 5.2. The results show that the first order diffraction has highest intensity when the angle of incident equal to 20 degree. Fig. 5.3 shows the pattern of ASD at incident angle equal to 20 degree.

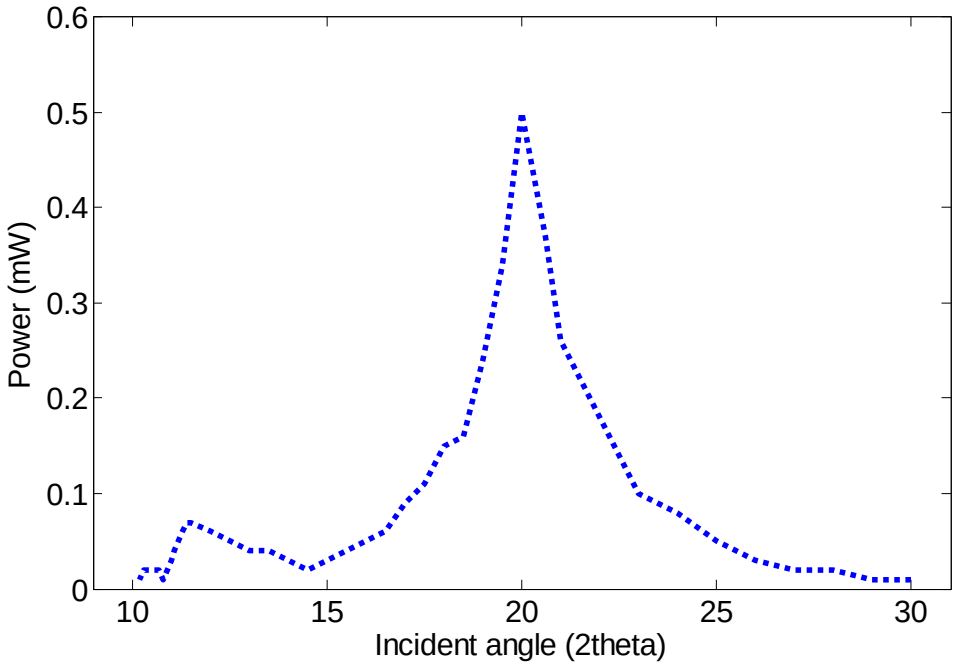


**Figure 5.2** The characteristic of incident angle and diffraction power.

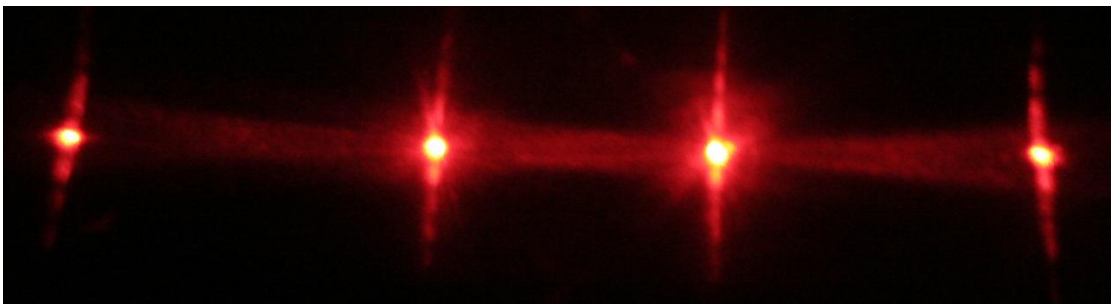

**Figure 5.3** The pattern of zero and first order of anisotropic self-diffraction.

## 5.2 Experimental setup for measuring the width of PR grating

As shown in Fig. 5.1, polarized laser diode has been used to observe phase grating in the crystal. The probe beam was expanded by using lens, $L_1$, and then incident on crystal for illuminating on its induced phase grating pattern. Then, the image bearing beam of the grating was magnified by using lens, $L_2$, and was recorded by CMOS camera. The magnified lens has been used because the path grating of two interference wave is smaller than the pixels size of CMOS camera. From the results in previous topic, the optimum angle that can produce the highest intensity of diffraction was equal to 20 degree $(2\theta_{io})$. Therefore, the grating produced from this optimum angle is investigated in this topic. Interference fringes form with path grating $\Lambda = \lambda / 2\sin\theta_i$, where $\lambda$ is writing beam wavelength, and $\theta_i$ is the incident angle inside the crystal that can be obtained by using Snell's laws as shown in Fig. 5.4 ($\theta_{io}$ = 10 degree, and refractive index of Ce:$BaTiO_3$ = 2.36 , so $\theta_i$ = 4.22). By calculation, path grating in our case is about 4.3 μm. To avoid the annihilation of grating by probe beam, the polarization of probe beam was perpendicular to the writing beam and c-axis of crystal. For calibrating the magnification of the probe system, first, the 50 lines per millimeter gating was recorded and reconstructed. The magnified pattern of this standard grating can be directly measured by image processing. After that, the real width pattern and magnified pattern have been compared to find the magnification of the probe system. This magnified system will be used to calculate for the real width of PR grating.

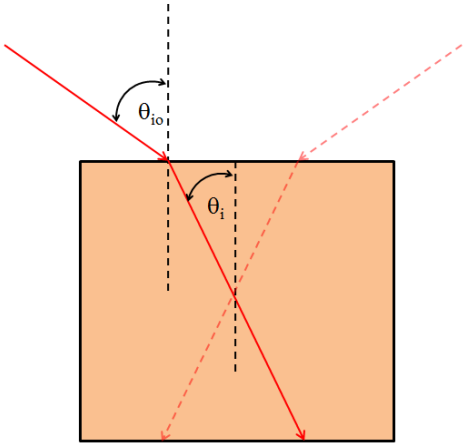


**Figure 5.4** Snell's laws.

## 5.3 Experimental results

The recorded image of standard grating which was used to calibrate magnification of probe beam is shown in Fig. 5.5. This image is not clear because the position of grating is slightly out of focal length of the magnified lens. The sharp reconstructed image of standard grating and its transverse intensity profile are illustrated in Fig. 5.6 and Fig. 5.7. The measured width size of 10 periods grating with sharp pattern is equal to 4,300 μm. Therefore, its single period is 430 μm. However, the actual width of this standard grating is 20 μm. From calculation, the magnification of this system is 21.5 times.

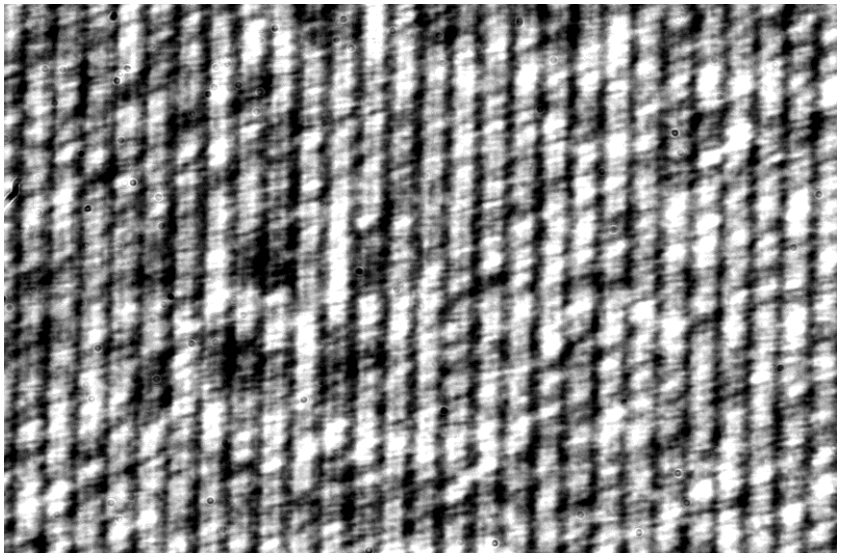

**Figure 5.5** Recorded hologram of standard grating.

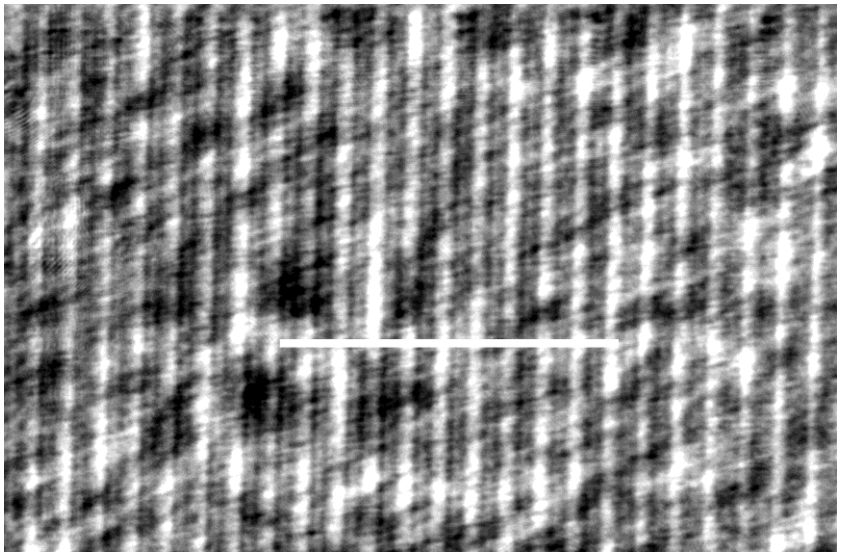

**Figure 5.6** Reconstructed hologram of standard grating.

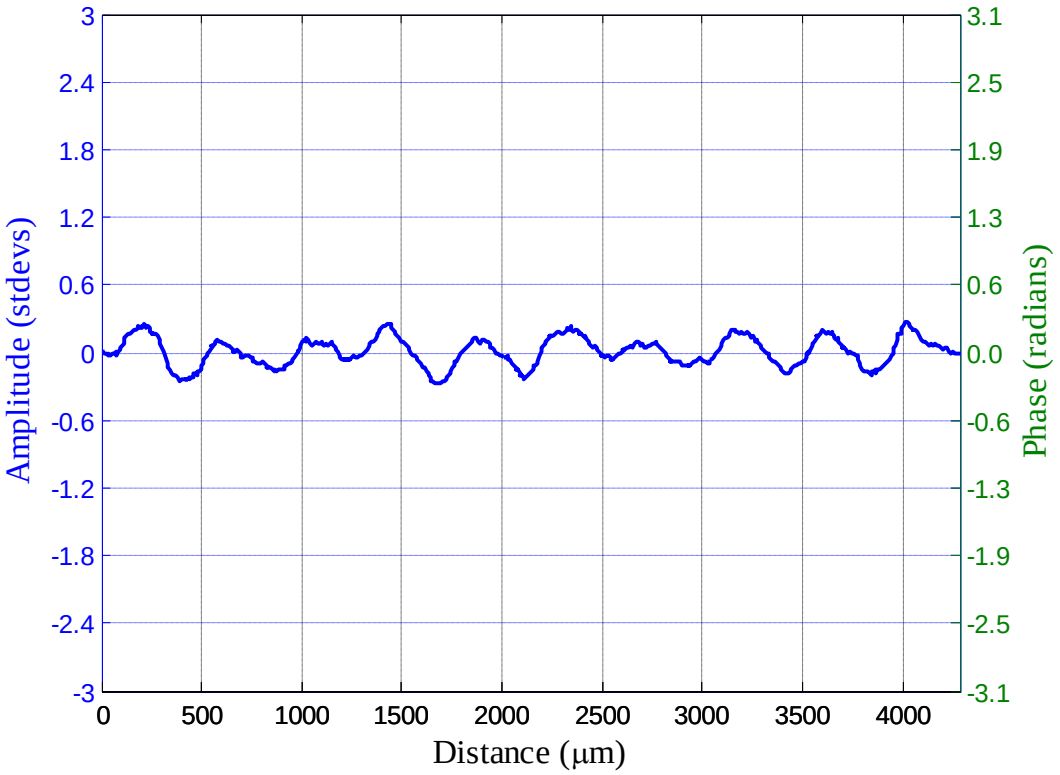


**Figure 5.7** Transverse intensity profile of Fig. 5.6.

Figure 5.8 shows the reconstructed grating image of Ce: BaTiO3 crystal by using DH technique. Due to width size of grating is very small, 10 periods of grating has been measured. The cross section plot of considered area is shown in Fig. 5.9. The 10 period has size of 860 μm, so the single period is 86 μm. By calculating with the magnification of the system, the actual phase grating width from this technique in this crystal is 4 μm. The computation of path grating equation from the previous section was 4.3 μm.

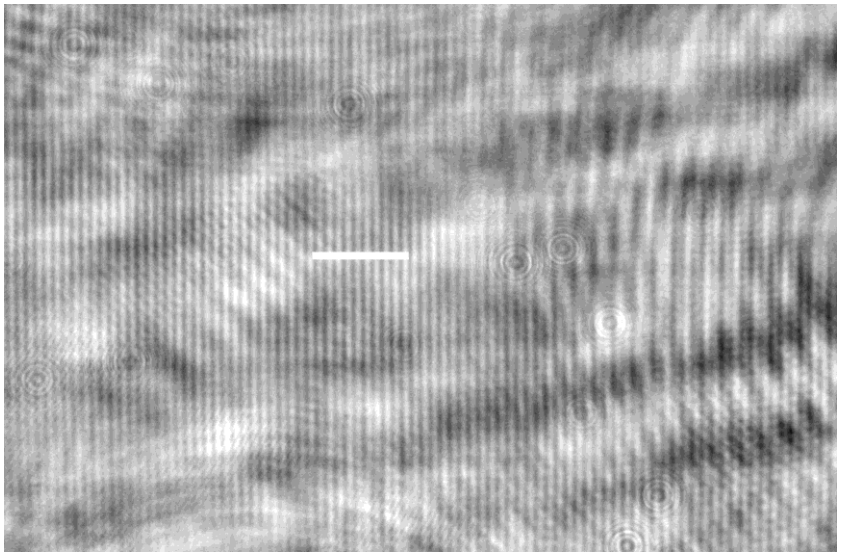

**Figure 5.8** Reconstructed hologram of phase grating inside the crystal.

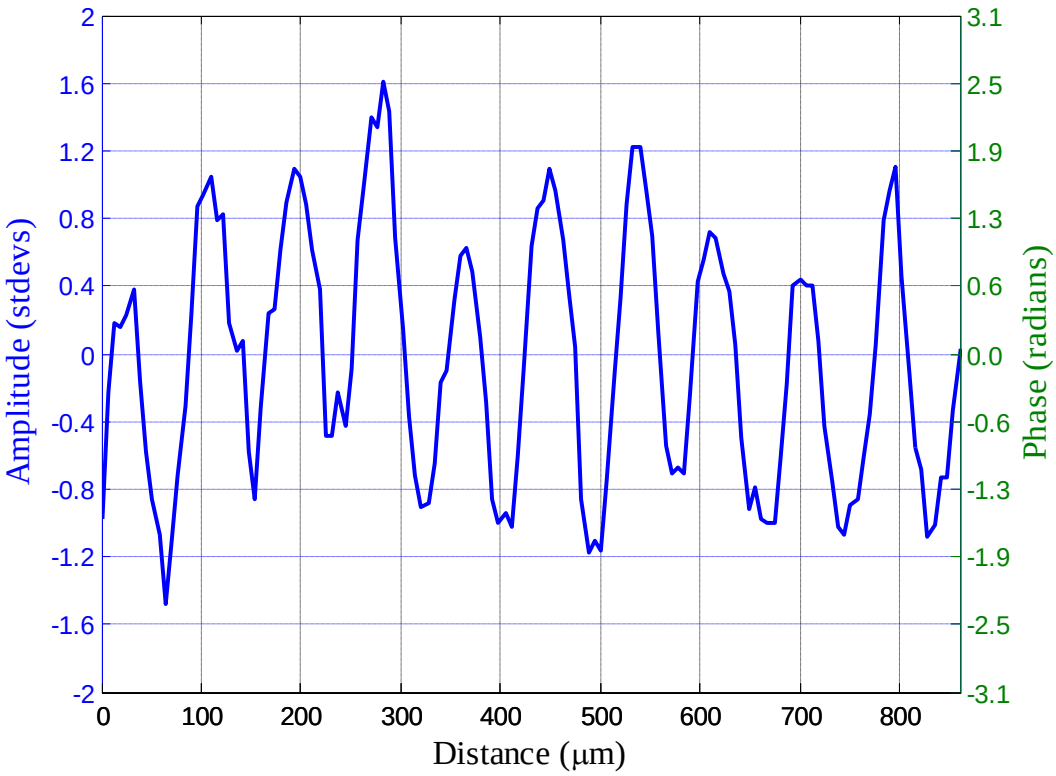


**Figure 5.9** Transverse intensity profile of Fig. 5.7.

# CHAPTER 6

# CONCLUSIONS

## 6.1 Summary of fingerprint moisture investigation using TIRDIH

In this study, we have proposed and demonstrated the moisture effect of fingerprint recording by RDIH based on TIR. By using the interference of diffracted and nondiffracted beams from the target in recording process, only one input beam has been used in our scheme. So the setup is more compact than the previous systems. The reconstructed images of RDIH also found that they are the same with the result images from TDIH. The result images of different moisture finger have been shown and found that they look different. The perfect fingerprint patterns have been observed, when moisture percentages of fingerprint are in the range of 50% - 60% which are measured from skin moisture checker. Moreover, the contrast of fingerprint patterns with high moisture could be resolved by changing the incident angle of light. For example, the incident angle inside prism $\theta_{ii}$ , which causes the TIR between prism and air (refractive index of air is 1), is equal to 41.14 degree. This angle is good for the fingerprint with moisture of 54%. When the moisture of fingerprint is increased, the air in valley of fingerprint will be replaced by the water (refractive index of water is 1.33). Therefore, the incident angle $\theta_{ii}$ that cause TIR for this case is about 61 degree. By using this angle in the experimental setup, the undistinguishable pattern could be resolved. However, this resolved technique cannot be applied with the soak fingerprint because there is a lot of water at the ridge and valley of fingerprint and it cannot be distinguished anymore.

## 6.2 Summary of glass bottle inspection using DIH

In this work, we have proposed the technique to measure radius of curvature and detect the defects inside glass bottles by using DIH technique. By using our experimental setup configuration, the glass bottle radius of curvature has been obtained. The defects inside glass

bottle are easily detected. These two configurations may be combined to one experimental configuration.

## 6.3 Summary of direct measurement of PR grating in Ce:$BaTiO_3$ crystal

We have proposed the alternate method for measuring the photorefractive grating on ASD by using digital holography. In our method, in-line hologram with single beam has been used to analyze phase grating in the crystals instead of using two beams. The diffracted wave from grating can be interfered with nondiffracted wave. The width of phase grating that reconstructed and measured by digital holography technique is not far different from the computation of path gating.

## 6.4 Future work

As described in summaries, DH is the one of powerful investigating tools. In future work, we would like to develop fingerprint scanner using DH technique to record fingerprint in three dimensions (not only patterns but also including the depth of fingerprint). The depth of patterns may be helpful and have impact on the scanning and security systems [44].

The advantage of DIH technique is the record without focusing lens. When the position of bottle is changed, this technique still detects the defect. Therefore, the detection of defect inside glass bottle may be applied to glass bottle industry. When change the type of glass bottle, the detecting system will not change as the conventional system.

The photorefractive effects are still widely researched. In future, we would like to applied DH technique to investigate the other type of grating such as reflective grating and higher order ASD grating.

Moreover, DH is easy to apply with the other system. In future work, we will apply DH with other research fields such; optical tweezers, thermal expansion of material. Finally, the reconstructed program will be developed to Graphics User Interface (GUI) for the comfortable when operated.

## REFERENCES


[1] R.Halmshaw, *NON-DESTRUCTIVE TESTING*, Edward Arnold, London, 1991.

[2] Paul E. Mix, *Introduction to Nondestructive testing: a training guide*, Wiley-Interscience, New Jersey, 2005.

[3] D. Gabor, "A new microscopic principle," *Nature.* **161**, 777-778 (1948).

[4] D. Gabor, "Microscopy by reconstructed wavefronts," *Proc. Roy. Soc*. **197**, 454-487 (1949)

[5] D. Gabor, "Microscopy by reconstructed wavefronts: 2," *Proc. Phys. Soc*. **64**, 449-469 (1951)

[6] U. Schnars and W. Jüptner, "Direct recording of holograms by a CCD target and numerical reconstruction,"*Appl. Opt.* **33,** 179-181 (1994).

[7] G. Situ, J. P. Ryle, U. Gopinathan, and J. T. Sheridan, "Generalized in-line digital holographic technique based on intensity measurements at two different planes," *Appl. Opt.* **47,**711-717 (2008).

[8] W. Xu, M. H. Jericho, I. A. Meinertzhagen, and H. J. Kreuzer, "Digital In-Line Holography of Microspheres," *Appl. Opt.* **41,** 5367-5375 (2002).

[9] G. Pan and H. Meng, "Digital holography of particle fields: reconstruction by use of complex amplitude," *Appl. Opt.* **42,** 827-833 (2003).

[10] F.Soulez, L. Denis, C. Fournier, E.Thiébaut, and C.Goepfert, "Inverse-problem approach for particle digital holography: accurate location based on local optimization," *J. Opt. Soc. Am. A***24,** 1164-1171 (2007).

[11] Y. Yang, G. Li, L. Tang, and L. Huang, "Integrated gray-level gradient method applied for the extraction of three-dimensional velocity fields of sprays in in-line digital holography," *Appl. Opt.* **51,** 255-267 (2012).

[12] J.Gao, D. R. Guildenbecher, P. L. Reu, and J. Chen, "Uncertainty characterization of particle depth measurement using digital in-line holography and the hybrid method," *Opt. Express* **21,** 26432-26449 (2013).

[13] A. S. G. Singh, T.Schmoll, B.Javidi, and R. A. Leitgeb, "In-line reference-delayed digital holography using a low-coherence light source," *Opt. Lett.* **37,** 2631-2633 (2012).

[14] W. M. Ash and M. K. Kim, "Digital holography of total internal reflection," *Opt. Express* **16,** 9811-9820 (2008).

[15] W. M. Ash III, L. Krzewina, and M. K. Kim, "Quantitative imaging of cellular adhesion by total internal reflection holographic microscopy," *Appl. Opt.* **48**, H144-H152 (2009).

[16] S. Sumriddetchkajorn and S. Phoojaruenchanachai, "Geometrical optics analysis for reduction of trapezoidal image distortion in a single prism-based optical fingerprint scanner," *Opt. Laser. Eng.* **45**, 229-239 (2007).

[17] M. Kawakoe and A. Tojo, "Fingerprint pattern classification," *Pattern Recognition* **17**, 295-303 (1984).

[18] R. D. Bahuguna and Tom Corboline, "TECHNICAL NOTE Prism fingerprint sensor that uses a holographic optical element," *Appl. Opt.* **35**, 5242-5245 (1996).

[19] Y. Jie and Z. Jihong, "Fingerprint sensor using a polymer dispersed liquid crystal holographic lens," *Appl. Opt.* **49**, 4763-4766 (2010).

[20] H. -F. Lin, H. -T. Jan, C. -F. Chen, and H. -C. Hsu, "Optical design for enhanced prism type fingerprint scanner image contrast with asymmetrical aspheric lens," *Optik* **121**, 2250-2253 (2010).

[21] M. C. Potcoava and M. K. Kim, "Fingerprint biometry applications of digital holography and low-coherence interferography," *Appl. Opt.* **48**, H9-H15 (2009).

[22] S. Plaipichit, P. Atta, P. Buranasiri, C. Ruttanapun, and P. Jindajitawat, "Fingerprint verification by using low coherence digital holography," in ICPS 2013: International Conference on Photonics Solutions, Proc. SPIE, **8883**, 888315 (2013).

[23] A. Tonatiuh Saucedo, Fernando Mendoza Santoyo, Manuel De la Torre-Ibarra, Giancarlo Pedrini, and Wolfgang Osten, "Endoscopic pulsed digital holography for 3D measurements," Opt. Express **14**, 1468-1475 (2006).

[24] Li Xu, Carl C. Aleksoff, and Jun Ni, "High-precision three-dimensional shape reconstruction via digital refocusing in multi-wavelength digital holography," Appl. Opt. **51**, 2958-2967 (2012).

[25] Ichirou Yamaguchi, Takashi Ida, Masayuki Yokota, and Kouji Yamashita, "Surface shape measurement by phase-shifting digital holography with a wavelength shift," Appl. Opt. **45**, 7610-7616 (2006).

[26] Yuichi Kikuchi, Daisuke Barada, Tomohiro Kiire, and Toyohiko Yatagai, "Doppler phase-shifting digital holography and its application to surface shape measurement," Opt. Lett. **35**, 1548-1550 (2010).

[27] A. Ashkin, G. D. Boyd, J. M. Dziedzic, R. G. Smith, A. A. Ballman, J. J. Levinstein, and K. Nassau, "Optically Induced Refractive Index Inhomogeneities in $LiNbO_3$ and $LiTaO_3$," *Appl. Phys. Lett.***9**, 72-74 (1966).

[28] R. L. Townsend and J. T. LaMacchia, "Optically Induced Refractive Index Changes in $BaTiO_3$," *J. Appl. Phys.***41**, 5188 (1970).

[29] S.Ducharme and J. Feinberg, "Speed of the photorefractive effect in a $BaTiO_3$ single crystal," *J. Appl. Phys*. **56**, 839 (1984).

[30] D. A. Temple, R. S.Hathcock, and C.Warde, "Intensity dependent photorefractive properties of $BaTiO_3$," *J. Appl. Phys*. **67,** 6667 (1990).

[31] M.Zgonik, K. Nakagawa, and P. Günter, "Electro-optic and dielectric properties of photorefractive $BaTiO_3$ and $KNbO_3$," *J. Opt. Soc. Am. B***12**, 1416-1421 (1995).

[32] M. C. Gower and P. Hribek, "Mechanisms for internally self-pumped phase-conjugate emission from $BaTiO_3$ crystals," *J. Opt. Soc. Am. B***5**, 1750-1757 (1988).

[33] N. V. Kukhtarev, E. Krazig, H. C. Kulich, and R. A. Rupp, "Anisotropic self-diffraction in $BaTiO_3$" *Appl. Phys. B* **35**, 17 – 21 (1984).

[34] D. A. Temple and C. Warde, "High-order anisotropic diffraction in photorefractive crystals," J. Opt. Soc. Am. B **5**, 1800-1805 (1988).

[35] C.C. Sun, B. Wang, and J.-Y. Chang, "Photorefractive Incoherent-to-Coherent Optical Converter Based on Anisotropic Self-Diffraction in $BaTiO_3$," *Appl. Opt*. **37**, 8247-8253 (1998).

[36] B. Wang and C. C. Sun, "Precise Measurement of Thermal-Induced Refractive-Index Change in $BaTiO_3$ on the Basis of Anisotropic Self-Diffraction," *Appl. Opt*. **40**, 672-677 (2001).

[37] Changxi Yang, Yuheng Zhang, Pochi Yeh, Yong Zhu, Xing Wu, "Photorefractive properties of Ce: BaTiO3 crystals," *Opt. Commun.* **113**, 416-420 (1995).

[38] H. Song, S. X. Dou1, and P. Ye, "Origin of the wavelength-dependence of effective trap density in photorefractive $BaTiO_3$:Ce," *J. Appl. Phys*. **88**, 6981 (2000)

[39]M. de Angelis, S. De Nicola, A. Finizio, G. Pierattini, P. Ferraro, S. Pelli, G. Righini3 and S. Sebastiani, "Digital-holography refractive-index-profile measurement of phase gratings," *Appl. Phys. Lett.* **88**, 111114 (2006).

[40] Ivan Turek and Norbert Tarjányi, "Investigation of symmetry of photorefractive effect in $LiNbO_3$," Opt. Express 15, 10782-10788 (2007).

[41] J. P. Fugal, T. J. Schulz, and R. A. Shaw, "Practical methods for automated reconstruction and characterization of particles in digital inline holograms," *Meas. Sci. Technol.***20,** 075501 (2009).

[42] J.W. Goodman, *Introduction to Fourier Optics*, chapter 4, McGrawiHill, Singapore, 1996

[43] U. Schnars and W Jueptner, *Digital holograpgy: digtal hologram recording, numerical reconstruction, and related technique*, chapter 3, Springer, Berlin, 2005.

[44] D. Maltoni, D. Maio, A. K. Jain, and S. Prabhakar, *Handbook of Fingerprint Recognition*, Springer, London, 2009.

# APPENDIX A

## Fourier transformation of image with MATLAB®

The Fourier transformation and inverse Fourier transformation were described by Eq. (2-7) and (2-8) respectively in chapter 2. In this section describes the transformation of image using Fourier transform function in MATLAB® program. Three samples of image included square, triangle, and circle shape are transformed by FFT function. The MATLAB code example is shown in Table A1.

**Table A1.** MATLAB code example for transforming image with FFT function

```
clear all;
close all;
colormap gray;
imgsrc='image name.png'; %the name of sample image that use to transform
OB=imread(imgsrc);
OB=rgb2gray(OB);
figure(1)
imshow(OB);
FT=fftshift(fft2(OB));
FT=mat2gray((abs(FT)));
figure(2)
imshow(FT);
```

The samples of image which are transformed by FFT function, have been shown in Fig. A.1

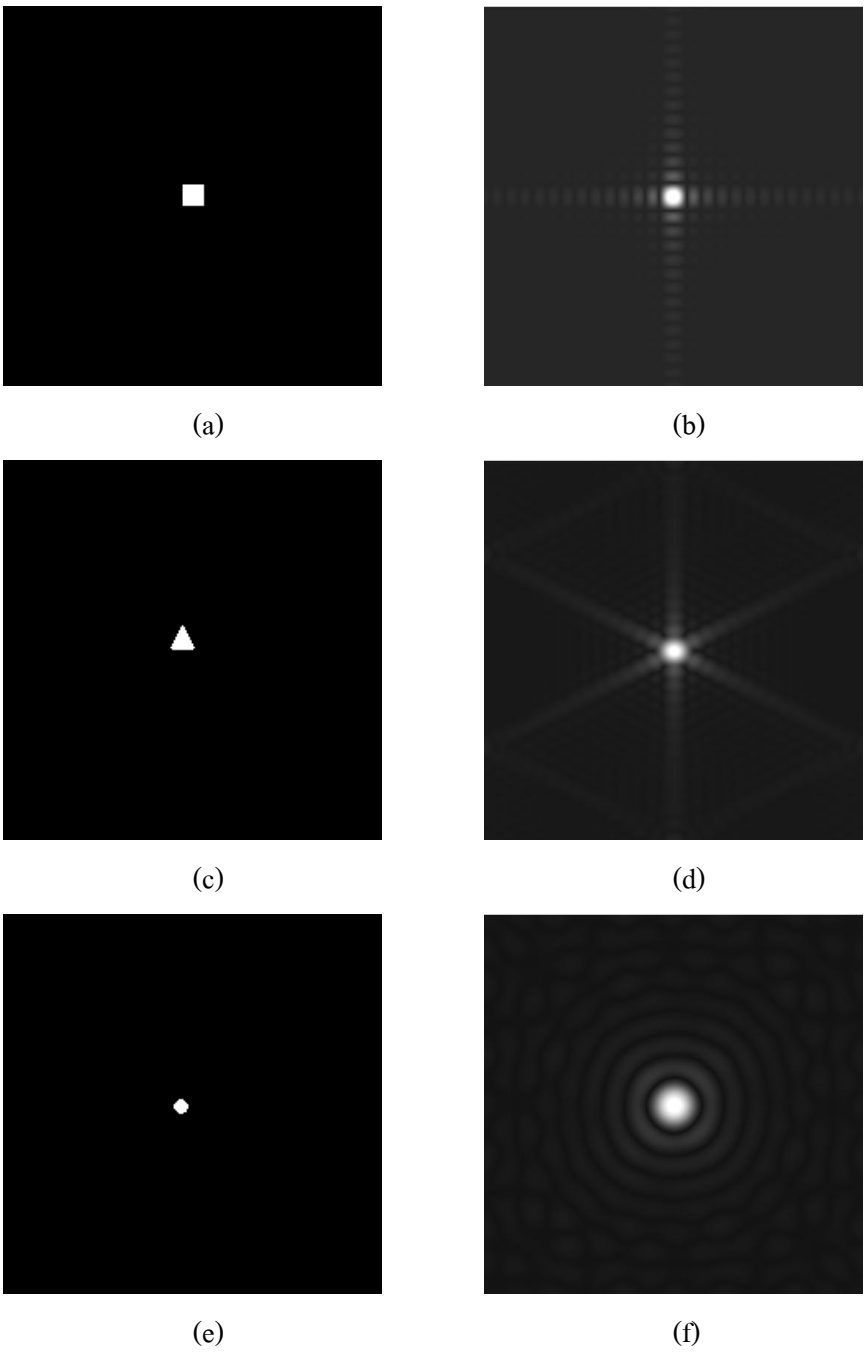


**Figure A.1.** The samples image; (a) square aperture, (b) FFT of square aperture, (c) triangle aperture, (d) FFT of triangle aperture, (e) circle aperture, and (f) FFT of circle aperture.

# APPENDIX B

## Source codes for reconstructing digital hologram

As described in chapter 2, there are two reconstruction methods that use in this thesis; Huygens convolution method (HCM) and angular spectrum method (ASM). Therefore this section show the two source codes which use to reconstruct digital hologram.

**Table B1.** MATLAB code example for reconstructing digital hologram using HCM.

```
clear all;
close all;
colormap gray;
imgsrc='image name.png'; %image name
H=imread(imgsrc);
H=rgb2gray(H);
imagesc(H)
figure(1)
imshow(H);
title('Recorded digital hologram')
H=double(H);
H=transpose(H);
lambda=635e-9; %wavelength, unit:m
del_px=6.42e-6; %pixels size, unit:m
del_py=6.42e-6; %pixels size, unit:m
M=3456; %number of pixels
N=2304; %number of pixels
z=296e-3; %reconstructed distance, unit:m
x=1:M;
y=1:N;
```

```
[X,Y]=meshgrid(x, y);
dim=((X-((M/2)-1)).*del_px).^2+((Y-((N/2)-1)).*del_py).^2;
TF_K=exp((1i*pi/(z*lambda)).*dim);
TF_K=transpose(TF_K);
RH=fftshift(fft2(fftshift(H.*TF_K)));
RH=mat2gray((abs(RH)).^2);
RH=transpose(RH);
figure(2)
imshow(RH);
text(10,10,strcat('\color{white}z=',sprintf('%3.0f%',z*1e3),'mm'));
title('Reconstructed digital hologram')
```

**Table B2.** MATLAB code example for reconstructing digital hologram using ASM.

```
clear all;
close all;
colormap gray;
imgsrc='image name.png'; %image name
H=imread(imgsrc);
H=rgb2gray(H);
imagesc(H)
figure(1)
imshow(H);
title('Recorded digital hologram')
H=double(H);
H=transpose(H);
lambda=635e-9; %wavelength, unit:m
del_px=6.42e-6; %pixels size, unit:m
del_py=6.42e-6; %pixels size, unit:m
M=3456; %number of pixels
N=2304; %number of pixels
z=296e-3; %reconstructed distance, unit:m
SP_OB=fftshift(ifft2(fftshift(H)));
deltafx=1/(M*del_px);
deltafy=1/(N*del_py);
k=2*pi/lambda;
x=1:M;
y=1:N;
[X,Y]=meshgrid(x, y);
dim=((1)-(((X-((M/2)-1)).*deltafx.*lambda).^2)-(((Y-((N/2)-1)).*deltafy.*lambda).^2)).^0.5;
```

```
TF_K=exp((-1i).*k.*z.*dim);

TF_K=transpose(TF_K);

RH=fftshift(fft2(fftshift(SP_OB.*TF_K)));

RH=mat2gray((abs(RH)).^2);

RH=transpose(RH);

figure(2)

imshow(RH);

text(10,10,strcat('\color{white}z=',sprintf('%3.0f%',z*1e3),'mm'));

title('Reconstructed digital hologram')
```

## APPENDIX C

### Publication in international journals

[1] S. Plaipichit, P. Buranasiri, C. Ruttanapun, and P. Jindajitawat, "The Direct Measurement of the Photorefractive Grating on Anisotropic Self Diffraction Using Digital Holography," *Integrated Ferroelectrics: An International Journal.* **156**(1), p. 160-167 (2014).

[2] S. Plaipichit and P. Buranasiri, "Moisture effect of fingerprint using total internal reflection digital in-line holography," *Opt. Eng.* **53**(11), p.112315-1 – 112315-5 (2014).

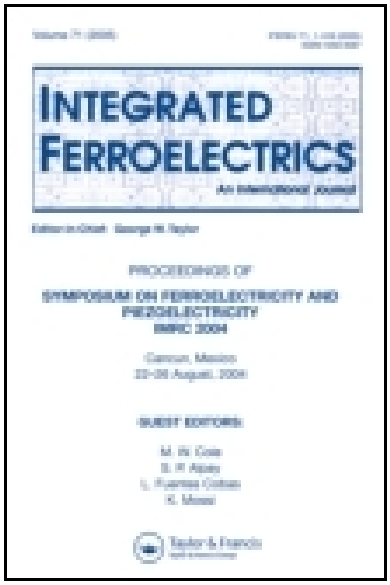


Integrated Ferroelectrics: An International Journal

Publication details, including instructions for authors and subscription information:
http://www.tandfonline.com/loi/ginf20

# The Direct Measurement of the Photorefractive Grating on Anisotropic Self Diffraction Using Digital Holography

Suwan Plaipichit[a], Prathan Buranasiri[a], Chesta Ruttanapun[a] & Phumin Jindajitawat[a]

[a] Department of Physics, Faculty of Science, King Mongkut's Institute of Technology Ladkrabang, Bangkok 10520, Thailand

Published online: 20 Jun 2014.

**To cite this article:** Suwan Plaipichit, Prathan Buranasiri, Chesta Ruttanapun & Phumin Jindajitawat (2014) The Direct Measurement of the Photorefractive Grating on Anisotropic Self Diffraction Using Digital Holography, Integrated Ferroelectrics: An International Journal, 156:1, 160-167, DOI: 10.1080/10584587.2014.907107

**To link to this article:** http://dx.doi.org/10.1080/10584587.2014.907107

*Integrated Ferroelectrics*, 156:160–167, 2014

ISSN: 1058-4587 print / 1607-8489 online
DOI: 10.1080/10584587.2014.907107





# The Direct Measurement of the Photorefractive Grating on Anisotropic Self Diffraction Using Digital Holography

SUWAN PLAIPICHIT,* PRATHAN BURANASIRI, CHESTA RUTTANAPUN, AND PHUMIN JINDAJITAWAT

Department of Physics, Faculty of Science, King Mongkut's Institute of Technology Ladkrabang, Bangkok 10520, Thailand

*In this paper, the measurement of grating period in photorefractive anisotropic self diffraction by using digital holography technique is proposed. In our experimental setup, He –Ne laser beam with wavelength of 632.8 nm has been separated and then incident on photorefractive cerium doped barium titanate crystal to produce photorefractive index grating. The transmitted probe beam, which contains phase and amplitude has been expanded and recorded on digital camera. To explore the grating periods, both phase and amplitude of the images are reconstructed by numerical process using computer. Then the grating periods in photorefractive anisotropic self diffraction have been measured. The results show grating periods, holograms and their reconstruction.*

**Keywords** Digital holography; photorefractive; self diffraction; phase grating

## 1. Introduction

Barium titanate ($BaTiO_3$) has been well known as one of the ferroelectric materials, and also has been recognized as photorefractive (PR) materials. $BaTiO_3$ has been used in many fields such as electronics, electrochemistry, and data storage. Due to the fact that refractive index of this PR crystal is easily changed by light incidence, $BaTiO_3$ is particular advantage for PR nonlinear optic fields. Recently, $BaTiO_3$ is one of the few electro-optic crystals that can exhibit anisotropic self diffraction (ASD), a phenomenon of PR effect that the polarizations of the incident and the diffracted light have different direction.

In 1966, Ashkin et al. found that refractive index of $LiNbO_3$ and $LiTaO_3$ were changed by optically induced and called "optical damage" [1]. Several years later, this phenomenon has been studied on $BaTiO_3$ by using holographic storage technique [2]. Some properties and application of $BaTiO_3$ such as intensity dependence, electro optics, and so on were observed by several researchers [3–6]. Kukhtarev *et al.* first found that polarization of incident beam and diffracted beam of $BaTiO_3$ crystal were perpendicular to each other and called "anisotropic self diffraction" [7]. After that, there were some applications of ASD with $BaTiO_3$ have been studied by several authors [8, 9]. Recently, the PR grating of $LiNbO_3$ was measured by using digital holography [10]. However, there were still few study

Received July 23, 2013; in final form January 7, 2014.
*Corresponding author. E-mail: ivirusjung@gmail.com
Color versions of one or more of the figures in the article can be found online at www.tandfonline.com/ginf.

of PR grating of ASD on Ce:$BaTiO_3$ crystal with wavelength of 632.8 nm. In this paper, the direct measurement method of photorefractive anisotropic self diffraction (PRASD) grating inside Ce:$BaTiO_3$ crystal by using digital holography technique has been proposed. Holograms from the data sets presented in this paper are reconstructed using the method described by Fugal *et al.* [11].

## 2. Theory

### *2.1 Photorefractive Effect*

The PR effect is a kind of nonlinear optic phenomena, which occurs in the electro-optics materials. In PR materials, the local index of refraction can be changed, when the light beams interfered on their surfaces. By assuming that the PR media are doped, their donor impurities can be ionized when they have been absorbed photons. Let the density of donor impurities be $N_D$ and $N^i{}_D$, which are their ionized. The rate equation for $N^i{}_D$ can be written as

$$\frac{\partial_D^i}{\partial t} = sI(N_D - N_D^i) - \gamma_R N N_D^i \tag{1}$$

where $N$, $s$, $I$, and $\gamma_R$ are electron density, cross section for photoexcitation, light intensity, and electron-ionized trap recombination rate, respectively. This equation can be explained on two parts. First, $sI(N_D - N^i{}_D)$ is the rate of electron generation and $\gamma_R N N^i{}_D$ is the rate of trap capture. Because of mobility of electron can be affected by the electron density, now, the rate equation can be written as

$$\frac{\partial N}{\partial t} - \frac{\partial N_D^i}{\partial t} = \frac{1}{q}\nabla \cdot \mathbf{j} \tag{2}$$

where $q$ is an electron charge and $\mathbf{j}$ is a current density, which consists of contributions from the drift of charge due to an electric field and the diffusion due to the gradient of carrier density. Thus, this can be written as

$$\mathbf{j} = qN\mu\mathbf{E} + k_B T \mu \nabla N \tag{3}$$

where $\mu$ is the mobility tensor, $\mathbf{E}$ is the electric field, $k_B T$ is the product of the Boltzmann constant and temperature. The electric field is followed by Poisson equation

$$\nabla \cdot \varepsilon\mathbf{E} = \rho(\mathrm{r}) = -q(N + N_A - N_D^i) \tag{4}$$

where $\varepsilon$ is dielectric tensor, $\rho(\mathbf{r})$ is charge density and $N_A$ is density of acceptor impurity. The Eqs (1) – (4) have been called band transport model or Kukhtarev's Equations [12].

### *2.2 Anisotropic Self Diffraction*

In an anisotropic bulk crystal, the phase matching conditions need to be satisfied by the writing beams (incident beams) to create the anisotropic self diffraction. As shown in Fig. 1, the optical axis is in the direction parallel to the plane of incident. Where $\mathbf{K}_{e1}$ and $\mathbf{K}_{e2}$ are the wave vector of two writing beams with extraordinary polarization. $\mathbf{K}_{o1}$ and $\mathbf{K}_{o2}$ are the wave vector of diffracted beams with direction of polarization perpendicular to c-axis

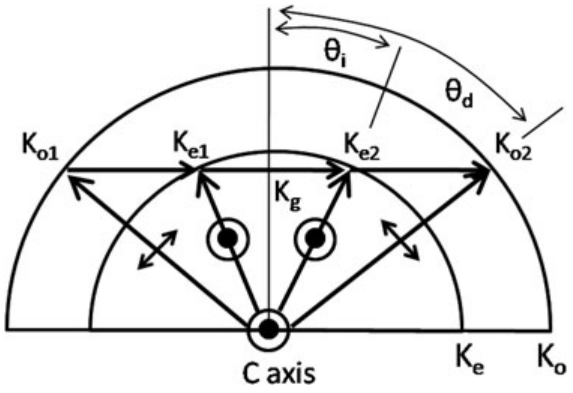


**Figure 1.** The wave vector diagram of anisotropic self diffraction.

(ordinary polarization). Thus, the grating wave vector, $\mathbf{K}_g$, can be defined by

$$\mathbf{K}_g = \mathbf{K}_{e2} - \mathbf{K}_{e1} \tag{5}$$

Now, the wave vectors of the diffracted higher order beams can be written as

$$\mathbf{K}_{o1} = \mathbf{K}_{e1} - \mathbf{K}_g, \ \mathbf{K}_{o2} = \mathbf{K}_{e2} + \mathbf{K}_g \tag{6}$$

The incident angle outside crystal can be expressed as [8]

$$\theta_{io} = \sin^{-1}\left[\left(\frac{n_o^2 - n_e^2}{8}\right)^{1/2}\right] \tag{7}$$

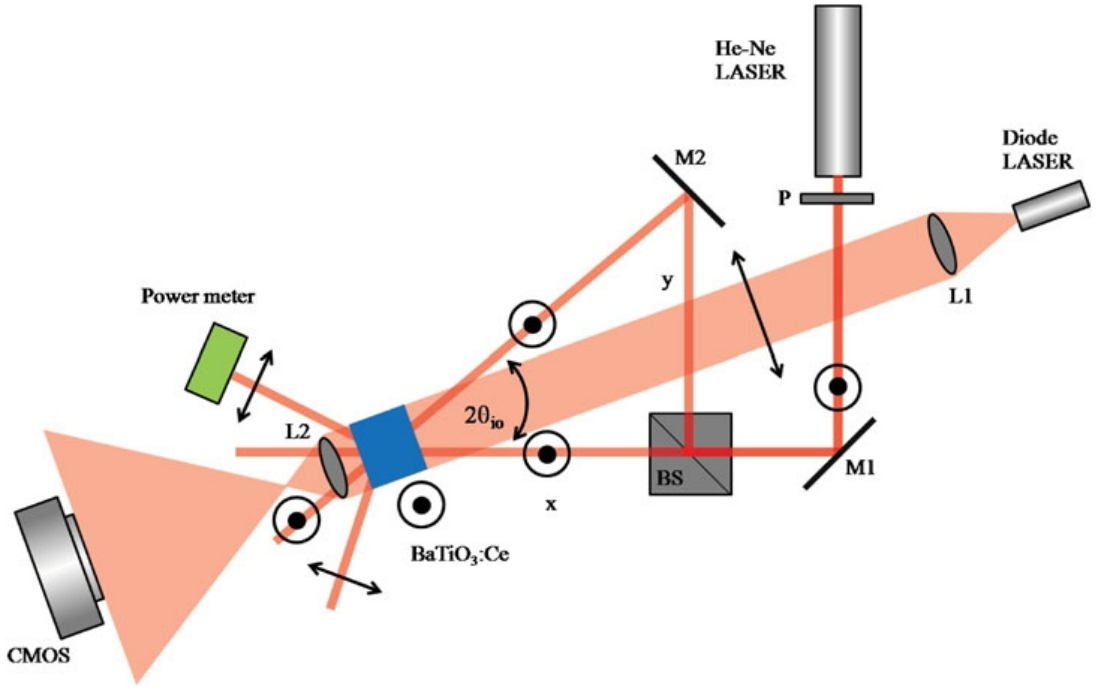


**Figure 2.** Experimental setup for measuring phase grating: P, polarizer; M's, mirror; BS, beam splitter; L's, lenses.

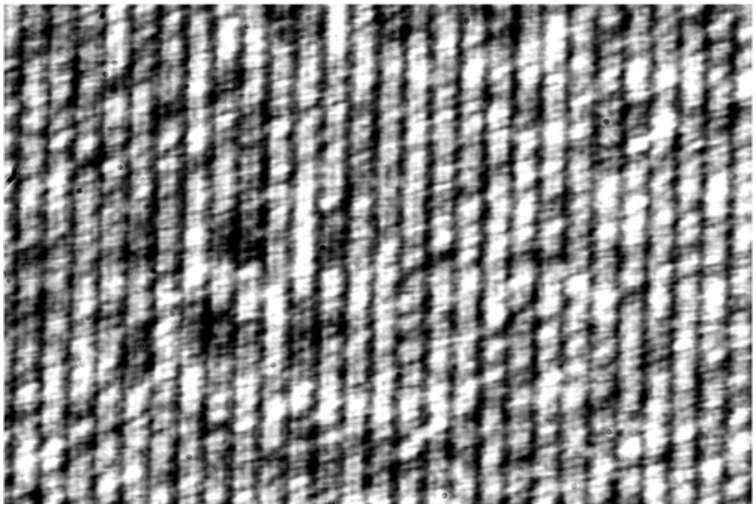

**Figure 3.** Recorded hologram of standard grating.

where $n_o$ is the ordinary refractive index and the $n_e$ is extraordinary refractive index of the crystal. Furthermore, under Bragg condition as shown in Figure 1, the incident light $\mathbf{K}_{e1}$ and $\mathbf{K}_{e2}$ not only construct the grating $\mathbf{K}_g$ but also couple to second order beams, $\mathbf{K}_{o1}$ and $\mathbf{K}_{o2}$, respectively. This is the regime of anisotropic self- diffraction.

### *2.3 Reconstruction Method*

In this paper, holograms are reconstructed by numerical process based on discrete Fresnel transform, which was describe by Schnars and Jueptner [13] and Fugal *et al.* [11]. The reconstructed field with $N \times N$ matrix of the images at any distance $z$ and wavelength $\lambda$ is given by

$$\begin{aligned} U(x, y, z) &= \exp\left[-i\pi\lambda z\left(\tfrac{x^2}{N^2 p_x^2} + \tfrac{y^2}{N^2 p_y^2}\right)\right] \\ &\times \sum_{k=0}^{N-1}\sum_{l=0}^{N-1} h(k, l)\exp\left[-i\tfrac{\pi}{\lambda z}\left(k^2 p_x^2 + l^2 p_y^2\right)\right]\exp\left[i2\pi\left(\tfrac{kx}{N} + \tfrac{ly}{N}\right)\right] \end{aligned} \tag{8}$$

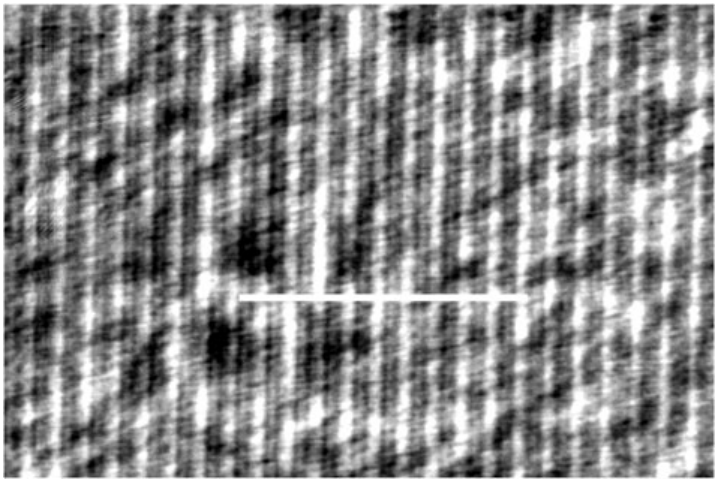

**Figure 4.** Reconstructed hologram of standard grating.

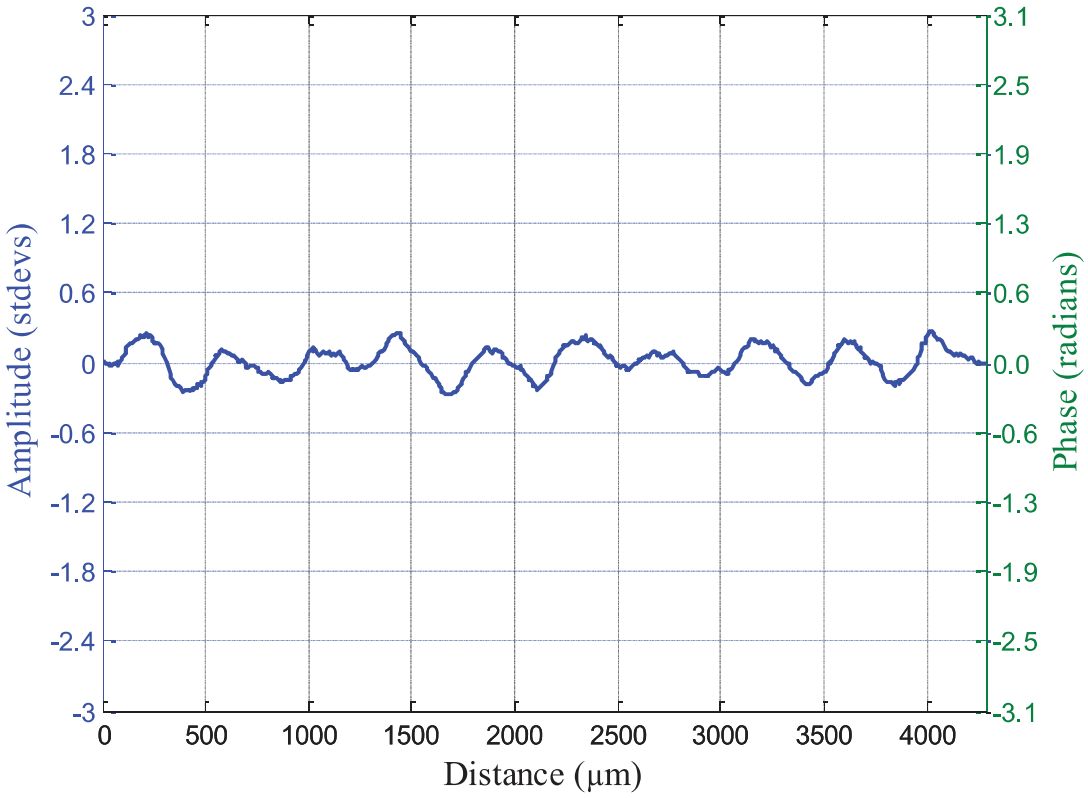


**Figure 5.** Cross section plot of Fig. 4.

where $h(k, l)$ is the intensity distribution of the hologram, and $p_x$, and $p_y$ are pixel sizes of CMOS chip.

## 3. Experimental Setup

A schematic of photorefractive grating measurement on anisotropic self diffraction using digital holography is shown in Fig. 2. The unpolarized He – Ne laser with wavelength

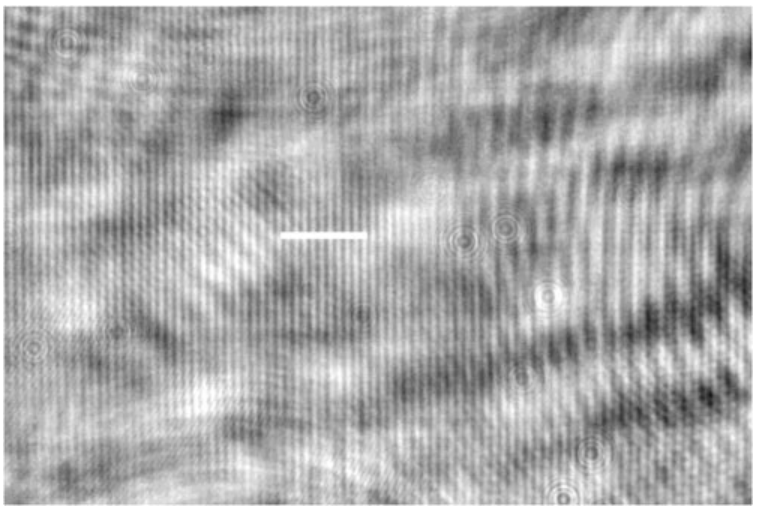

**Figure 6.** Reconstructed hologram of phase grating in the crystal.

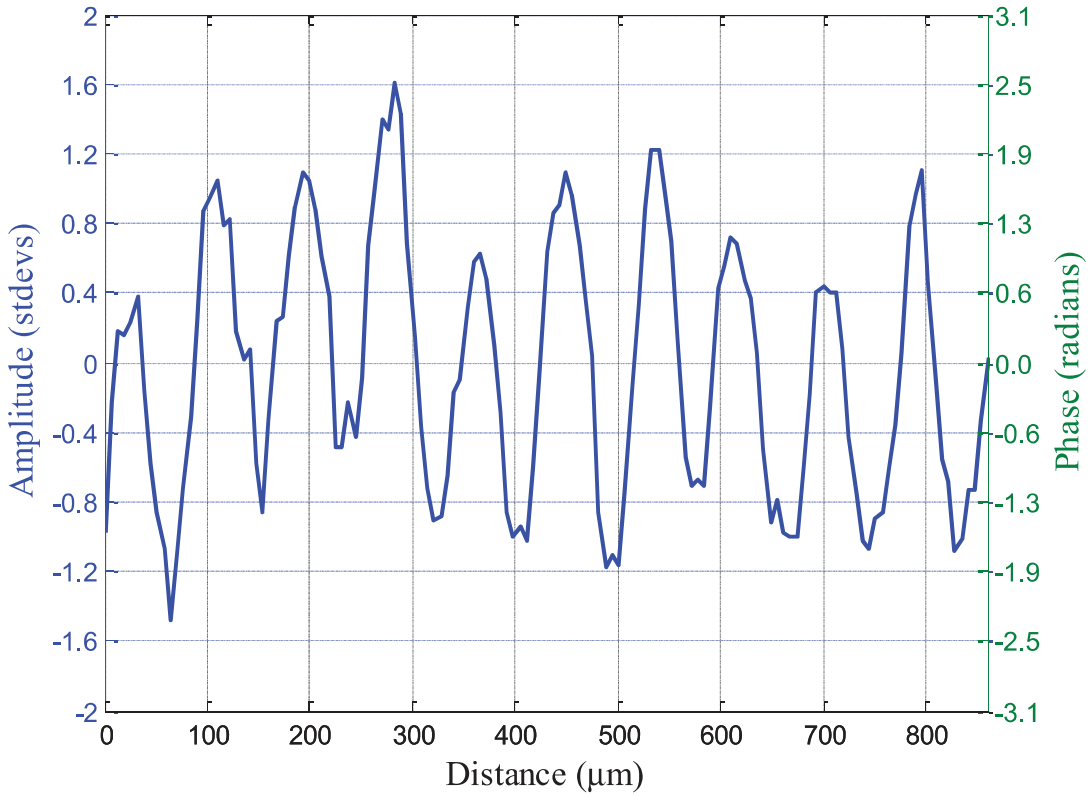


**Figure 7.** Cross section plot of Fig. 6.

of 632.8 nm has been used as the writing beam. The polarized beam from polarizer, P, was separated by using a beam splitter, and then incident on PR Ce:$BaTiO_3$ crystal. The incident angle of two beams on the crystal was calculated by using trigonometry function $2\theta_{io} = \tan^{-1}(y/x)$, where y is distance between beam splitter, BS, to mirror, $M_2$, and x is distance between beam splitter to crystal. The dimensions of the crystal were 5.6 mm $\times$ 5.6 mm $\times$ 6.4 mm (a $\times$ b $\times$ c). The intensity of self diffracted beam was measured by power meter. Polarized diode laser with wavelength of 635 nm has been used to observe phase grating in crystal. The probe beam was expanded by lens, $L_1$, and incident on crystal for illuminating on its induced phase grating pattern. Then, the image beam bearing of the grating was magnified by lens, $L_2$, and was recorded by CMOS camera. We used a Canon EOS 350D with 3456 $\times$ 2304 pixels, 6.4 $\mu$m pixel pitch, and 22.2 mm $\times$ 14.7 mm size as an image detector.

The angle between the writing beams, which incident on a face of the crystal is equal to 20 degrees ($2\theta_{io}$), *i.e.* the optimum angle that generated strongest phase grating. Interference fringes form with path grating $\Lambda = \lambda_w/(2\sin\theta_i)$, where $\lambda_w$ is writing beam wavelength. The incident angle inside the crystal, $\theta_i$, can be obtained by using Snell's laws. By calculation, path grating in our case was 4.3 $\mu$m. To avoid the annihilation of grating by probe beam, the polarization of probe beam was perpendicular to writing beam and c-axis of crystal. For calibrating the magnification of the probe system, first, the 50 lines per millimeter gating was recorded and reconstructed. Phase grating pattern was recorded when self diffracted beam had the most intensity.

## 4. Results and Discussion

The recorded image of standard grating which was used to calibrate magnification of probe beam is shown in Fig. 3. This image is not sharp and clear because the position of grating is slightly out of focal length of the magnified lens. The sharp reconstructed image of standard grating and its cross section plot are illustrated in Figure 4 and Fig. 5. The width size of 10 periods grating with sharp pattern was measured equal to 4300 $\mu$m. Therefore, its single period is 430 $\mu$m. However, the actual width of this standard grating is 20 $\mu$m. From calculation, the magnification of this system is 21.5 times.

Figure 6 shows the reconstructed grating image of Ce:$BaTiO_3$ crystal by using digital holography technique. Due to width size of grating is very small, 10 periods of grating has been measured. The cross section plot of considered area is shown in Fig. 7. The 10 period has size of 860 $\mu$m, so the single period is 86 $\mu$m. By calculating with the magnification of the system, the actual phase grating width from this technique in this crystal is 4 $\mu$m. The computation of path grating equation from the previous section was 4.3 $\mu$m.

## 5. Conclusions

We have proposed the alternate method for measuring the photorefractive grating on ASD by using digital holography. In our method, in-line hologram with single beam has been used to analyze phase grating in the crystals instead of using two beams. The diffracted wave from grating can be interfered with undiffracted wave. The width of phase grating that reconstructed and measured by digital holography technique is not different far from the computation of path gating. In future work, we will continue our method to observe the generation of phase grating in real time.

## Funding

This research was supported reconstructed program "HoloViewer" from Physics Department, Michigan Technological University [11].

## References

1. A. Ashkin, G. D. Boyd, J. M. Dziedzic, R. G. Smith, A. A. Ballman, J. J. Levinstein, and K. Nassau, Optically induced refractive index inhomogeneities in $LiNbO_3$ and $LiTaO_3$. *Appl. Phys. Lett.* **9**, 72–72 (1966).
2. R. L. Townsend and J. T. LaMacchia, Optically induced refractive index changes in $BaTiO_3$. *J. Appl. Phys.* **41**, 5188 (1970).
3. S. Duchame and J. Fienberg, Speed of the photorefractive effect in a $BaTiO_3$ single crystal. *J. Appl. Phys.* **56**, 839 (1984).
4. M. C. Gower, and P. Hribek, Mechanisms for internally self-pumped phase-conjugate emission from $BaTiO_3$ crystals. *J Opt Soc Am B.* **5**, 1750–1757 (1988).
5. D. A. Temple, R. S. Hathcock, and C. Warde, Intensity dependent photorefractive properties of $BaTiO_3$. *J. Appl. Phys.* **67**, 6667 (1990).
6. M. Zgonik, K. Nakagawa, and P. Gunter, Electro-optic and dielectric properties of photorefractive $BaTiO_3$ and $KNbO_3$. *J. Opt. Soc. Am. B.* **12**, 1416–1421 (1995).
7. N. V. Kukhtarev, E. Krazig, H. C. Kulich, and R. A. Rupp, Anisotropic self-diffraction in $BaTiO_3$. *Appl. Phys. B.* **35**, 17–21 (1984)
8. C. C. Sun, B. Wang and J. Y. Chang, Photorefractive Incoherent-to-Coherent Optical Converter Based on Anisotropic Self-Diffraction in $BaTiO_3$. *Appl. Opt.* **37**, 8247–8253 (1998).

9. B. Wang, and C. C. Sun, Precise Measurement of Thermal-Induced Refractive-Index Change in $BaTiO_3$ on the Basis of Anisotropic Self-Diffraction. *Appl. Opt.* **40**, 672–677 (2001).
10. M. de Angelis, S. de Nicola, A. Finizio, G. Pieratttini, P. Ferraro, S. Pelli, and S. Sebastiani, Digital-holography refractive-index-profile measurement of phase gratings. *Appl. Phys. Lett.* **88**, 111114 (2006).
11. J. P. Fugal, T. J. Schulz, and R. A. Shaw, Practical methods for automated reconstruction and characterization of particles in digital in-line holograms. *Meas. Sci. Technol.* **20**, 075501 (2009).
12. N. V. Kukhtarev, V. B. Markov, S. G. Odulov, M. S. Soskin, and V. L. Vinetskii, Holographic storage in electrooptic crystals. II. Beam coupling – light amplification. *Ferroelectrics.* **22**, 961–964 (1979).
13. U. Schnars and W. Jueptner, Direct recoding of hologram by a CCD target and numerical reconstruction. *Appl Opt.* **33**, 179–181 (1994).

Optical Engineering 74

OpticalEngineering.SPIEDigitalLibrary.org

# Moisture effect of fingerprint using total internal reflection digital in-line holography

Suwan Plaipichit
Prathan Buranasiri

SPIE.

# Moisture effect of fingerprint using total internal reflection digital in-line holography

**Suwan Plaipichit and Prathan Buranasiri***
King Mongkut's Institute of Technology Ladkrabang, Faculty of Science, Department of Physics, Chalongkrung Road, Bangkok 10520, Thailand

**Abstract.** Total internal reflection (TIR) is normally important in an optical fingerprint scanner. The moisture effect in a fingerprint scanner based on TIR has been explored by using digital in-line holography (DIH). First, the reflection and the transmission technique set up for DIH have been explored by using a positive resolution test target with a line width of 200 $\mu$m. From experimental results, the reconstructed image of the reflected DIH is perfect as the image of the transmitted DIH. Due to the advantage for opaque object imaging of the reflected DIH, reflected DIH based on TIR has been selected to investigate the moisture effect of the fingerprint. Fingerprints with moistures of 39%, 54%, 69%, and a soaked finger have been observed. A laser diode of 635 nm and a complementary metal oxide semiconductor camera were used in all of the experimental setups in this research. The reconstructed image of the fingerprint gives a sharper image than the directed recorded image. The fingerprint with higher moisture provided a darker fingerprint image, while the optimum amount of moisture that gives the most complete finger pattern is 54%. 
[DOI: 10.1117/1.OE.53.11.112315]

Keywords: digital in-line holography; fingerprint; skin moisture; low coherence.

Paper 140193SS received Feb. 1, 2014; revised manuscript received Jun. 3, 2014; accepted for publication Jun. 5, 2014; published online Jun. 25, 2014.

## 1 Introduction

Holography, the imaging technique of a recorded and reconstructed image in three dimensions was invented by Gabor.[1] The recording process requires the interference of the object beam and reference beam on photographic film. Then it uses the reading beam shining on the photographic film to see the image in three dimensions. This process is called reconstruction. Due to the conventional holography waste photographic film, digital holography was developed. The image, which consists of the phase and amplitude, is recorded on electronic devices such as charge couple devices (CCDs) or complementary metal oxide semiconductors (CMOS). The three-dimensional image is numerically reconstructed using a computer.[2] Digital holography would be typically classified into two types, i.e., off-axis and in-line configurations. The digital in-line holography (DIH) is the simplest configuration with which to record a hologram. There are various configurations of DIH, such as transmission, reflection, and total internal reflection (TIR). Transmitted DIH (TDIH) configuration could record and reconstruct the interferogram, which is placed at different plane.[3] An example of this is particle characterization.[4–7] Since TDIH may not be used in investigation of an opaque object, reflected DIH (RDIH) has been developed. As with normal holography, RDIH needs the interference of an object beam and a reference beam to complete the recording process. By using the reference-delayed technique, however, the system could record a hologram with only one input beam. In this configuration, a twice-reflected beam from an object, which consists of the phase difference, was interfered and recorded with a CCD camera.[8] By using the technique of TIR holographic microscopy some properties of biology cells have recently been explored.[9,10] In addition, the basic concept of TIR was widely applied in fingerprint scanner applications.[11,12] The early system, however, provided unsharp patterns. A number of methods have been invented for resolving this problem. For example, the holographic plate which when placed on the prism was used to correct the distortion of the pattern.[13,14] Another example, an asymmetrical aspheric lens, was invented to get better contrast for the fingerprint pattern.[15] Recently, the fingerprint patterns were explored using a digital holography technique based on the angular spectrum method,[16] which is based on the Michelson interferometer. In our previous work, the digital hologram patterns of a fingerprint pattern were obtained by using the reflection from a glass slide.[17] Interference patterns from the top and bottom occurred and were distributed in the recorded images.

However, from our point of view, the imaging technique of fingerprinting still has value for continuing exploration. In this paper, a digital holographic fingerprint scanner based on a combination of RDIH and TIR has been presented. In our configuration, instead of using two input beams as with previous systems, only one input beam is used so the system may be cheaper and more compact. The reflected field, which is diffracted at the edge of the fingerprint pattern, is interfered with the undiffracted field. We also show that the reconstruction of RDIH provide the same results as TDIH in Sec. 4. By using our technique, the results of various moistures on a fingerprint have been explored and shown.

## 2 Imaging Method

### 2.1 *Transmitted Digital In-Line Holography*

The experimental configuration of TDIH that was used in this paper is shown in Fig. 1(a). An expanded beam

*Address all correspondence to: Prathan Buranasiri, E-mail: kbpratha@kmitl.ac.th

propagates through the positive pattern test target. Then, it is separated into two beams, i.e., object and reference beams, by the thin opaque line of the target. The object beam was diffracted by the object pattern; the other one is a reference beam, since it is just transmitted through the target without any distortion. The holographic interference pattern is obtained by the superposition of these two beams and recorded on a CMOS camera. The holograms from data sets that are presented in this paper are reconstructed using the numerical method based on Huygens–Fresnel filtering described by Fugal et al.[18] Suppose $[h(x,y)]$ represents the two-dimensional (2-D) diffracted optical field which propagated along the $z$ direction to the CMOS plane. It can be expressed by using the Huygens–Fresnel principle[19] as the following

$$h(x,y) = \frac{z}{j\lambda}\iint O(\xi,\eta)\frac{\exp(jk\rho)}{\rho^2}\mathrm{d}\xi\,\mathrm{d}\eta, \tag{1}$$

where $O(\xi,\eta)$ is a 2-D optical field at the object plane, $\rho = [z^2 + (x-\xi)^2 + (y-\eta)^2]^{1/2}$ is the distance from any point on the object plane $(\xi,\eta)$ to the CMOS plane $(x,y)$, $z$ is the propagation distance, and $k = 2\pi/\lambda$ is the wavenumber of the light. By using the convolution method, the hologram function can be rewritten as

$$h(x,y) = F^{-1}\{F[O(\xi,\eta)]\cdot F[g(\xi,\eta,x,y)]\}, \tag{2}$$

where the impulse response $g(\xi,\eta,x,y)$ is given by

$$g(\xi,\eta,x,y) = \frac{z}{j\lambda}\frac{\exp[jk\rho]}{\rho^2}, \tag{3}$$

The optical field at the image plane $(\xi\prime,\eta\prime)$ can be reconstructed by using the inverse Fourier transform of the filtered Huygens–Fresnel as

$$R(\xi\prime,\eta\prime) = F^{-1}\{F[h(x,y)]\cdot F[g(\xi,\eta,x,y)]\}. \tag{4}$$

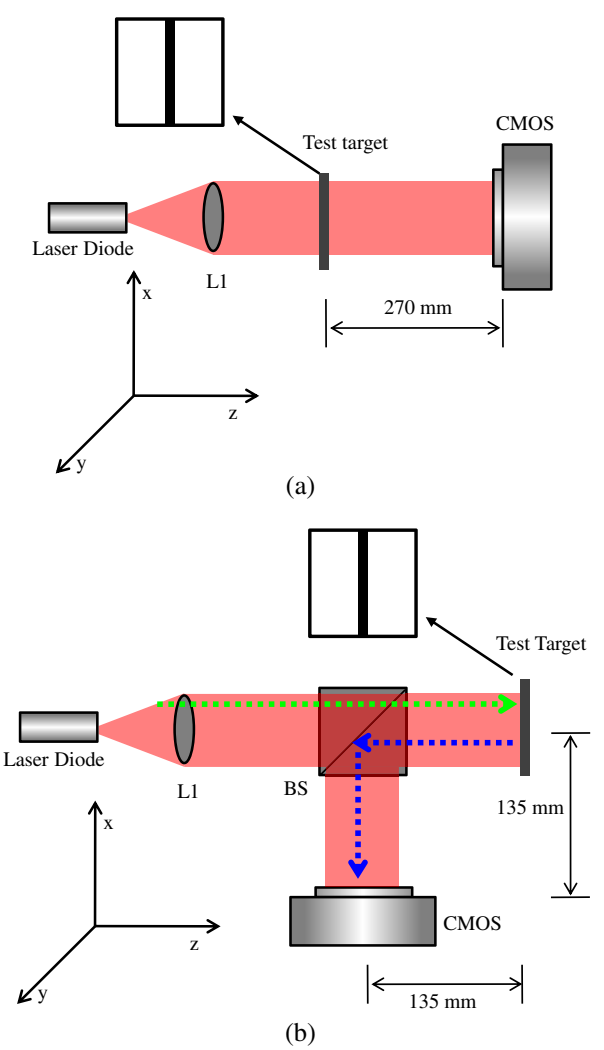


**Fig. 1** Experimental setup for recording a digital in-line holography (DIH) and reflected DIH (RDIH) of resolution test target: (a) Transmission DIH (TDIH) and (b) RDIH.

### 2.2 *Reflected Digital In-Line Holography*

The concept of RDIH is illustrated in Fig. 1(b). The expanded beam is incident on the target, which has a thin opaque line, and then it reflects back because of the polished surface. There are two different beams reflected at this surface. The first one reflects with diffraction at the edge of the opaque pattern; the other one reflects on the clear surface of the target without any diffraction. The interference of these two beams is recorded on a CMOS camera and then is numerically reconstructed in the same way as in basic DIH. The results have been shown in Sec. 4

### 2.3 *Total Internal Reflection for Reflected Digital In-Line Holography*

The concept of TIR has been widely used in fingerprint scanners. Figure 2 depicts the geometry of TIR, which is used to image the fingerprint pattern. TIR has occurred when the incident angle is larger than the critical angle between the prism and air boundary. There are two areas from which you can obtain the pattern in fingerprint imaging based on TIR. Here, the light reflects with TIR at the valley of the fingerprint providing, a bright pattern, and scatters at the ridge of the fingerprint, providing a dark pattern. Then they are interfered on the CMOS plane. This principle

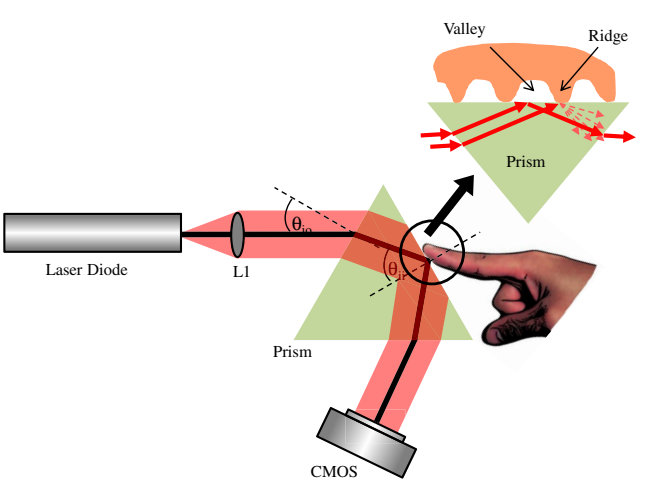


**Fig. 2** The schematic of digital holographic fingerprint scanner using total internal reflection.

will be applied to RDIH for imaging a fingerprint in the next section. Here we call this method total internal reflection DIH (TIRDIH).

## 3 Experimental Setup

First, our experimental setup has been done in the cases of both TDIH and RDIH as described in Sec. 2, which shows that the RDIH can be used instead of the TDIH in the case of an opaque object as described in Sec. 1. In our experiment, the distance between the camera and test target is 270 mm in both cases. Then, the RDIH has been applied to fingerprint imaging using the TIRDIH as described in Sec. 2.3. The experimental setup TIRDIH has been shown in Fig. 2. In the setup, a laser diode (LDM115G/633/1, 1 mW, 635 nm) was used as the light source. The expanded beam from the laser diode was collimated by lens $L_1$ ($f_1 = 175$ mm and 25.4 mm diameter) and then incident on an equilateral glass prism (N-BK7 with a refractive index: $n = 1.52$) with angle $\theta_{io}$. The refracted beam transmitted through the prism and then reflected at the boundary between the prism and air with angle $\theta_{ii}$. In the experiment, the TIR between the boundary of the prism and air was obtained when $\theta_{io}$ was equal to 29.0 deg, (i.e., $\theta_{ii} = 41.14$). Then, the interference patterns of various moistures of fingerprints were recorded with a CMOS camera (Canon EOS 350D, Japan, $3456 \times 2304$ pixels, 6.41-$\mu$m pixel pitch).

Four samples of different moistures of fingerprints, i.e., 39%, 54%, 69% and wet fingerprint, were used in the experiment. Since the maximum measurable range of the skin moisture checker (Scalar model MY808s) is only about 70%, we have used 69% of moisture as the highest one to avoid the saturated value of the instrument. Each reconstructed image is shown and compared in Sec. 4.

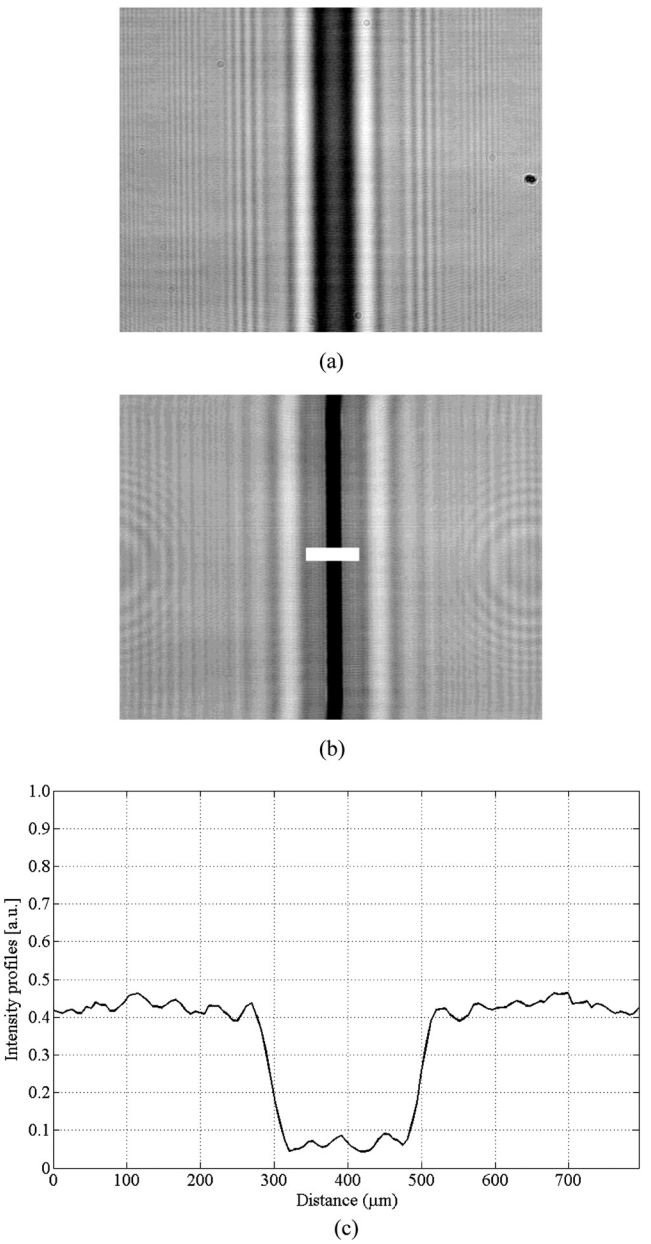


**Fig. 3** Hologram and its profile from TDIH: (a) recorded hologram, (b) reconstructed hologram, and (c) transverse intensity profile of (b).

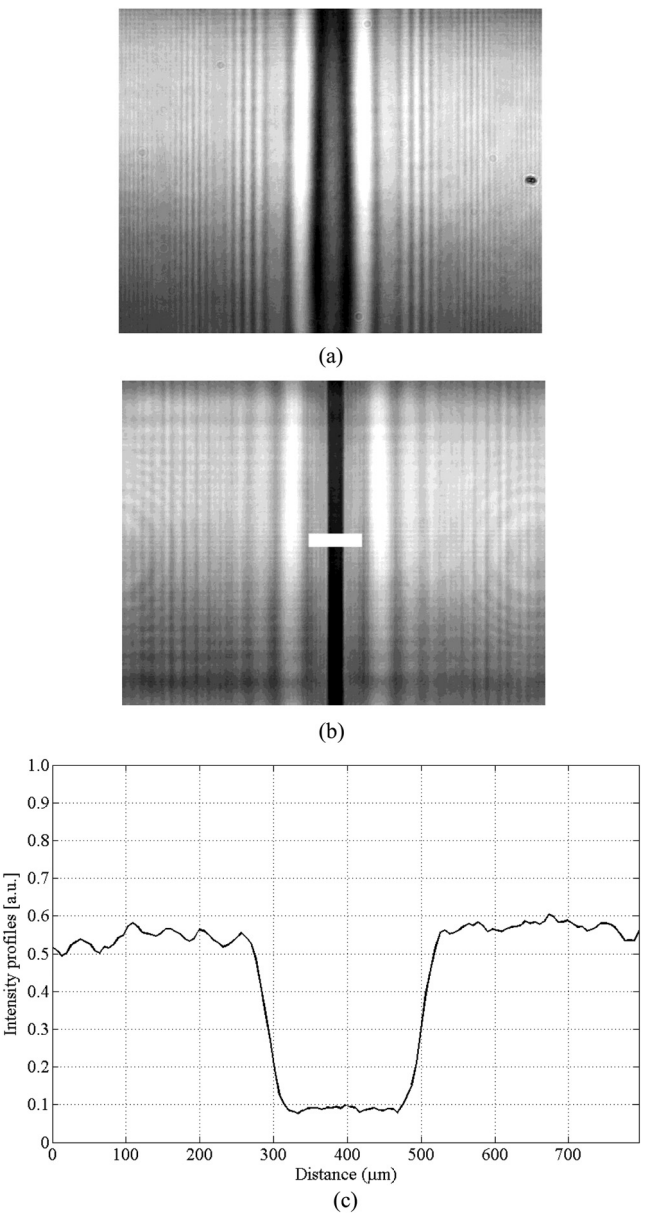


**Fig. 4** Hologram and its profile from RDIH: (a) recorded hologram, (b) reconstructed hologram, and (c) transverse intensity profile of (b).

## 4 Experimental Results

### 4.1 *Test Target Hologram*

In this section, the experimental results of the TDIH and the RDIH have been shown. Figure 3(a) shows the transmitted hologram patterns, which were recorded in the experimental setup from Fig. 1(a). The image recorded on the CMOS plane appeared as a defocused pattern. The numerical reconstruction of Fig. 3(a) at the plane of $z = 270$ mm from the CMOS is shown in Fig. 3(b). At this plane, the pattern of the test target was focused. The transverse intensity profile of Fig. 3(b) is illustrated in Fig. 3(c). The cross-section plots have been found corresponding to the standard value of the width of the resolution of the test target (200 $\mu$m).

Figures 4(a)–4(c) represent the recorded hologram pattern, reconstructed hologram pattern, and the transverse intensity profile of the RDIH in Fig. 1(b). From our RDIH results, the image can be reconstructed as in the case of TDIH. The pattern of thee test target is focused at the plane of $z = 270$ mm as in the TDIH case. Moreover, the pattern width is the same as that of the TDIH case.

### 4.2 *Fingerprint Hologram*

The hologram pattern of a fingerprint with a moisture of 54.0% and its best numerically reconstructed image are shown in Figs. 5(a) and 5(c), respectively. The reconstructed image was a better profile than the recorded image. Figures 5(b)–5(e) represent the best reconstructed fingerprint holograms of different moistures. From our observation, the

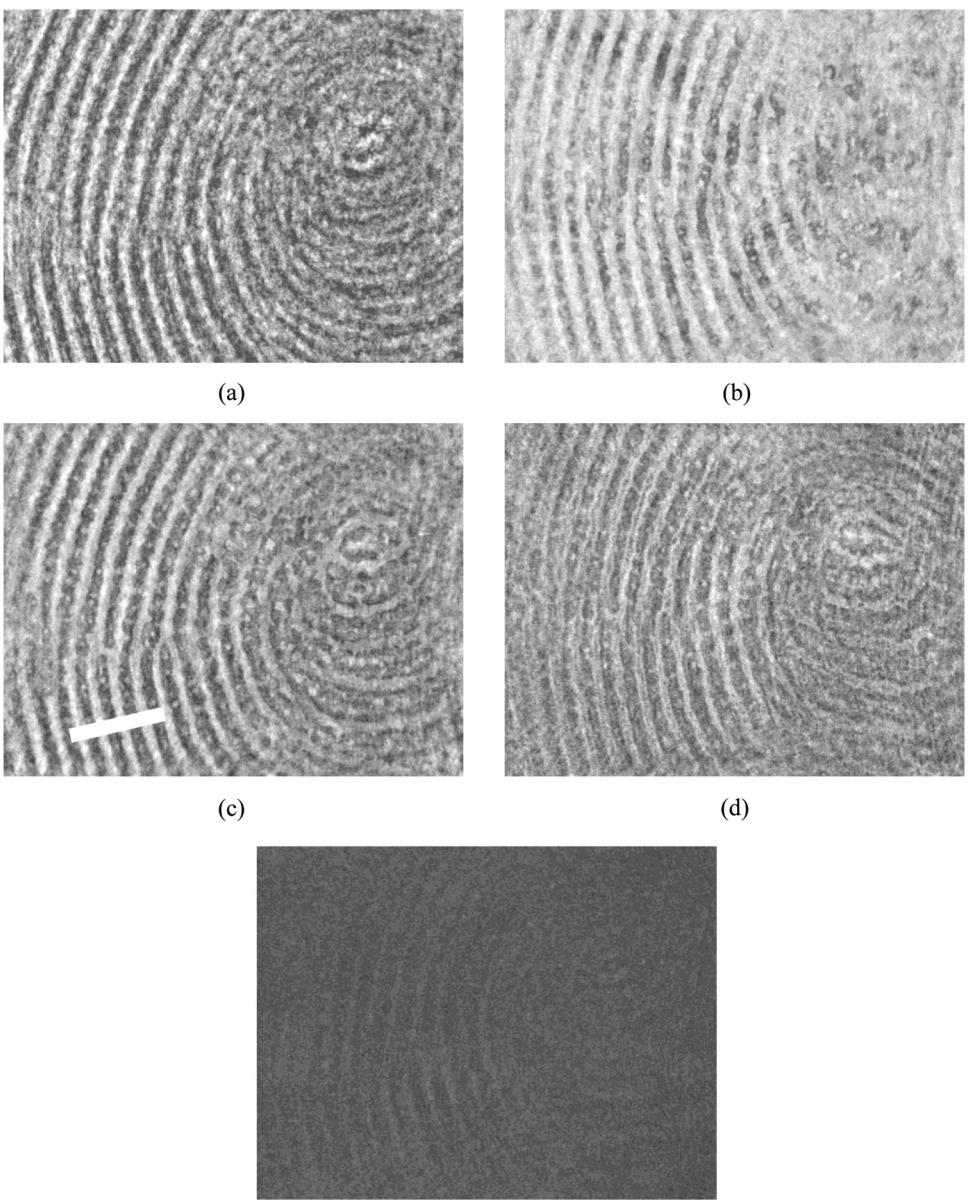


**Fig. 5** Recorded hologram: (a) with moisture of 54.0%. Reconstructed holograms: (b) with moisture of 39.0%, (c) with moisture of 54.0%, (d) with moisture of 69.0%, and (e) wet fingerprint.

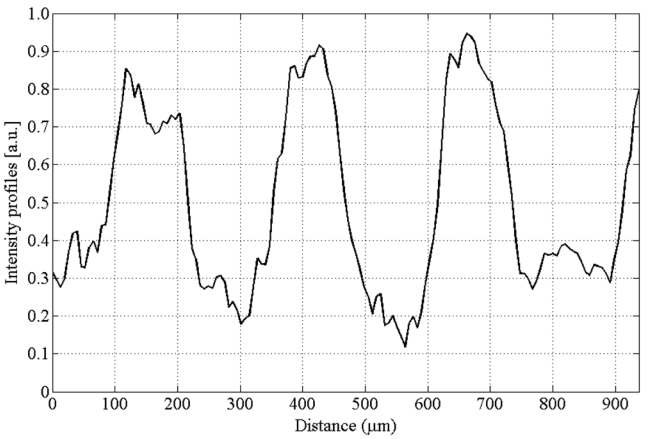


**Fig. 6** Transverse intensity profiles of fingerprint with moisture of 54.0%.

image of the fingerprint with a moisture of 39.0% [Fig. 5(b)] was incomplete because the ridge of the fingerprint was not completely close to the glass prism. When the fingerprint had enough moisture for coupling the fingerprint to the prism, the fingerprint pattern image would be perfect as illustrated in Fig. 5(c). We observed the ridge of the fingerprint was the dark pattern which is obtained from the scattering of light, and the valley of the fingerprint was the bright pattern which is obtained from the TIR of the light inside the prism, as described in Sec. 2. However, the fingerprint with too much moisture may give a worse image pattern as shown in Fig. 5(d). Since the gaps between fingerprint valleys and the prism are full of moisture the TIR cannot occur. However, the ridge patterns still occurred while the valley patterns were darker than the image of the fingerprint with a moisture of 54.0%. The wet fingerprint gives the worst pattern because there is a lot of water between the fingerprint and the prism. In this case, the ridge and valley of the fingerprint cannot be distinguished, as is presented in Fig. 5(e). Moreover, the intensity of the image will be decreased when the moisture of the fingerprint increases. The transverse intensity profile of the fingerprint pattern from Fig. 5(c) is shown in Fig. 6. The width of the fingerprint had been measured and it is about 150 $\mu$m.

## 5 Conclusion

In this study, we have proposed and demonstrated the moisture effect on fingerprint recording by the RDIH based on TIR. By using the interference of diffracted and undiffracted beams from the target in the recording process, only one input beam has been used in our scheme. So the setup is more compact than the previous systems. The reconstructed images of the RDIH also found that they are the same as the result images from the TDIH. The result images of different moistures for fingers have been shown and it was found that they look different. Perfect fingerprint patterns have been observed when the moisture percentages of fingerprint are in the range of 50% to 60%, which are measured with a skin moisture checker.

### Acknowledgments

This research has been supported reconstructed tool from Physics Department, Michigan Technological University.

### References

1. D. Gabor, "A new microscopic principle," *Nature* **161**, 777–778 (1948).
2. U. Schnars and W. Jüptner, "Direct recording of holograms by a CCD target and numerical reconstruction," *Appl. Opt.* **33**(2), 179–181 (1994).
3. G. Situ et al., "Generalized in-line digital holographic technique based on intensity measurements at two different planes," *Appl. Opt.* **47**(5), 711–717 (2008).
4. W. Xu et al., "Digital in-line holography of microspheres," *Appl. Opt.* **41**(25), 5367–5375 (2002).
5. G. Pan and H. Meng, "Digital holography of particle fields: reconstruction by use of complex amplitude," *Appl. Opt.* **42**(5), 827–833 (2003).
6. F. Soulez et al., "Inverse-problem approach for particle digital holography: accurate location based on local optimization," *J. Opt. Soc. Am. A* **24**(4), 1164–1171 (2007).
7. Y. Yang et al., "Integrated gray-level gradient method applied for the extraction of three-dimensional velocity fields of sprays in in-line digital holography," *Appl. Opt.* **51**(2), 255–267 (2012).
8. A. S. G. Singh et al., "In-line reference-delayed digital holography using a low-coherence light source," *Opt. Lett.* **37**(13), 2631–2633 (2012).
9. W. M. Ash and M. K. Kim, "Digital holography of total internal reflection," *Opt. Express* **16**(13), 9811–9820 (2008).
10. W. M. Ash, L. Krzewina, and M. K. Kim, "Quantitative imaging of cellular adhesion by total internal reflection holographic microscopy," *Appl. Opt.* **48**(34), H144–H152 (2009).
11. S. Sumriddetchkajorn and S. Phoojaruenchanachai, "Geometrical optics analysis for reduction of trapezoidal image distortion in a single prism-based optical fingerprint scanner," *Opt. Laser. Eng.* **45**(1), 229–239 (2007).
12. M. Kawakoe and A. Tojo, "Fingerprint pattern classification," *Pattern Recognit.* **17**(3), 295–303 (1984).
13. R. D. Bahuguna and T. Corboline, "TECHNICAL NOTE Prism fingerprint sensor that uses a holographic optical element," *Appl. Opt.* **35** (26), 5242–5245 (1996).
14. Y. Jie and Z. Jihong, "Fingerprint sensor using a polymer dispersed liquid crystal holographic lens," *Appl. Opt.* **49**(25), 4763–4766 (2010).
15. H.-F. Lin et al., "Optical design for enhanced prism type fingerprint scanner image contrast with asymmetrical aspheric lens," *Optik* **121** (24), 2250–2253 (2010).
16. M. C. Potcoava and M. K. Kim, "Fingerprint biometry applications of digital holography and low-coherence interferography," *Appl. Opt.* **48**(34), H9–H15 (2009).
17. S. Plaipichit et al., "Fingerprint verification by using low coherence digital holography," *Proc. SPIE* **8883**, 888315 (2013).
18. J. P. Fugal, T. J. Schulz, and R. A. Shaw, "Practical methods for automated reconstruction and characterization of particles in digital inline holograms," *Meas. Sci. Technol.* **20**(7), 075501 (2009).
19. J. W. Goodman, *Introduction to Fourier Optics*, Chapter 4, McGraw Hill, Singapore (1996).

**Suwan Plaipichit** is a PhD candidate at the King Mongkut's Institute of Technology Ladkrabang. He received his BS and MS degrees in applied physics from the King Mongkut's Institute of Technology Ladkrabang in 2008 and 2010, respectively. His current research interests include nonlinear optics, photorefractive effect, and digital holography. He is a member of SPIE.

**Prathan Buranasiri** received his BS degree in physics from Ramkhamhaeng University, Thailand. Then he went to the United States to pursue his graduate degree and received his MSc in physics and a PhD in electrical engineering from the University of Alabama in Hunstville and the University of Dayton, respectively. He is currently an instructor at the Department of Physics of King Mongkut's Institute of Technology Ladkrabang, Bangkok, Thailand. During his Ms and PhD degree work, he specialized in the nonlinear photorefractive effect. His recent research interests include photonic bandgap structure and their applications, optical properties in nanocarbon materials, photorefractive materials, and fiber optic communication system. He is a member of SPIE.

## AUTHOR BIOGRAPHY

**Name:** Suwan Plaipichit

**Date of Birth:** May 24, 1985

**Address:** 102/26 M.4, Keha-Romklao, Klongsongtonnoon sub-district,
Lat-Krabang district, Bangkok, 10520, Thailand

**E-mail:** ivirusjung@gmail.com

**Education:**

| | |
|---|---|
| 1992-1997 | Wat Pak Bueng school, Lat-Krabang, Thailand |
| 1998-2003 | Debsirin Romklao school, Lat-Krabang, Thailand |
| 2004-2007 | King Mongkut's Institute of Technology Ladkrabang, Bangkok, Thailand |
| | **B.Sc. Applied Physics,** Major Scientific Instrument and Industrial |
| | **Thesis:** Bullet Analysis and Comparison for Forensic Science |
| | **Advisor:** Prof. Jiti Nookaew |
| | **GPA:** 3.13 |
| 2008-2009 | King Mongkut's Institute of Technology Ladkrabang, Bangkok, Thailand |
| | **M.Sc. Applied Physics** |
| | **Thesis:** Adjustable High Voltage Direct Current Power Supply for $CO_2$ Laser |
| | **Advisor:** Dr.Prathan Buranasiri |
| | **GPA:** 3.83 |